

***Impact of telomere shortening on cell cycle  
progression and induction of senescence***

**Fachbereich für Chemie  
der Universität Hannover**

**zur Erlangung des Grades eines  
Doktor der Naturwissenschaften**

**Dr. rer. nat.**

**genehmigte Dissertation  
von**

**Master of Science Satyanarayana Ande**

**geboren am 05.06.1975, in Vijayawada (Indien)**

**2004**

Referent : Prof. Dr. Walter H. Müller  
Fachbereich für Biochemie  
Medizinische Hochschule Hannover  
Hannover, Deutschland

Koreferent : PD Dr. K. L. Rudolph  
Abteilung für Gastroenterologie, Hepatologie und Endokrinologie  
Medizinische Hochschule Hannover  
Hannover, Deutschland

Tag der Promotion: 06.02.2004

**Declaration:** Here with I declare that the study has been done by my own under the guidance of PD Dr. K. L. Rudolph and all the information provided is novel and true and has not been submitted to any other institute or university to obtain any other degree.

## **Acknowledgements**

I am very grateful to my supervisor PD Dr. K. L. Rudolph and to the Chairman of the Department of Gastroenterology, Hepatology and Endocrinology Prof. Dr. M. P. Manns for giving me the opportunity to pursue my research in Hannover Medical School and their encouragement and support through out my doctoral work. I would very much like to thank Prof. Dr. W. H. Müller, Department of Biochemistry, Hannover Medical School for his advise and valuble suggestions during my doctoral thesis work.

I would very much like to thank Prof. Thomas Scheper, Dean, Faculty of Chemistry, University of Hannover, Prof. Dr. Gaestel, Department of Biochemistry, Hannover Medical School and Prof. Jacobsen, Department of Plant Molecular Biology, University of Hannover for their advise and conducting necessary examinations for my doctoral thesis. I would like to thank Dr. Malek, Hannover Medical School for his valuable suggestions and discussions.

I would like to thank Dr. J. Buer and Dr. Lauber, Department of Cell Biology, GBF for their help and valuable suggestions in doing microarray analysis.

I would like to thank my colleagues Martina, Andre, Meta, Sonja, Steffi, Ruben and Christoph for valuable discussions and co-operation through out my research work.

I would like to thank all the people of Department of Gastroenterology, Hepatology & Endocrinology. I am very thankful especially to Prof. Dr. Trautwein group and Dr. Kubicka group for their co-operation and valuable discussions. My special thanks to Dr. Wüstefeld, Dr. Zender, Dr. Kühnel and Dr. Liedke for their help and discussions.

I thank Prof. Ungewickell, Department of Biology, Hannover Medical School for helping me with fluorescence microscopy and Dr. Krauter, Department of Hematology, Hannover Medical School, for RT-PCR and Prof. Dittmur, GBF, Braunschweig for FACS analysis.

## Contents

Title page.....	1
Declaration.....	2
Acknowledgements.....	3
Contents.....	4
<b>Abstract.....</b>	<b>7</b>
<b>1. Introduction.....</b>	<b>8</b>
1.1 Structure and Function of Telomeres.....	8
1.2 Telomere binding proteins and their function.....	9
1.3 DNA end replication problem.....	12
1.4 Telomerase.....	13
1.5 Telomerase independent telomere elongation.....	15
1.6 Telomere shortening and M1/M2 model of cellular senescence and crisis.....	16
1.7 The DNA-damage hypothesis of telomere dysfunction.....	17
1.8 The phenotypic and molecular characteristics of cellular senescence.....	19
1.9 Premature senescence.....	20
1.10 mTERC knock-out mouse: An invaluable model system for the study of the impact of telomere shortening <i>in vivo</i> .....	22
1.11 Liver regeneration: An <i>in vivo</i> model system for the study of cell cycle initiation and progression.....	23
1.12 Telomere shortening in aging and disease .....	24
1.13 The impact of telomere shortening on liver regeneration in telomerase deficient mice.....	25
1.14 Summary and the focus of present study.....	25
<b>2. Materials and Methods.....</b>	<b>27</b>
2.1 Chemicals.....	27
2.2 Radioactive material.....	29
2.3 Molecular markers.....	29
2.3.1 DNA-Markers.....	29
2.3.2 RNA-Markers.....	30
2.4 Enzymes.....	30
2.5 Antibodies.....	30
2.6 Tissue Culture Reagents.....	30
2.7 Oligonucleotides.....	30

2.8	Kits.....	31
2.9	Other materials.....	32
2.10	Laboratory equipment.....	32
2.11	Mice.....	33
2.12	DNA Extraction and Genotyping.....	33
2.13	Partial hepatectomy and <i>in vivo</i> BrdU labeling.....	34
2.14	Immuno-histochemical detection of BrdU.....	35
2.15	Hematoxylin and Eosin (H&E) staining.....	36
2.16	Senescence Associated $\beta$ -gal Staining.....	36
2.17	BrdU and Telomere probe co-staining.....	36
2.18	SA- $\beta$ -gal -BrdU co-staining.....	37
2.19	SA- $\beta$ -gal -Telomere probe co-staining.....	37
2.20	Q-FISH on inter-phase nuclei of isolated hepatocytes.....	38
2.21	Apoptotic TUNNEL assay.....	39
2.22	Determination of IL-6 serum levels.....	39
2.23	RNA extraction and cDNA synthesis.....	39
2.24	High density oligonucleotide microarray hybridization and analysis.....	40
2.25	Liver perfusion, nuclei preparation and flow cytometry.....	41
2.26	Propidium iodide (PI) staining for FACS analysis.....	41
2.27	Anti-BrdU (FITC) -PI double staining for FACS analysis.....	42
2.28	Quantitative real time PCR.....	42
2.29	Cell culture.....	43
2.30	Retrovirus preparation and infection.....	43
2.31	Cloning using the pGEMT-Easy vector.....	44
2.32	In-gel southern blotting for TRF (Telomere Restriction Fragment) length analysis.....	44
2.33	LB (Luria-Bertani) medium.....	45
2.34	LB (Luria-Bertani) plates.....	45
2.35	Bacterial transformation and culture.....	45
2.36	Plasmid mini preparation.....	46
2.37	Plasmid maxi preparation.....	46
2.38	Restriction digestion and insert verification.....	47
2.39	PCR Product extraction from the agarose gel.....	47
2.40	Freezing of cells.....	47
2.41	Thawing of cells.....	48

2.42	Human liver cirrhosis samples and histology.....	48
<b>3.</b>	<b>Results.....</b>	<b>49</b>
3.1	Telomere shortening limits the number of cells participating in organ regeneration....	49
3.2	Critical telomere shortening at the cellular level blocks cell cycle re-entry of a sub-population of liver cells in G3 mTERC <sup>-/-</sup> mice.....	51
3.3	Non-proliferating cells with critically short telomeres in mTERC <sup>-/-</sup> are senescent.....	53
3.4	Differentially expressed genes in response to induction of senescence in vivo.....	57
3.5	Cells with sufficient telomere reserves in G3 mTERC <sup>-/-</sup> mice compensate for impaired organ regeneration by an additional round of replication.....	64
3.6	Inhibition of S-phase entry, impaired G2/M progression, and additional round of cell division in regenerating liver of G3 mTERC <sup>-/-</sup> mice.....	66
3.7	Apoptosis does not account for the differences in the regenerative response between mTERC <sup>+/+</sup> and G3 mTERC <sup>-/-</sup> .....	70
3.8	Mitogenic responses are not disrupted by telomere shortening and are essential to reveal senescence phenotype in mTERC <sup>-/-</sup> mice.....	71
3.9	mTERC <sup>-/-</sup> have critically short telomeres and further telomere shortening in the subsequent cell division is not necessary to reveal increased senescence phenotype.....	73
3.10	The <i>in vitro</i> phenotype of replicative senescence induced by telomere shortening is dependent on mitogen stimulation.....	75
3.11	The enhanced expression of cell cycle inhibitors induced by telomere shortening is mitogen dependent.....	83
3.12	Inhibition of MEK/MAPK pathway partially abrogates the co-operation between mitogen stimulation and senescence signalling.....	86
3.13	Hepatocyte-specific senescence in human liver cirrhosis.....	88
3.14	Hepatocyte specific senescence correlates to fibrosis progression in cirrhosis.....	90
<b>4.</b>	<b>Discussion.....</b>	<b>91</b>
<b>5.</b>	<b>References.....</b>	<b>99</b>
	Curriculum Vitae.....	111

## **Zusammenfassung**

Telomerverkürzungen begrenzen die regenerative Kapazität von primären menschlichen Zellen in vitro durch die Induktion von zellulärer Seneszenz. Das Stadium der Seneszenz tritt auf, wenn Telomere eine kritisch kurze Länge erreichen. Seneszenz ist durch einen permanenten Wachstumsarrest gekennzeichnet. In dieser Arbeit haben wir Leberregeneration in Telomerase defizienten Mäusen untersucht, um zu erfassen, ob das in vitro Modell der zellulären Seneszenz auch für die durch Telomerverkürzung begrenzte Organregeneration in vivo zutrifft. Unsere Arbeiten zeigen, dass Telomerverkürzungen auf zellulärer Ebene in einem Organ heterogen auftreten und dass kritisch kurze Telomere eine Subpopulation von Zellen kennzeichnen, die im Rahmen der Regeneration vom Zellzykluseintritt gehemmt sind. Diese Subpopulation von nicht-proliferierenden Zellen zeigt Seneszenz-assoziierte- $\beta$ -Galaktosidase-Aktivität - ein biochemischer Marker zellulärer Seneszenz. Genexpressionsanalysen zeigten eine Hochregulation von Zellzyklusinhibitoren, die unter anderem auch Targetgene des p53-Gens enthielten, welches als Markergen von Seneszenz gilt. Unsere Studien zur Induktion und Aufrechterhaltung zellulärer Seneszenz in primären menschlichen Fibroblasten und Mausleber haben eine Zellzyklusabhängigkeit des Seneszenz-Signalwege aufgezeigt. Die Seneszenz-Signalwege sind schwach aktiv in ruhenden Zellen, wohingegen in Zellen, die zum Zellzykluseintritt angeregt werden, eine volle Aktivierung der Seneszenz-Signalwege auftritt. Die Amplifizierung der Seneszenz-Signalwege durch Mitogenstimulation ist zum Teil durch den MEK/MAPK-Signalweg vermittelt. Unsere Analyse humaner Leberproben zeigte, dass Seneszenz-assoziierte- $\beta$ -Galaktosidase-Aktivität in 84% von Leberzirrhoseproben auftritt aber nicht in nicht-zirrhosischen Kontrolllebergewebe. Diese Daten indizieren, dass die Telomerhypothese zellulärer Seneszenz für die Entstehung von menschlicher Leberzirrhose zutrifft, ein Krankheitsstadium, dass durch den Verlust hepatozellulärer Regenerationsfähigkeit gekennzeichnet ist. Unsere Arbeiten indizieren, dass zelluläre Seneszenz in vivo auftritt und funktionellen Einfluss auf Organregeneration hat. Im Mausmodell zeigen unsere Arbeiten, dass die gehemmte Organregeneration in Organen mit kurzen Telomeren durch zusätzliche Zellteilungsrunden von Zellen mit ausreichender Telomerlänge kompensiert werden kann. Diese Ergebnisse indizieren, dass das Ergebnis chronischer Erkrankungen und chronisch regenerativer Prozesse während der Alterung von der Balance zwischen regenerierenden und nicht-regenerierenden Zellen abhängt, eine Balance, die durch die Telomerlänge auf zellulärer Ebene bestimmt wird.

## **Abstract**

**Telomere shortening limits the regenerative capacity of primary cells *in vitro* by inducing cellular senescence characterized by a permanent growth arrest of cells with critically short telomeres. To test if this *in vitro* model of cellular senescence applies to impaired organ regeneration induced by telomere shortening *in vivo*, we monitored liver regeneration after partial hepatectomy in telomerase deficient mice. Our study shows that telomere shortening is heterogeneous at the cellular level and inhibits a subpopulation of cells with critically short telomeres from entering the cell cycle. This subpopulation of cells with impaired proliferative capacity shows senescence associated  $\beta$ -galactosidase activity a marker of senescence. Expression profiling of the effected organ shows upregulation of cell cycle inhibitors including downstream targets of p53 - a marker gene of replicative senescence. Our studies on induction and maintenance of replicative senescence in primary human cells and in mouse liver show that the replicative senescence pathway is cell cycle dependent. It operates at a low level in cells with shortened telomeres but becomes fully activated when cells are stimulated to enter the cell cycle. The amplification of replicative senescence signalling by mitogen-stimulation is in part mediated through MEK/MAPK-pathway. Our analysis on human liver samples reveals that senescence-associated  $\beta$ -galactosidase staining is present in 84% of cirrhosis samples but not in non-cirrhotic livers indicating that the telomere hypothesis applies to cirrhosis formation, which is characterized by cessation of hepatocyte regeneration. This study provides experimental evidence for the existence of an *in vivo* process of cellular senescence induced by critical telomere shortening that has functional impact on organ regeneration. We show in the mouse model that impaired regeneration of an organ with shortened telomeres can be accomplished by cells with sufficient telomere reserves that are capable of additional rounds of cell division. These findings indicate that the outcome of chronic diseases and tissue regeneration during aging depends on the balance of proliferative to non-proliferative cells determined by telomere length at cellular level.**

**Stichworte:** Zelluläre Seneszenz, Organ Regeneration, Telomerverkürzung

**Keywords:** Cellular senescence, Organ regeneration, Telomere shortening

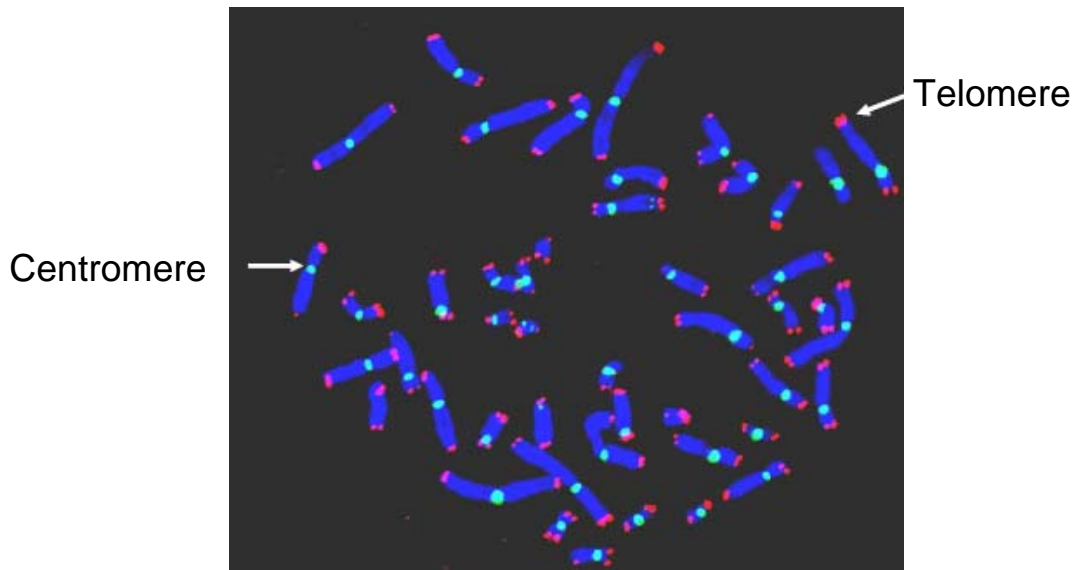


# 1. Introduction:

## 1.1 Structure and Function of Telomeres

Telomeres are specialized nucleo-protein structures that form the physical ends of linear eukaryotic chromosomes (1, 2). The name ‘telomere’ (telos=end; meros=part) and the observation of the specialized genetic structures at the ends of chromosomes dates back to 1938. Using cytogenetic approaches, Muller and McClintock independently observed that natural chromosome ends, unlike random DNA breaks, had special properties that protected them from end-to-end fusions. Due to extensive research efforts for the past few years, now it is known that highly conserved telomere structures at the ends of linear chromosomes consist of tandem repeat DNA sequences and associated proteins (1, 2). Mammalian telomeric DNA is composed of G-rich tandem repeats of the sequence (TTAGGG)<sub>n</sub>, which in humans extends 10-15 kilo bases (Kb) where as in inbred mouse strains it is approximately 40 – 60 Kb (3, 4, 5). The sequence of human telomeres was identified by Moyzis in 1988 (6). Cytologically, telomeres in a variety of plants and animals are heterochromatic, implying a high degree of DNA folding (7). The bulk of telomeric DNA is double stranded, but the extreme terminus of telomeric DNA consists of a 3’ overhang of approximately 200 bases. The G-strand overhang is the substrate to which telomeric repeats are added by telomerase (8, 9).

Recent discoveries suggest that telomeres exist in at least two different states or architectures: an ‘open’ and a ‘closed’ complex. The ‘closed’ complex is thought to represent the state that caps and protects chromosome ends. In mammals and some other species a lasso-like structure, called the t-loop, has been observed (10, 11). In the t-loop model for this higher order ‘closed’ complex structure, the 3’- single-stranded overhang folds back into the double-stranded telomeric tracts, providing one solution to the end-protection problem. The ‘open’ complex is probably not only required for the telomerase to access the end of the telomeric DNA for telomere elongation (see below), but most likely the opening of the tertiary telomere structure is also necessary to allow telomeric DNA replication during S-phase. Therefore it is likely that different telomere states – open or closed - are cell cycle-dependent.

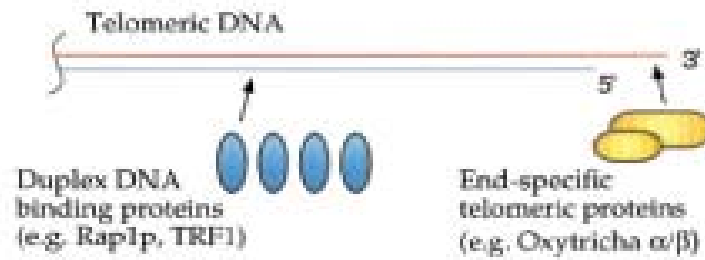
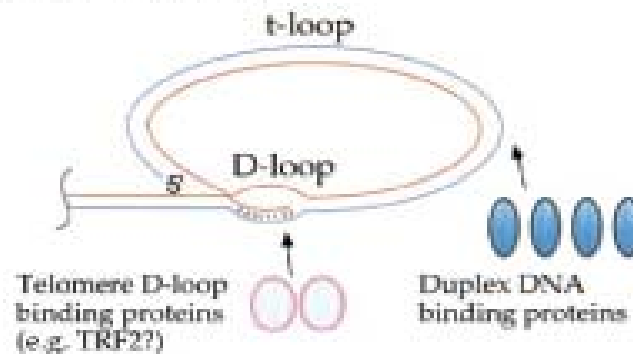


**Figure 1.1.1** Structure of metaphase chromosomes. (5) (Liu Y, Kha H, Ungrin M, Robinson MO, Harrington L. Preferential maintenance of critically short telomeres in mammalian cells heterozygous for mTERT. *Proc. Nat. acad. sci.*, 2002, 99, 3597-3602).

Maintenance of functional telomeres at chromosome ends is required for the prolonged survival of most organisms with linear chromosomes. The primary function of telomeres is to cap and protect the chromosomal ends (12, 13). Telomeres are also involved in several essential biological functions. They protect chromosomes from recombination, end-to-end fusion, and recognition as damaged DNA (12-16), provide a means for complete replication of chromosomes, contribute to the functional organization of chromosomes within the nucleus (17), participate in the regulation of gene expression (18), and serve as a molecular clock that controls the replicative capacity of human cells and their entry into senescence (see below, 19-21).

## 1.2 Telomere binding proteins and their function

The terminal regions of the telomeric double-stranded DNA repeats in humans (and other species) are thought not to be packaged into nucleosomes (22), but together with the single-stranded overhang serve the crucial function of providing binding sites for sequence-specific DNA-binding proteins that bind to and stabilize telomeres (23-25) and possibly involve in telomere mediated responses (12-16, 26). Some of these proteins are necessary for the formation of higher order telomere structures, such as T loops, D loops (10, 11) or G-quartets (27), which appear to be essential for telomere capping function.

**A. The classical view****B. The new view**

**Figure 1.2.1** Classical versus new view of telomere structure (11) (C.W.Greider, Telomeres do D-loop, T-loop. *Cell*, 97, 419-422).

These DNA-binding proteins in turn recruit other proteins to the telomere, forming a multi-protein telomeric cap (14, 28). The most striking feature of these telomeric proteins is that they bind to double-stranded DNA via a structurally conserved DNA-binding domain of the Myb/homeodomain type (29). Myb/homeo-domains belong to the common helix–turn–helix (HTH) family of DNA-recognition motifs found in many transcription regulators.

Two Myb-related telomere repeat binding proteins, TRF1 and TRF2, have been characterized and play important, but apparently distinct, roles in telomere length homeostasis (23, 24, 29). TRF1 and TRF2 and their associated proteins have the primary responsibility of stabilizing the complex and forming the t-loop (10, 11). Some degree of stabilization is intrinsic to the telomere overhang due to the G-rich nature of the TTAGGG repeats that form quadruplex structures. TRF1 is important in intra-telomeric coiling and it acts as a negative regulator of telomere length and function (23). TRF2 also binds along the length of the telomere but appears to be particularly abundant at the base of the t-loop and is important for its stabilization and formation (24). These duplex telomere DNA binding proteins also have their own associated proteins (13, 14, 28).

One such protein is Rap1p, which is integrated into the t-loop complex and interacts with TRF2, but its specific role in humans is unknown (25). Tankyrase has the ability to inhibit TRF1, thereby releasing it from the t-complex and allowing telomerase and other enzymes to bind (30). TIN2 promotes TRF1 function and causes it to bind to telomeres (31). The single-stranded G-rich overhang binds Pot1 which is the terminal transducer of TRF1 telomere length control (32).

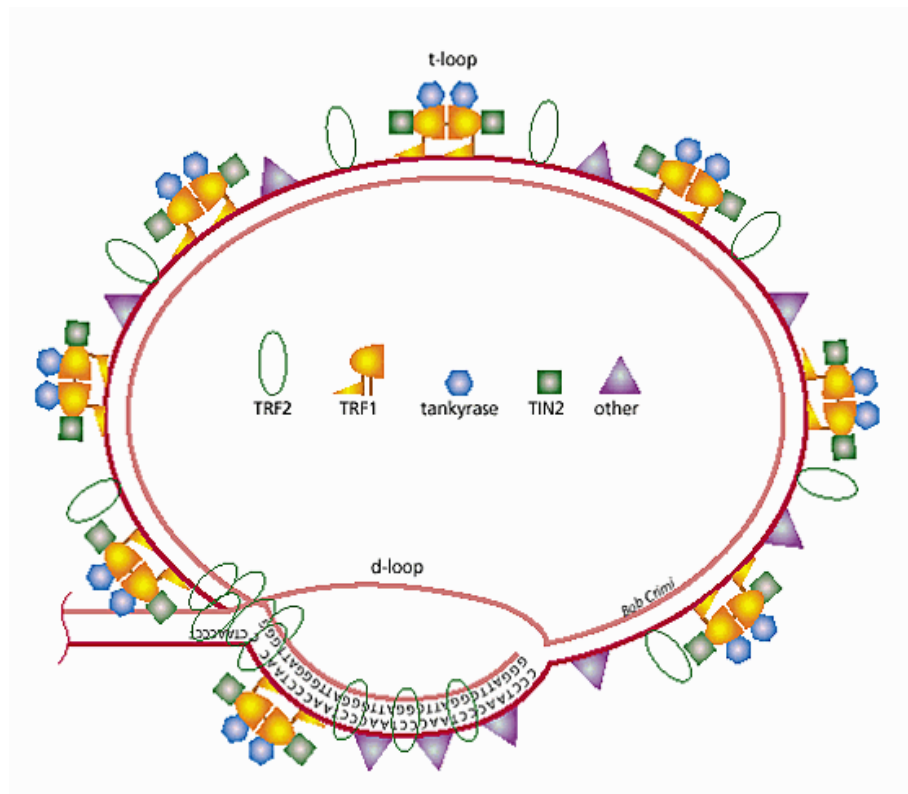


**Figure 1.2.2** T-loop, D-loop structure of mammalian telomere. (33) (Shay, JW: At the end of the millennium, a view of the end. *Nat Genet* 1999, **23**:382–383.)

The DNA damage response complex RAD50/MRE11/NBS1 also co-operates with TRF2 (34). The MRE11 complex functions conventionally in homologous recombination to repair DNA double strand breaks (35). At the telomere, however, it is thought to stabilize the T-loop where the single stranded tail invades the duplex telomere. Based on its function in vitro, the role of NBS1 during the S phase may be to unwind the T-loop via a helicase (34). Ku70 and Ku86, together with DNA-PKcs, form an enzyme called DNA dependent protein kinase (DNA-PK), which is involved in DNA double strand break (DSB) repair by NHEJ and in V(D)J recombination. Ku proteins also interact with TTAGGG repeats and with telomeric proteins TRF1 and TRF2 (36).

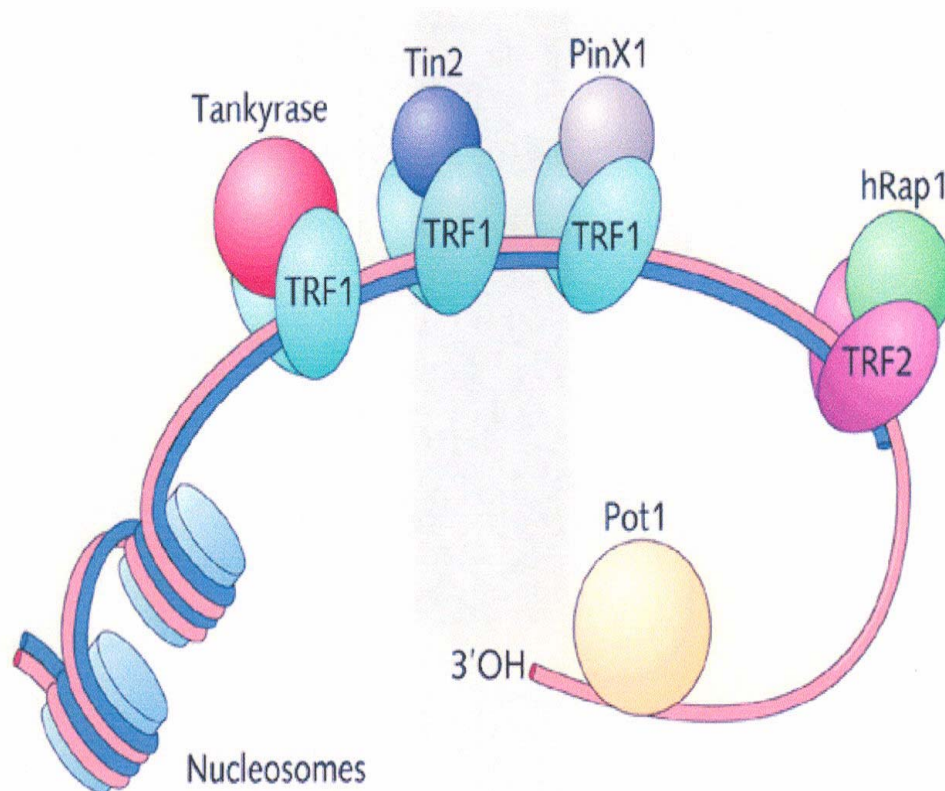


**Figure 1.2.3** The nucleo-protein complex, telomeres with its associated binding proteins (37) (Rhodes D, Fairall L, Simonsson T, Court R, Chapman L. Telomere architecture. *Embo Rep.* 2002, 3, 1139-45).

It appears that in addition to these known telomere binding proteins there might be several other proteins which involve in telomere stabilization and integrity and telomere mediated responses. Identification and functional analysis of these proteins lead to a better understanding of the structure and integrity of the telomeres. A selective disruption of the telomere integrity might be a new therapeutic approach to inhibit cancer cell growth, whereas stabilization of telomeres could be useful to prevent chromosomal instability and cancer initiation.

### 1.3 DNA end replication problem

Replication of linear chromosomes presents a special problem and Watson and Olovnikov independently hypothesized that linear DNA progressively loses some of its sequence at the very ends each time a cell divides (38). Their theoretical hypothesis was later proven by showing that DNA polymerase can only synthesize a new strand of DNA as it moves along the template strand in the 3' → 5' direction. This occurs on the 3' → 5' strand

(leading strand) of a chromosome as the DNA polymerase can move un-interruptedly from an origin of replication until it meets another bubble of replication or the end of the chromosome. In contrast, DNA-synthesis using the 5' → 3' strand (lagging strand) as the template is discontinuous and requires small RNA-primers for initiation of DNA-replication. When the replication fork opens sufficiently, DNA polymerase binds to the RNA-primer and begins to synthesize a section of complementary strand - called an Okazaki fragment - proceeding in the opposite direction of the movement of the replication fork. This continues until close to the end of the chromosome. Later, DNA ligase, ligates the Okazaki fragments together. However, the molecular requirements of the process are such that 5' end of each newly-synthesized strand can not be replicated completely. Thus each of the daughter chromosomes will have a shortened telomere (the end replication problem). It is estimated that human telomeres lose about 50-100 base pairs from their telomeric DNA after each round of replication (19-21). This represents about 10-15 TTAGGG repeats.

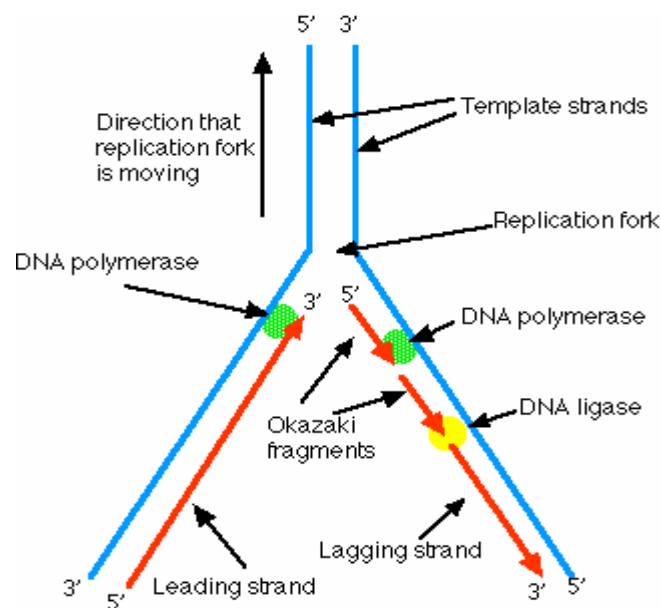


**Figure 1.3.1** The end replication problem (The cell cycle: DNA replication, mitosis and cancer, Chapter 17, *Addison wisely Longman*)

#### 1.4 Telomerase

The DNA polymerase's inability to complete DNA replication until the extreme ends of the telomeres was compensated for by the reverse transcriptase enzyme telomerase, which synthesizes telomere repeat units *de novo* by adding one nucleotide at a time, to single-stranded chromosome ends (39). Telomerase enzyme was discovered in the unicellular

protozoan *Tetrahymena thermophila* (40). The telomerase holoenzyme consists of two essential components: telomerase RNA component (TERC) (41), which serves as a template for the synthesis of telomere sequence and the telomerase reverse transcriptase (TERT), which is the catalytic component of the enzyme (42). When a chromosome is replicated, the 3' hanging parental fragment containing the G-rich sequence GGGTTA is recognized by the telomerase complex. Using its own RNA as a complementary primer, the telomerase mimics reverse transcriptases and elongates the hanging DNA fragment in the 5' to 3' direction. Replication of the lagging strand can now be completed using the telomeric extensions as a template for synthesis using DNA polymerase.

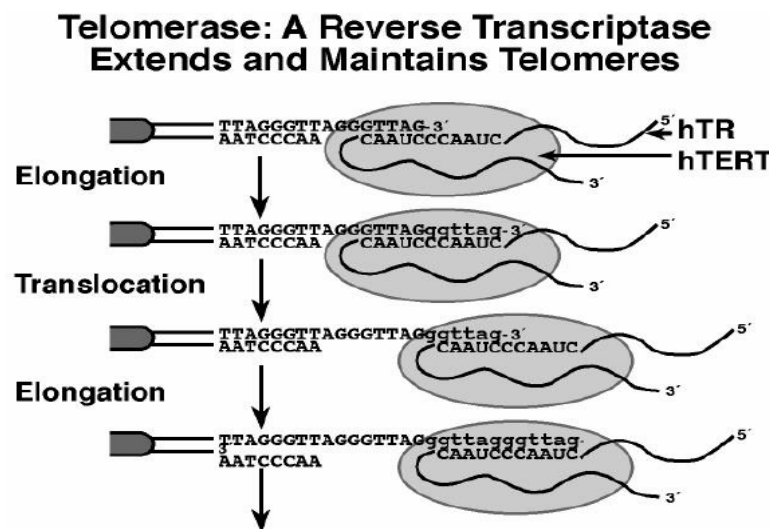


**Figure 1.4.1** Structure of telomerase holoenzyme and the mechanism of action at the telomeric ends. (43) (Blackburn EH, The telomere and telomerase: nucleic acid-protein complexes acting in a telomere homeostasis system. A review. *Biochemistry (Mosc)*. 1997, 62, 1196-201).

In cells with active telomerase, the telomere-telomerase complex comprises a dynamic system in which telomeric DNA length is continually being built up and shortened in a regulated way that maintains telomere length homeostasis and retains telomere functionality (43). The action of telomerase is regulated by sequence-specific DNA binding proteins that bind the telomeric DNA repeats. The human holoenzyme requires the proteins p23 and hsp90 to assemble the telomerase components *in vivo* (44). The telomerase gene was recently mapped to 5p15.33 as one of the most distal genes on chromosome 5p (45). This has raised questions about whether its proximity to the telomere might result in it being regulated by ‘telomere position effect’ mechanisms. Telomere position effect (TPE) results in the

reversible silencing of genes near telomeres by a mechanism that depends both on telomere length and on the distance to the gene (18, 46). Because telomeres in most human cells shorten with age, TPE would provide a mechanism to incrementally alter phenotype with increasing cellular age. The existence of TPE in mammalian cells raises the possibility that some presenescent changes could be "programmed" by the progressive shortening of telomeres with ongoing cell division, leading to altered patterns of gene expression that might affect both cell and organ function (18, 46).

In humans, telomerase expression is tightly regulated. It is active only during embryogenesis, whereas its postnatal activity is suppressed in most somatic tissues but remains active in a subset of cells, such as germ cells (47), stem cells, progenitor cells (48), and activated lymphocytes (49-51). TERC is ubiquitously expressed, whereas TERT expression is suppressed and acts as a rate limiting factor in most somatic cells and tissues leading to inevitable loss of telomere repeats at a rate of 50-100bp (52, 53). Postnatal suppression of telomerase expression in most somatic tissues is thought to represent a potent anti-tumor barrier not allowing the immortal growth of transformed cells (54). The molecular mechanism for postnatal inactivation of telomerase in humans is not well known and remains to be elucidated. Several lines of evidence suggest that the existence of repressors rather than the absence of activators might control the tight regulation of TERT expression in humans (55, 56). Contrary to most normal tissues, over 80% of human cancers show expression and activity of telomerase (57).

### **1.5 Telomerase independent telomere elongation**

Although telomerase is the most prevalent mechanism used for maintenance of telomeric DNA, a small percentage of tumors and immortalized cell lines have been described that do not contain telomerase activity. These lines utilize an Alternative Lengthening of Telomere (ALT) mechanism to circumvent the telomeric checkpoint (58). Characteristics of human ALT cells include great heterogeneity of telomere size (ranging from undetectable to abnormally long) within individual cells, and ALT-associated PML bodies (APBs) that contain extrachromosomal telomeric DNA, telomere-specific binding proteins, and proteins involved in DNA recombination and replication (59). Activation of ALT during immortalization involves recessive mutations in genes that are as yet unidentified. Evidence from unicellular eukaryotes suggests that recombination between telomeric repeats may be one mechanism for telomerase-independent telomere stabilization. Although the molecular



mechanism for telomere maintenance in the absence of telomerase remains speculative, new results from mammalian systems also implicate a mechanism based upon homologous recombination in the ALT pathway (58).

### 1.6 Telomere shortening and M1/M2 model of cellular senescence and crisis

Replicative senescence was first described more than 30 years ago, for human fibroblasts in culture and has been called the Hayflick limit (19). The number of divisions that normal cells complete before they senesce depends on the species, age and genetic background of the donor, as well as the particular cell type (5, 20, 21). Upon completing a finite number of divisions, cell growth is arrested with G1 content in human cells (60, 61) and G1 or G2 content in mammalian cells (62). Once thus arrested, they cannot be stimulated to enter the S phase of the cell cycle by any known combination of physiological mitogens. This stage of a permanent cell cycle arrest has been termed cellular senescence.

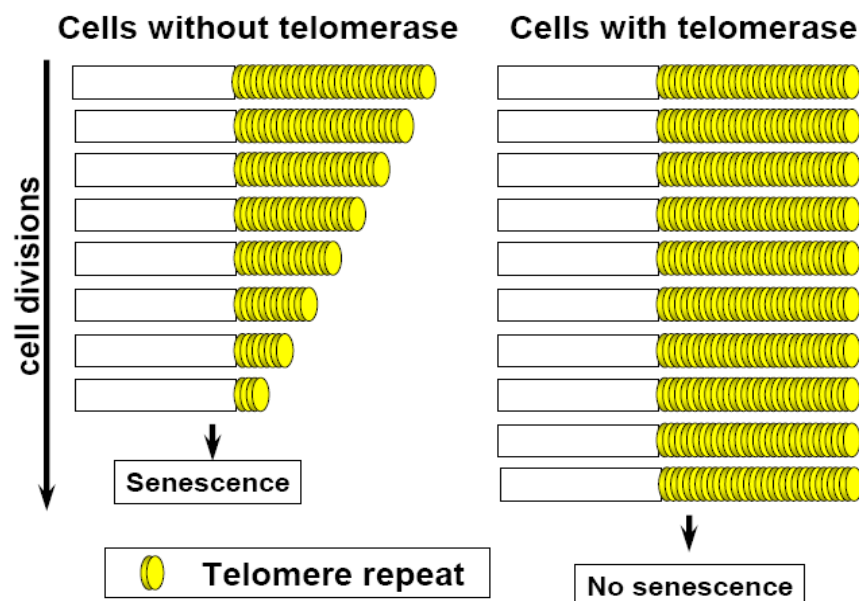


**Figure 1.6.1** Induction of cellular senescence after a finite number of divisions due to telomere shortening in the absence of telomerase activity

A two-stage model of cellular senescence M1/M2 has been proposed and the tumor suppressors p53 and Rb/p16 are part of the first mortality stage M1 or replicative senescence (54, 63). M1 is initiated when a few telomeres become shortened to a critical level and the chromosome ends become recognized as DNA damage signals leading to an activation of cell cycle check-points. In the absence of the gene products inducing these check-points (e.g. p53

or p16/Rb), cells continue to divide despite the prevalence of telomere dysfunction and ultimately reach a second checkpoint termed the “crisis” point (M2) which is characterized by massive rates of cell death and chromosomal instability (54). First experimental evidence for a relationship between telomere length and senescence was provided by the observation that telomeres of cultured somatic cells continuously shorten until cell growth is arrested at the M1 stage (19, 54). Experimental proof for the telomere hypothesis of cellular aging has come from experiments showing that the ectopic expression of hTERT leads to cellular immortalization and a bypass of senescence (64).

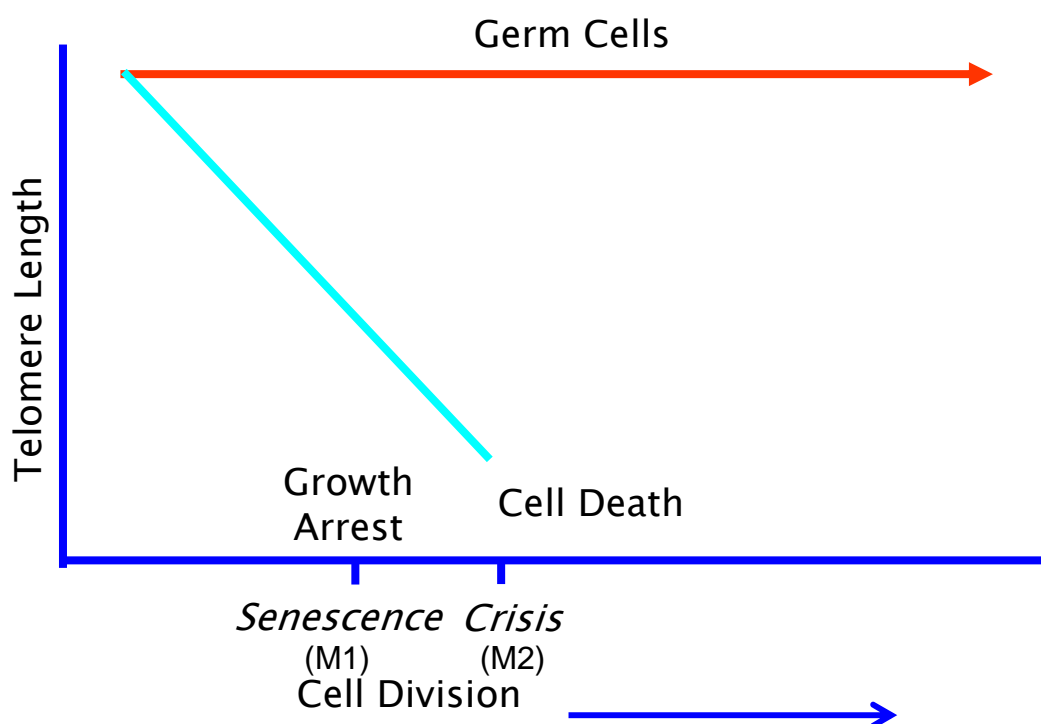


**Figure 1.6.2** M1/M2 model of cellular senescence (65) (Linskens MH, Harley CB, West MD, Campisi J, Hayflick L. Replicative senescence and cell death. *Science* 1995, **267**, 17).

### 1.7 The DNA-damage hypothesis of telomere dysfunction

A current hypothesis is that critical telomere shortening leads to telomere shortening and dysfunctional telomeres and this uncapping of chromosomal ends trigger responses similar to DNA-damage signaling including the p53-dependent DNA-damage pathway that leads to growth arrest or apoptosis (12-16, 62, 66). p53 DNA binding activity and transcriptional activity have been reported to increase upon replicative senescence. Moreover, p21, a well-recognized p53 target gene whose expression markedly increases in senescent

cells (67, 68). An important question concerns the signaling components upstream of p53 and p16/Rb that alert cells to telomere dysfunction. The ATM kinase is likely to be involved in the induction of senescence as well as in apoptosis. So far there is no suggestion on how the expression level of p16 is increased in cells experiencing telomere damage or other forms of DNA damage. In each case, p53 and p21 are induced and high levels of p16 accompany a reduction in pRb phosphorylation (67, 68). Perhaps the irreparable damage caused by the uncapping of multiple telomeres mimics by the ultimate consequences of extensive genome-wide radiation damage. Telomere-directed senescence may thus reflect the results of persistent damage, irrespective of its original proximate cause. In accordance with this hypothesis a recent study shows that critical telomere shortening in senescent cells activate DNA damage checkpoint responses which are similar to the responses induced by cells bearing DNA double-strand breaks. This involves telomeric foci of phosphorylated histone H2AX and their co-localization with DNA repair and DNA damage checkpoint factors such 53BP1, MDC1 and NBS1 and activation of CHK1, CHK2, MDC1 which are all down stream targets of ATM and p53 (16).

In mTERC<sup>-/-</sup> mice, an *in vivo* model to study the impact of telomere shortening, the cell cycle inhibitor p53 has been identified as a mediator of adverse effects of telomere shortening in organ regeneration *in vivo* (62). Deletion of p53 in mTERC<sup>-/-</sup> mice rescued defects in homeostasis of high-turnover organs without rescuing telomere length, chromosomal capping, or fusions of the chromosomes. This observation suggests p53 as a downstream target of telomere dysfunction *in vivo* by inducing apoptosis or cell cycle arrest in response to critical telomere shortening (62). Interestingly the activation of p53 in response to telomere shortening might in part be independent of ATM. The ATM<sup>-/-</sup> mTERC<sup>-/-</sup> mice have premature aging phenotype and impaired organ homeostasis and show no rescue of these phenotypes as has been found in p53<sup>-/-</sup> mTERC<sup>-/-</sup> mice (69). Another mediator of apoptosis induced by telomere dysfunction in mTERC<sup>-/-</sup> mice is Ku86 (36), which plays a role in non-homologous endjoining. Absence of Ku86 prevents chromosomal fusions and apoptosis induced by telomere dysfunction but does not rescue the growth deficit of cells and organs with critically short telomeres (70). These studies from mTERC<sup>-/-</sup> mice have given the first experimental evidence that telomere dysfunction acts upon regeneration process *in vivo* during aging and in response to acute or chronic injury.

### 1.8 The phenotypic and molecular characteristics of cellular senescence

Cellular senescence induced by telomere shortening is characterized by typical changes in cell morphology and size (flattened cells with enlarged cytoplasm) (19, 71), and senescence-associated beta-galactosidase (SA- $\beta$ -Gal) activity at pH6 (72). The findings on molecular level suggest that once cells undergo replicative senescence they express one or more inhibitors of cell cycle progression that can act in a trans-dominant manner (68). The growth arrest associated with cellular senescence has been studied most extensively in cultured human fibroblasts (19-21, 60). It is clear from these studies that many genes, including at least three proto-oncogenes, remain mitogen-inducible in senescent cells (73). Thus senescent cells do not fail to proliferate due to a general breakdown of growth factor signal transduction. Rather, it is now known that replicative senescence causes the selective repression of a few positive-acting, growth regulatory genes whose expression has been shown to be important for G1 progression and DNA synthesis. In fibroblasts, these inhibited genes include the c-fos proto-oncogene (74), the helix-loop-helix ID-1 and ID-2 genes (75), and the E2F-1 and E2F-5 (76, 77) components of the E2F transcription factor. In addition, the retinoblastoma tumor suppressor protein (pRb) remains in its growth suppressive form (that is, remains constitutively underphosphorylated) (78, 79). Phosphorylation of pRb during G1 phase is carried out by cyclinD-Cdk4/6 and cyclin E-Cdk2 complexes (79). Phosphorylation of Rb is an essential event for the release of E2F transcription factors that promote the expression of late G1 genes whose products are required for S-phase initiation and progression (79). In addition to these deficiencies in positive growth-regulators, senescent human fibroblasts over-express two negative growth regulators: the p21 and p16 inhibitors of cyclin dependent protein kinases (CDKs) (67). In senescent cells even though there is abundant cyclin D-Cdk4/6 and cyclin E-Cdk2 complexes they lack cyclin D and cyclin E associated kinase activities which is due to increased inhibitory binding of p21 to these complexes rather than inhibitory phosphorylation of kinase activity (67). The high levels of p21 and p16 are very likely responsible for the accumulation of inactive CDK complexes (67, 68), and thus the constitutive under phosphorylation of pRb in senescent cells. Furthermore, because p21 can inhibit E2F by both pRb dependent and pRb-independent mechanisms, the high level of p21 may well be also responsible for the lack of E2F activity in senescent cells (67, 68). However, in addition to this essentially irreversible arrest of cell proliferation, senescent cells display two other striking phenotypic changes. First, senescent cells acquire resistance to apoptotic stimuli (80). The mechanism by which senescent cells resist apoptotic

death is not well understood. Second, senescent cells show sometimes striking changes in differentiated functions with altered chromatin re-organization (81). Very little is known about the mechanisms that lead to chromatin remodeling and differentiated gene expression in senescent cells.

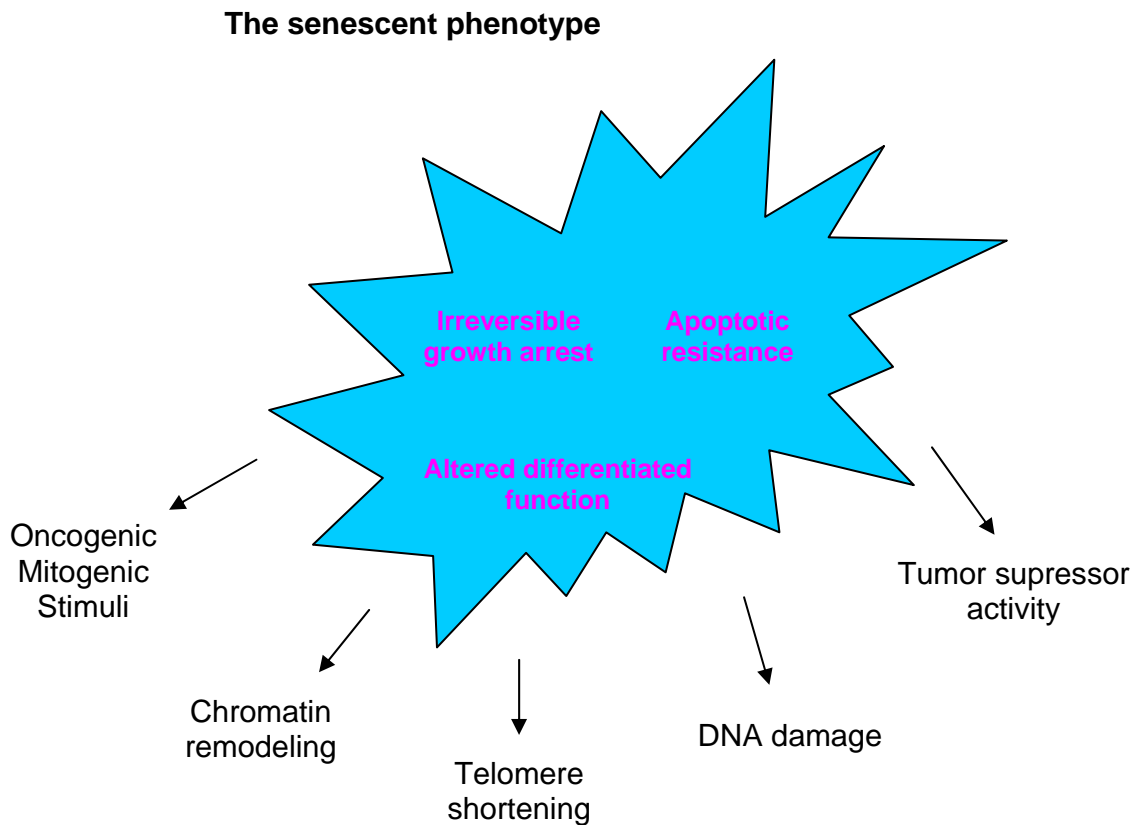


**Figure 1.8.1** Characteristics of cellular senescence. (82) (Itahana K, Dimri G, Campisi J. Regulation of cellular senescence by p53. *Eur J Biochem.* 2001, 268, 2784-91).

### 1.9 Premature senescence

Beside induction of cellular senescence by critical telomere shortening, several other factors include oxidative stress, DNA damaging agents and uncontrolled stimulation of several mitogenic pathways can also induce senescence irrespective of telomere length (83-86). An example of such premature senescence is the induction of a permanent growth arrest by overstimulation of the ras/raf/MEK/MAPK pathway (86). This arrest involves similar signaling pathways as the senescence program induced by critical telomere shortening and both programs have the same morphological markers (87). In primary human cells this premature senescence program leads to activation/upregulation of p53 and p16 (84, 86) and this "premature senescence program" has been implicated to function as a tumor suppressor

mechanism, preventing growth of cells with deregulated ras signaling (87). In addition, the "premature senescence" program gives a plausible explanation for the telomere independent onset of senescence in primary cell cultures indicating that abnormal mitogenic signaling induced by growth factors in the culture medium provokes a mitogenic stress-induced senescence response similar to the over-stimulation of the ras pathway (88, 89). Another stress-condition that has been linked to activation of a senescence program is oxidative stress and DNA-damage (83). It has been demonstrated that oxidative stress can co-operate with senescence induced by telomere shortening (90) whereas low oxygen condition can extend the lifespan of primary mouse embryonal fibroblasts (91). According to this finding the activation of senescence might depend on multiple factors including cellular stresses and telomere shortening. In line with this hypothesis, a recent study has shown that in primary human fibroblasts the activation of senescence during *in vitro* passage represents a mix of different senescence stimuli including oxidative and mitogenic stresses as well as telomere shortening (92). The inter-connection between these different senescence stimuli has yet to be explored.

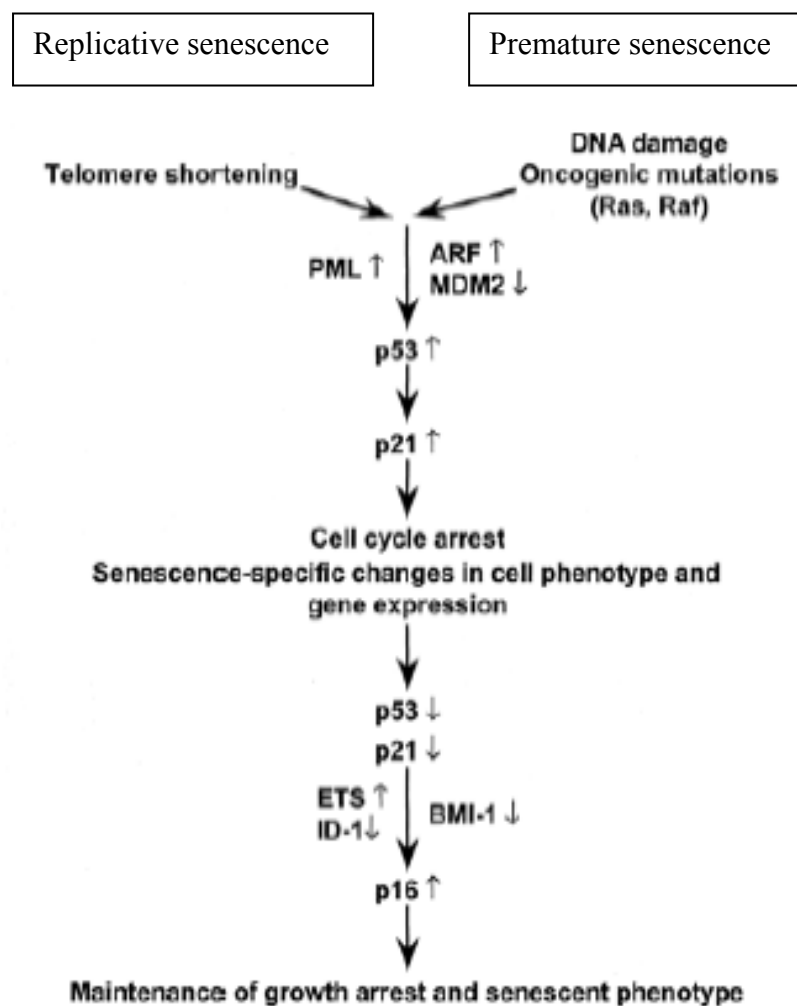


**Figure 1.9.1** Replicative senescence and premature senescence are indistinguishable to each other and share common morphological as well as molecular markers of senescence (87) (Chen QM. Replicative senescence and oxidant-induced premature senescence. Beyond the control of cell cycle checkpoints. *Ann N Y Acad Sci.* 2000, 908, 111-25).

### **1.10 mTERC knock-out mouse: An invaluable model system for the study of the impact of telomere shortening *in vivo***

The first animal model system to study the consequences of telomere shortening at organismal level *in vivo* was the telomerase deficient mice lacking the RNA component of telomerase (mTERC<sup>-/-</sup>), which is essential for telomerase activity (93). The telomerase function was not required for normal murine growth and development. The first generation (G1) mTERC<sup>-/-</sup> mice lack telomerase activity but – due to very long telomeres in laboratory mice do not show a significant phenotype (94). However, after breeding successive generations of telomerase-deficient mice, multiple phenotypes were uncovered in late generation mice (G3-G6), including defects in cell proliferation, wound healing, and the apoptotic loss of spermatogonia resulting in sterility (94, 95). In addition the phenotypes associated to telomere dysfunction include: elevated rates of embryonic mortality due to a defective closure of the neural tube (96), small size and severe intestinal atrophy (97), spleen atrophy and reduced proliferation of B and T lymphocytes upon mitogenic stimulation, as well as impaired germinal center function upon immunization (97).

In response to chronic liver damage, mTERC<sup>-/-</sup> mice prematurely develop cirrhosis -- the end stage of chronic liver diseases in humans (98). In addition, the mice show premature aging of highly proliferative organs and a curtailed stress response leading to a reduced lifespan (99). The prevalence of premature aging phenotypes depends on the telomere length (99) and appears in earlier generations of mTERC<sup>-/-</sup> inter-crosses in mouse strains with shorter telomeres as compared to those with longer telomeres (97). In addition, it has been shown that regenerative defects in mTERC<sup>-/-</sup> mice are caused by the prevalence of very short telomeres independent of the average telomere length (100). Overall, these results support an essential role of telomeres and telomerase for the well-being and survival of organisms (93-100).

### 1.11 Liver regeneration: An *in vivo* model system for the study of cell cycle initiation and progression

Liver has unique ability to regulate its growth and mass. Adult hepatocytes are normally quiescent and remain in G0 stage of the cell cycle but their ability to divide is not lost and they readily enter cell cycle in response to injury (101, 102). Therefore, hepatocytes constitute a conditional renewal cell system that may proliferate *in vivo* under well-defined conditions. This capacity is of physiological relevance in numerous liver diseases such as viral and alcoholic hepatitis, metabolic disorders, and post-liver surgery. Partial hepatectomy (70% liver resection) is a widely used method to study liver regeneration in animals. Liver regeneration following partial hepatectomy (PH) usually does not require the activation of liver precursor (''stem'') cells. Instead, liver mass is replenished by the proliferation of adult hepatocytes. After PH the remnant liver cells enter the cell cycle in a highly synchronized manner and restore the lost mass in 1 to 2 rounds of cell division within a week (101, 102). This makes it a highly valuable model system to study the cell cycle initiation and progression under *in vivo* conditions. The term regeneration is not biologically correct because the removed lobes or segments do not grow back. Instead, restoration of liver mass occurs by the compensatory hyperplasia of the cells in the remaining lobes. During liver regeneration the liver cells continue to perform crucial metabolic functions such as glucose regulation, synthesis of many blood proteins, secretion of bile, and biodegradation of toxic compounds required for homeostasis (101).

Liver regeneration is a multi-step process with at least two critical steps: the transition of the quiescent hepatocytes into the cell cycle (priming) and the progression beyond the restriction point in the G1 phase of the cell cycle (101). A large number of genes are either newly expressed or increase their expression during liver regeneration after PH. The first phase of gene expression after PH, referred to as the immediate early phase, occurs very rapidly after the operation and lasts for approximately 4 hrs (101, 103). The second phase of gene expression after partial hepatectomy is referred to as delayed early gene response. Extensive work by Taub and colleagues identified and defined the roles of as many as 70 genes participate in the immediate early response to PH. The proto-oncogenes c-fos, jun-B, c-jun and c-myc were the first genes to be identified in this group (104). During this phase the cells become competent to enter cell cycle and acquire the capacity to respond to a set of factors that make the cells progress through the G1 phase and replicate. The factors include IL-6, hepatocyte growth factor (HGF), epidermal growth factor (EGF), tumor necrosis factor



$\alpha$  (TNF- $\alpha$ ), transforming growth factor-  $\alpha$ , insulin, and other receptor ligands that have been implicated in various stages of hepatocyte proliferation. These ligands, through complex molecular mechanisms, activate transcription factors including NF- $\kappa$ B, signal transducer and activator of transcription 3 (STAT3), activator protein 1 (AP-1), and CCAAT/ enhancer-binding protein (C/EBP) $\beta$  that initiate a cascade of gene expression that ultimately is responsible for proliferation (101, 105).

Cell cycle genes activated after PH include p53, mdm2, p21, cyclins and cyclin dependent kinases (106). The increased abundance of p21, an inhibitor of the cell cycle after growth stimulation by cyclin D1, reflects the characteristic feature of liver regeneration after partial hepatectomy that is, not only stimulators but also repressors are activated. Examples of cell cycle repressors activated after partial hepatectomy include TGF $\beta$ , activin, p21 and p53 (106). Perhaps it is the dual activation of stimulators and repressors that makes liver regeneration a precisely regulated growth process that never goes beyond its predicted end point.

The highly synchronized proliferation of more than 90% of remnant liver cells after PH not only provide an opportunity to study the cell cycle initiation and progression under *in vivo* conditions, but also gives an opportunity to study the role of different genes in different phases of cell cycle progression. Similarly, since telomere shortening affects the proliferative capacity of cells it is possible to identify the consequences of telomere shortening on cell cycle initiation and progression *in vivo* by using the liver regeneration system.

### **1.12 Telomere shortening in aging and disease**

The telomere hypothesis of cellular aging has fueled speculations whether telomere shortening impacts on the regenerative capacity of tissues and organs during aging and chronic disease. In line with this hypothesis a variety of studies have shown telomere shortening during aging in a variety of human tissues and organs including liver (107-112). In addition, it has been demonstrated that different chronic diseases which induce elevated rates of cell turnover also induce accelerated telomere shortening. One example is accelerated telomere shortening in chronic liver disease (111,113) especially at the cirrhosis stage (114). These studies indicated that the telomere hypothesis of cell aging might apply to the development of liver cirrhosis at the end of chronic liver disease. Further support for this hypothesis came from the observation that the p53/p21-pathway is activated in liver cirrhosis

(115). The p53/p21 pathway is the major signaling pathway mediating the replicative senescence stage in response to critical telomere shortening (see above). The observation of telomere shortening in chronic liver disease and cirrhosis is in accordance with the fact that cell turnover is elevated during this process (116) while telomerase is not active in human liver due to the lack of TERT-expression (117). Despite the evidence that telomere shortening might limit liver regeneration in humans it remains an open question whether telomere shortening is in fact affecting hepatocytes. Given the massive changes in organ architecture at the cirrhosis stage it remains a possibility that changes in telomere length at this stage would simply reflect differences in telomere length between different cell types.

### **1.13 The impact of telomere shortening on liver regeneration in telomerase deficient mice.**

Previous studies on liver regeneration in mTERC<sup>-/-</sup> mice gave the first experimental support for the telomere-hypothesis of cirrhosis formation (98). In these studies three different models of liver regeneration were analyzed: 1. Synchronized proliferation of hepatocytes in response to partial hepatectomy (PH), 2. Clonal expansion of hepatocytes in the model of acute liver failure in albumin-urokinase-plasminogen-activator transgenic mice, and 3. Continuous destruction and concomitant proliferation of hepatocytes in the carbon tetrachloride model of chronic liver damage. In all three model systems telomere shortening significantly impaired the regenerative capacity of the liver resulting in reduced survival in the model of acute liver failure and the development of premature liver cirrhosis in the model of chronic liver damage (98). Impaired liver regeneration correlated with an increased frequency of anaphase bridges (a prominent sign of telomere dysfunction) (118), with perturbed cell cycle progression during the G2/M stage of the cell cycle, and with an elevated rate of hepatocyte apoptosis (98). Interestingly the adenoviral mediated gene delivery of mTERC to the liver of mTERC<sup>-/-</sup> mice rescued telomere dysfunction, and the premature development of liver cirrhosis by re-activating telomerase (98). These data indicated that telomerase gene delivery can rescue cirrhosis formation which is induced by critical telomere shortening *in vivo*. But it is not known about the consequences of telomere shortening on the other stages of cell cycle.

### **1.14 Summary and the focus of present study**

Telomere shortening is prevalent during aging, chronic diseases of elevated cell turn over and appears to be an inevitable consequence in the absence of telomerase. From a variety

of studies it is clear that telomere shortening affects cell proliferation which in turn affects regeneration of tissues and organs. mTERC<sup>-/-</sup> mouse is an invaluable model system to study the consequences of telomere shortening *in vivo*. The DNA damage response pathways involving ATM, p53 and their downstream targets and their associated factors are known to be involved in telomere shortening induced replicative senescence.

A further understanding on the signaling and consequences of cellular senescence could lead to new therapeutic approaches to treat regenerative defects during aging and chronic diseases. Our study focussed on exploring the consequences of telomere shortening on cell cycle initiation and progression *in vivo* by analyzing liver regeneration in response to partial hepatectomy (PH) in late generation mTERC<sup>-/-</sup> mice and mTERC<sup>+/+</sup> control mice. The study focussed on the impact of telomere shortening at G1/S transition stage of regenerating liver cells and analysed the gene expression changes induced by telomere shortening at this cell cycle stage. In addition, we focused on the question whether telomere shortening induced replicative senescence signaling is constitutively operative at the same intensity irrespective of external factors or modulated by mitogen stimulation which induces a proliferative response.

## 2. Materials and Methods

### 2.1 Chemicals

<u>Chemical</u>	<u>Supplier</u>
Acetone	Merck
Agarose (Electrophoresis grade)	Gibco
Agarose (Sea Plaque)	Gibco
Ammonium acetate	AppliChem
Ammonium sulphate	Merck
Ampicillin	Sigma
ATP (adenosin tri-phosphate)	Sigma
Bacto-Tryptone	Gibco
BES (N,N-bis (2-Hydroxyethyl)-2 aminoethansulfonsyre)	Sigma
5'-bromo-2'-deoxyuridine (BrdU)	Sigma
Bromophenol blue	Serva
BSA (Bovine Serum Albumin)	Sigma
Calcium chloride	Merck
Chloroform	J.T.Baker
Citric acid	Merck
3, 3'-diaminobenzidine tetra-hydrochloride (DAB)	Amersham
Deionised water	Ampuwa
Dimethyl formamide (DMF)	Sigma
Diethyl pyrocarbonate (DEPC)	Sigma
Dimethyl sulfoxide (DMSO)	Sigma
dNTPs	Invitrogen
EDTA (N,N;N',N'-Ethylenediaminetetraacetate)	Merck
Ethanol	J.T.Baker

Ethidium bromide	Sigma
Eosin Y solution aqueous	Sigma
Ficoll	Sigma
Formaldehyde	Merck
Formamide	Merck
Glucose	Sigma
Glycerol	Serva
Glycine	AppliChem
Glutaraldehyde	Sigma
Hemalum solution	Merck
Hepes (2-(4-(2-Hydroxyethyl)-1-piperazinyl)ethansulfonate)	ICN
Hydrochloric acid	Merck
Hydrogen peroxide	Merck
Hygromycin	Sigma
Isopropanol	J.T. Baker
IPTG (Isopropyl-beta-D-thiogalactopyranoside)	Roth
Magnesium chloride	Merck
Magnesium sulphate	Merck
Mayer's Haematoxylin solution	Sigma
Methanol	J.T. Baker
MOPS (3-(N-Morpholin)propanesulfonate)	Sigma
Mounting medium for fluorescence	Vectashield
Mounting medium with DAPI	Vectashield
Paraformaldehyde	Merck
PBS (phosphate buffered saline)	Gibco
Potassium chloride	Merck

Potassium hexacyanoferrate (II)	Merck
Potassium hexacyanoferrate (III)	Merck
Propidium iodide	Sigma
RNA Clean	Hybaid
RNase Away	Roth
Roti-phenol/Chloroform	Roth
Sodium hydroxide	Merck
Sodium acetate	AppliChem
Sodium chloride	Merck
Sodium dodecylsulphate (SDS)	Sigma
Sodium fluoride	Merck
Sucrose	Merck
SYBR Green	Sigma
Tris (Tris-(hydroxymethyl)-aminomethane)	AppliChem
Triton-X-100	Sigma
Tryptose phosphate broth	Gibco
Tween 20	Sigma
X-gal (5-Bromo 4-chloro 3-indolyl- beta-D-galactopyranoside)	Roth

## 2.2 Radioactive material

<sup>32</sup> P-γ-ATP	Amersham
-----------------------	----------

## 2.3 Molecular markers

### 2.3.1 DNA-Markers

100 bp-ladder	New England biolabs
1 kb-ladder	Life technologies
High molecular weight marker	Life technologies

### 2.3.2 RNA-Markers

RNA ladder (RNAI)	Roche
-------------------	-------

### 2.4 Enzymes

Collagenase	Sigma
Dispase	Sigma
DNase I, RNase-free	Boehringer, Mannheim
Hot star Taq polymerase	Qiagen
Lysozyme	Sigma
Proteinase K	Invitrogen
Pepsin	Sigma
Restriction Endonucleases	New England, Biolabs
RNase A	Sigma
Superscript II-RT	Invitrogen
T4 DNA ligase	Invitrogen
T4-Kinase (Polynucleotide-Kinase)	New England, Biolabs
Taq DNA polymerase	Qiagen

### 2.5 Antibodies

Anti-mouse-BrdU Antibody	Amersham
Anti-BrdU-FITC Antibody	Beckton Dickinson
FITC-conjugated goat anti-mouse IgG	Dako
Peroxidase anti-mouse IgG2a	Amersham

### 2.6 Tissue Culture Reagents

DMEM with Glutamax-1	Gibco
Foetal Bovine Serum (FBS)	Gibco
Trypsine/EDTA solution	Biochrom
Pencillin/Streptomycine	Biochrom

### 2.7 Oligonucleotides

All the oligonucleotides were purchased from MWG Biotech. (NC, USA).

Gene	Primer-pairs
Mouse-Nucb2	*5'-TTTGAACACCTGAACCACCA-3' **5'-CCGGTCATATTGCTCCAGAT-3'
Mouse-Prkri	*5'-CCGACCTCACCAAAGTGATT-3' **5'-TTCGTCAAGCTTCCCTTGTT-3'
Mouse-Plk	*5'-CTTCCTGAACGAGGATCTGG-3' **5'-AGGAGTGCCACACAAGGTCT-3'
Mouse-P21	*5'-TTGTGCTGTCTTGCACCTCT-3' **5'-AATCTGTCAGGCTGGTCTGC-3'
Mouse-Gadd45g	*5'-GGACCCTGACAATGTGACCT-3' **5'-AGCAGAACGCCTGAATCAAC-3'
Mouse-Faf1	*5'-GGAGCAGATTCGCAAAGAAC-3' **5'-CAGGCTCAGCATTTTCTTCC-3'
Mouse-Wee1	*5'-AACGGGCACTCTTCACAGAT-3' **5'-GCTGACAGAGCGGTTTCATTT-3'
Mouse-Klf4	*5'-ATGCAGTCACAAGTCCCCTC-3' **5'-GACCTTCTTCCCCTCTTTGG-3'
Mouse-p16	*5'-TCTGCTCAACTACGGTGCAG-3' **5'-CACCAGCGTGTCCAGGAAG-3'
Mouse-ARF	*5'-GCTCTGGCTTTCGTGAACAT-3' **5'-GTGAACGTTGCCCATCATC-3'
Mouse-rsp9	*5'-CTGGACGAGGGCAAGATGAAGC-3' **5'-TGACGTTGGCGGATGAGCACA-3'
Human-P21	*5'-GCGACTGTGATGCGCTAAT-3' **5'-GTCACCCTCCAGTGGTGTCT-3'
Human-P16	*5'-ACCAGAGGCAGTAACCATGC-3' **5'-AAGTTTCCCGAGGTTTCTCA-3'
Human-ARF	*5'-CCAGGTGGGTAGAAGGTCTG-3' **5'-GAGAATCGAAGCGCTACCTG-3'
Human-β-actin	*5'-GGACTTCGAGCAAGAGATGG-3' **5'-AGGAAGGAAGGCTGGAAGAG-3'

\* Forward primer \*\*Reverse primer

Telomere probe Cy3-OO-(CCCTAA)<sub>3</sub>

Applied Biosystems

Oligo dT (TTTTTT)<sub>3</sub> primer

MWG Biotech.

Salmon Sperm DNA

Amersham

## 2.8 Kits

Cell proliferation kit

Amersham

Gel extraction kit

Qiagen

*In situ* cell death detection kit, Fluorescein

Roche

Nucleotide removal kit

Qiagen

Opt EIA set: Mouse IL-6

Pharmingen

PGEM-T-Easy vector kit

Promega



Plasmid mini kit	Qiagen
Plasmid maxi kit	Qiagen

## 2.9 Other materials

High density oligonucleotide chips	Affymetrix
Bacterial Culture plates	Greiner
Cell culture dishes (10cm)	Greiner
Cell culture flasks (250ml)	Cell star
Culture plates (6 well)	Cell star
Centrifuge-Tubes, Ultra-Clear™	Beckman
Centrifuge tubes, sterile (10 ml)	Sarstedt
Centrifuge tubes, sterile (50 ml)	Sarstedt
FACS tubes	Falcon
Film cassettes	Kodak
Freezing vials	Nunc
PCR soft tubes	Biozym
Tissue Homogenizer	Braun
3 MM Filter paper	Whatman

## 2.10 Laboratory equipment

Gene-chip scanner	Affymetrix
Agilent Technologies 2100 Bioanalyzer	Agilent Technologies
Cell culture incubator	Heraeus
Cell culture laminar flow bench	Heraeus
Cryostat Microm HM 500 OM	Omega
Desktop centrifuge	Eppendorf
Elektrophoresis-Apparatus	Labtech, Pharmacia Biotech
FACS (FACScan)	Beckton Dickinson
Fluorescence microscope	Olympus
Gel doc	Biorad
Heat block	Eppendorf
Microscope	Olympus
Microscope equipped camera	Sony
Power-Supply	Biometra

PCR master cycler	Eppendorf
ABI prism 7700 Sequence detection system	PE applied Biosystems
Spectrophotometer	Contron
Ti-70-Rotor und SW 28.1-Swinging-Bucket-Rotor	Beckman
Ultra centrifuge	Beckman
Vortex	Omnilab

## 2.11 Mice

Ten to twelve weeks old male G3 mTERC<sup>-/-</sup> and littermate mTERC<sup>+/+</sup> (C57BL/6J strain) control mice were used for the *in vivo* experiments. Late generation mTERC<sup>-/-</sup> mice were obtained by crossing successive generations of mTERC<sup>-/-</sup> until third generation (G3) (94). The mice were bred and maintained in the animal facility, Medical School, Hannover, on a standard diet and in 12 hrs of light-dark periods.

## 2.12 DNA Extraction and Genotyping

mTERC<sup>+/+</sup>, mTERC<sup>-/-</sup> and mTERC<sup>+/-</sup> mice were identified from the mouse colony by PCR amplification method. The DNA was extracted from the mice tails by standard Phenol-Chloroform method. In brief, a small piece of tissue was cut from the tip of the mouse tail and digested in 500µl of lysis buffer (10mM NaCl + 10mM Tris-HCl (pH8.0) + 25mM EDTA pH8.0 + 0.5% SDS, 10ml of this buffer and 64µl of proteinase K) overnight with continuous shaking at 56°C. Then 1 ml of phenol/chloroform was added and continuously but gently shaken for 1 min at room temperature and centrifuged at 10,000 rpm for 5 min. The supernatant was collected and 1ml of chloroform was added and continuously shaken for 10 min at room temperature and centrifuged for 5 min at 10,000 rpm. To the supernatant 1 ml of iso-propanol was added (DNA precipitation) and gently shaken by inverting the eppendorf for 1 min and then centrifuged at 13,000 rpm for 10 min. The supernatant was discarded and the DNA pellet was washed twice with 70% ethanol and centrifuged at 13,000 rpm for 5 min. The DNA pellet was air dried for 5 min and dissolved in 50µl of TE buffer (10mM Tris-HCl (pH7.6), 1mM EDTA). Primer pairs and the reaction conditions used for genotyping are as follows: mTRR-5'-TTCTGACCACCACCTACTTCAAT-3', 5ppgK-5'-GGGGC TGCTAAAGCGCAT-3', mTRwtF-5' CTAAGCCGGCACTCCTTACAAG-3'. (1µg of DNA + 2.5µl 10X PCR buffer + 1.5µl 3mM MgCl<sub>2</sub> + 0.5µl dNTP's + 1.0 µl mTRR primer (10 pmol) + 1.0µl 5ppgK primer (10 pmol) + 1.0 µl mTRwtF primer (10 pmol) + 0.25µl Taq DNA polymerase + 15.25µl dH<sub>2</sub>O). The PCR cycle profile is as follows: initial denaturation

at 94°C for 30 sec, annealing at 55°C for 30 sec, and extension at 72°C for 30 sec. Thirty cycles of PCR amplification were performed and the PCR products were run on 2% agarose gel and visualized with ethidium bromide (25µl of 1mg/ml conc. for 100 ml of agarose gel). The primers amplify a fragment of 250bp for mTERC<sup>+/+</sup> and 180bp for mTERC<sup>-/-</sup> and both the fragments for mTERC<sup>+/-</sup>.

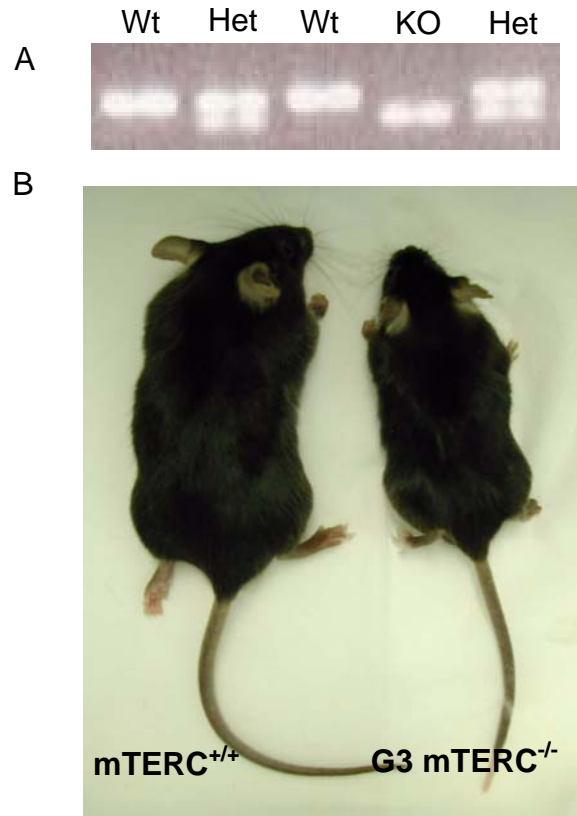


**Figure 2.12.1 (A)** Representative agarose gel electrophoresis photograph showing the positions of PCR products stained with ethidium bromide which indicate the genotype of the mice. A single band of 250bp represents wild type mouse where as two bands one at 250bp and second one at 180bp position represents the heterozygous and a single band at 180bp position represents the mTERC<sup>-/-</sup> knock-out mouse. **(B)** Photograph of wild type (mTERC<sup>+/+</sup>) and G3 mTERC<sup>-/-</sup> mice of 3 months old. Note: G3 mTERC<sup>-/-</sup> mouse is of smaller size compared to litter mate age matched mTERC<sup>+/+</sup> mice.

### 2.13 Partial hepatectomy and *in vivo* BrdU labeling

The mice were operated under sterile conditions in the early hours of the day between 8.00 and 11.00A.M., according to the protocol of Higgins and Anderson (119). Mice were anesthetized intraperitoneally (10µl/gm body weight of mouse) (1.9ml ketanest + 100µl Rompum + 3ml NaCl) and were subjected to 70% partial hepatectomy (PH), the left lateral, left median and right median lobes were separately isolated and then removed with a single

ligature. Care was taken to avoid disruption of the portal vein, biliary tract, and gallbladder. All animals resumed normal activities promptly after recovering from anesthesia. After 2 hours of BrdU pulse labeling mice were sacrificed at 24 (n=3), 30 (n=5), 32 (n=5), 36 (n=5), 48 (n=5), 72 (n=5), 96 (n=5) and 120 (n=3) hrs after PH. For BrdU pulse labeling 10 $\mu$ l/gm body weight labeling reagent (10:1 ratio, 5-bromo-2-deoxyuridine and 5-fluoro-2-deoxyuridine, Cell proliferation kit, Amersham) was administered 2 hrs before sacrifice. For continuous BrdU labeling (n=5) 0.8 mg/ml BrdU (Sigma) was given in sterile drinking water and fresh water was made after every 24 hours (Tough DF and Sprent J, 1994). To increase the sensitivity of the continuous BrdU labeling procedure 200 $\mu$ L of 1mg/ml BrdU in PBS were administered intra-peritoneally in 12 hr intervals between 24-72 (or 120) hrs after PH. After sacrifice of the mice the liver lobes were snap-frozen in liquid nitrogen and stored at -80°C until further use.

#### **2.14 Immuno-histochemical detection of BrdU**

7  $\mu$ m thick cryostat-sections were fixed in Ice-cold acetone-methanol (1:1) for 10 min followed by two 5 min washes in TBS-Tween (20mM Tris-HCl, 137mM NaCl, 0.1% Tween20, pH 7.6). The tissues were dehydrated in 70% ethanol for 30 min and air dried for about 30 min at room temperature. The endogenous peroxidase activity was blocked by incubating the slides in 3% H<sub>2</sub>O<sub>2</sub> in methanol for 10 min followed by two 5 min washes in TBS-Tween. Denaturation of cellular DNA was done by immersing the slides in alkaline formamide (95ml formamide / 5ml 1N NaOH) for 30 sec at 70°C followed by one 5 min wash in TBS-Tween at 70°C followed by incubation in 15mM tri-sodium citrate in formamide for 15 min at 70°C. The reaction was stopped by washing the slides in Ice-cold TBS-Tween twice, each wash for 5 min. A second fixation was carried out in 3% formaldehyde in PBS for 30 min followed by two 5 min washes in TBS-Tween followed by incubation in 0.2% glutaraldehyde in PBS for 10 min at room temperature. Then the slides were washed twice each wash for 5 min in TBS-Tween and incubated with anti-5-bromo-2'-deoxyuridine monoclonal antibody (Amersham) for over night at 4°C in a wet chamber. Then the slides were washed in TBS-Tween twice each wash for 5 min and incubated with peroxidase anti-mouse IgG2a secondary antibody for 30 min at room temperature followed by three 5 min washes in TBS-Tween. The detection was done by incubating them with the substrate 3, 3'-diaminobenzidine tetrahydrochloride (25mg DAB / 100 $\mu$ L substrate intensifier / 50ml PBS), for 20 min followed by two washes each wash for 5 min with double distilled water. Then the slides were counterstained with hemalum solution and mounted with mounting medium and

stored in dark until further analysis. A BrdU labeling index was determined by counting the number of BrdU positive cells randomly in 20 low power magnification fields (10X) and expressing the number of BrdU labeled nuclei as a percent of all nuclei counted.

### **2.15 Hematoxylin and Eosin (H&E) staining**

7µm thick cryostat sections were prepared from paraffin embedded liver tissue samples. The sections were de-paraffinized by incubating them in xylene solution 3x5 min. Then the sections were fixed in acetone for 2 min on ice followed by rehydration by incubating them consequently in 100%, 90% and 70% ethanol and finally in dH<sub>2</sub>O each 3 min. Then the slides were incubated in fresh hematoxylin for 15 min followed by washing with dH<sub>2</sub>O for 20 min. Then the slides were incubated with freshly prepared Eosin solution (which was acidified with acetic acid) for 1 min. Then the slides were washed with dH<sub>2</sub>O for 5 min followed by dehydration in 90% ethanol followed by 100% ethanol each 3 min. Finally the slides were air dried for 5 min and mounted with mounting medium.

### **2.16 Senescence Associated β-gal Staining**

Senescence-associated β-gal staining was carried out as described previously (72). In brief, 7µm cryostat sections were fixed in 3% formaldehyde for 5 min, followed by three washes in PBS at room temperature. The slides were incubated in freshly prepared SA- β-gal staining solution (1mg/ml of 5-bromo-4-chloro-3-indolyl β-D-galactoside (X-gal) in DMF / 40mM citric acid/sodium phosphate (pH 6.0) / 5mM potassium ferrocyanide / 5mM potassium ferricyanide / 150mM NaCl / 2mM MgCl<sub>2</sub>) at 37°C for over night. The stained sections were washed twice with PBS and counter-stained for 30 sec with eosin. The excess counter-stain was removed by two washes in PBS. All the samples were stained in triplicates. Analysis was done in blinded fashion. The number of SA-β-gal positive cells was counted randomly in 20 low power fields (10X) and expressed the number of positive cells as a percent of all cells counted.

### **2.17 BrdU and Telomere probe co-staining**

To combine BrdU staining with telomere probe Cy3-OO-(CCCTAA)<sub>3</sub> hybridization, 7 µm thick cryostat-sections were fixed in Ice-cold acetone-methanol (1:1) for 10 min followed by two 5 min washes in TBS-Tween (pH 7.6). The tissues were dehydrated in 70% ethanol for 30 min and air dried for about 30 min at room temperature. The endogenous peroxidase activity was blocked by incubating the slides in 3% H<sub>2</sub>O<sub>2</sub> in methanol for 10 min followed by

two 5 min washes in TBS-Tween. Denaturation of cellular DNA was done by immersing the slides in alkaline formamide (95ml formamide / 5ml 1N NaOH) for 30 sec at 70°C followed by one 5 min wash in TBS-Tween at 70°C followed by incubation in 15mM tri-sodium citrate in formamide for 15 min at 70°C. The reaction was stopped by washing the slides in Ice-cold TBS-Tween twice, each wash for 5 min. A second fixation was carried out in 3% formaldehyde in PBS for 30 min followed by two 5 min washes in TBS-Tween. Then the tissues were digested with acidified pepsin (100mg pepsin / 100ml H<sub>2</sub>O / 84μL conc. HCl) for 10 min followed by two 5 min washes in TBS-Tween. Then they were fixed by incubating in 0.2% glutaraldehyde in PBS for 10 min at room temperature. Then the slides were co-incubated with anti-5-bromo-2'-deoxyuridine monoclonal antibody (Amersham) and telomere probe hybridization mix [250μl final volume: 2.5μl 1M Tris-Cl, pH 7.2 / 21.4μl MgCl<sub>2</sub> (25mM MgCl<sub>2</sub> / 9mM citric acid / 82mM Na<sub>2</sub>HPO<sub>4</sub>, pH7.4) / 175μl de-ionized formamide / 12.5μl 10% (w/w) blocking reagent / 5μl 25μg/ml PNA Cy3-telomere probe / 33.6μL H<sub>2</sub>O] for over night at 4°C in a wet chamber. Then they were washed in TBS-Tween thrice each wash for 5 min and incubated with FITC-conjugated goat anti-mouse IgG secondary antibody (DAKO) for 30 min at room temperature followed by three 5 min washes in TBS-Tween. Then the slides were air dried for 10 min and mounted with 1:1 (v:v) mixed mounting solution with/without DAPI and stored in dark at 4°C until further analysis. The liver samples of the mice which were administered BrdU continuously until 120hrs were used for this double staining. Five samples from each group (mTERC<sup>+/+</sup> and G3mTERC<sup>-/-</sup>) were stained and analyzed at the same time. The quantification of the telomere fluorescence intensity was performed using TFL-TELO V1.0, a telomere analysis program developed by P.Landsdorp.

### 2.18 SA- β-gal -BrdU co-staining

For simultaneous detection of senescence and cell proliferation in the same sample, first SA-β gal staining at pH 6 was done (described above, 2.16) on 7μm sections of liver samples from mTERC<sup>+/+</sup> (n=5) and G3mTERC<sup>-/-</sup> (n=5) followed by BrdU staining as described above.

### 2.19 SA- β-gal -Telomere probe co-staining

To measure the telomere lengths in senescent cells and proliferating cells in the same sample first SA-β gal staining was carried out (described before, 2.16) followed by telomere probe hybridization (described above, 2.17) except that the pepsin digestion step is optimized

to 7 minutes to detect cytoplasmic senescent staining and at the same time to minimize background for telomere fluorescence intensity measurement.

## 2.20 Q-FISH on inter-phase nuclei of isolated hepatocytes

In situ Q-FISH on interphase nuclei of liver cells was performed as described previously (120). The tissue sections were fixed in 4% paraformaldehyde in PBS. After three washes in PBS, a second fixation was carried out in 4% formaldehyde for 10 min at room temperature, followed by enzymatic unmasking of the sections for 10 minutes at 37°C (enzyme mix: 100mg pepsin/ 50 mg collagenase / 100mg dispase / 84µl concentrated HCl / 100ml water). Fixation and washing steps were repeated as described, followed by dehydration of the slides. After 3 minutes of denaturation at 80°C, the slides were incubated with hybridization mix: (125µl final volume): 2.5µl 1 M Tris-Cl, pH 7.2 / 21.4µl MgCl<sub>2</sub> [25 mM MgCl<sub>2</sub> / 9mM citric acid / 8.2 mM NaH<sub>2</sub>PO<sub>4</sub>, pH7.4] / 175µl de-ionized formamide / 12.5µl 10% (w/w) blocking reagent / 5µl 25µg / ml PNA Cy3-telomere probe). The slides were washed twice in washing solution I (100ml final volume: 70ml formamide / 1ml 1M Tris-Cl, pH7.2 / 1ml 10% BSA / 28ml dH<sub>2</sub>O), followed by three washes in washing solution II (15ml 1M Tris-Cl, pH 7.2 / 15ml 1.5 M NaCl / 120µl Tween 20 (0.08% final) / 120ml H<sub>2</sub>O). After dehydration, the slides were mounted with 1:1 (v:v) mixed mounting solution with/without DAPI. Pictures were taken at an exposure time of 1.5 seconds for the Cy3 images and at 0.5 seconds for DAPI.

## 2.21 Apoptotic TUNNEL assay

The TUNNEL assay was performed on cryostat sections of frozen liver samples according to manufacturer protocol (In Situ cell death detection kit, Roche). In brief 7µm cryostat sections were fixed in 4% para-formaldehyde in PBS, pH 7.4 for 20minutes at room temperature followed by two 15 minute washes with PBS. Then the tissue sections were incubated in permeabilization solution (0.1% Triton X-100 in 0.1% sodium citrate) for 5 minutes on ice followed by 5minute wash with PBS. 50µL of tunnel reaction mix was applied directly on the top of the sections and incubated for 1 hour in a humidified chamber at 37°C. Then the slides were rinsed 3x1min in PBS and mounted with 1:1 (v:v) mixed mounting solution with/without DAPI and analyzed under fluorescent microscope. The number of apoptotic cells was counted in 20 high power fields (100X). All the counts were performed without knowledge of the day(s) after partial hepatectomy.

## 2.22 Determination of IL-6 serum levels

Blood-sera were obtained from mice at 1, 3, 6, 9 and 12 hrs after partial hepatectomy and stored at -80°C before testing. Serum IL-6 levels were determined using Pharmingen OptEIA™ Set: Mouse IL-6 kit according to manufacturer protocol. In brief, the micro-wells of 96 well plate were coated with 100µl per well with capture antibody diluted in coating buffer (0.1M carbonate buffer, pH 9.5). Then the plate was sealed with paraffin and incubated at 4°C over night with gentle shaking. Then the wells were aspirated and washed 3 times with 300µl wash buffer per well (PBS with 0.05% Tween 20). After the last wash the plate was inverted and blotted on to absorbent paper to remove any residual buffer. Then the wells were blocked with 200µl assay diluent per well and incubated at room temperature for 1 hr. The wells were aspirated and washed 3 times with 300µl of wash buffer. The standards and different dilutions of the samples were prepared and 100µl of each standard and sample were pipetted into appropriate well, sealed and incubated at room temperature for 2 hrs. The wells were aspirated and washed 5 times with 300µl of wash buffer. Then 100µl of working detector (detection antibody + Avidin-HRP) was added to each well, sealed and incubated for 1 hr at room temperature. The wells were aspirated and washed 7 times with 300µl of wash buffer each wash 30 sec. Then 100µl of substrate solution was added to each well and the plate was incubated for 30 min at room temperature in the dark. Then the reaction was stopped by adding 50µl of stop solution (1M H<sub>3</sub>PO<sub>4</sub> or 2N H<sub>2</sub>SO<sub>4</sub>). The absorbance was read at 450nm within 30 min after termination of the reaction.

## 2.23 RNA extraction and cDNA synthesis

The total RNA was extracted from the liver tissue and from the *in vitro* cultured cells according to manufacturer protocol (RNA Clean™, Hybaid). Briefly, the frozen liver tissue was homogenized with RNA Clean™ (2ml per 100mg tissue) in a glass-teflon homogenizer. 200µL of chloroform was mixed per 2ml of homogenate and shaken vigorously for 15 sec. and incubated on ice for 5min. The samples were centrifuged at 12,000xg at 4°C and the upper aqueous phase was carefully transferred to a fresh tube and an equal volume of iso-propanol was mixed to precipitate RNA and incubated for 15 min at -20°C. Then it was centrifuged for 15 min at 12,000xg at 4°C and the supernatant was discarded without disturbing the RNA pellet. The RNA pellet was washed with 70% ethanol and vortexed for few seconds and centrifuged for 8min at 7,500xg. The washing step was repeated once again. The RNA pellet was dried under vacuum for 10 min and dissolved in suitable volume of



RNAase free DEPC water. The quality of the RNA was checked on a denaturing agarose gel [(1.2gms agarose, 5 ml 20X MOPs buffer (400mM MOPs + 50mM sodium acetate + 10mM EDTA, pH 7.0 + 95ml dH<sub>2</sub>O, boiled and cooled to 50°C and 1.8 ml of 37% formaldehyde and 2 µl of 1mg/ml ethidium bromide were added] and run in the running buffer (50 ml 20X MOPs+20 ml 37% formaldehyde+930 ml dH<sub>2</sub>O). The concentration of the RNA was determined by spectrophotometer at 260nm (OD<sub>260</sub>). The RNA samples having an OD<sub>260/280</sub> ratio of 2 or more were used for micro-array analysis, cDNA synthesis and Quantitative Real Time PCR. 2µg total RNA was used to synthesize cDNA with oligo-dT primer and Superscript II-RT enzyme (invitrogen). The RT reaction was checked by amplifying a 130bp fragment of the house keeping genes RSP9 of mouse and β-actin of human.

## **2.24 High density oligonucleotide microarray hybridization and analysis**

Quality and integrity of the total RNA isolated from liver samples was checked by running all the samples on an Agilent Technologies 2100 Bioanalyzer (Agilent Technologies). Preparation of the biotinylated RNA probe was done as described (Affymetrix GeneChip Expression Analysis Manual, Affymetrix). Briefly, 5 µg total RNA was reverse transcribed to cDNA using 100 pmol of a T7T23V primer (Eurogentec; Seraing, Belgium) containing a T7 promotor. The concentration of biotin-labeled cRNA was determined by UV absorbance. In all cases, 12.5 µg of each biotinylated cRNA preparation were fragmented and placed in a hybridization cocktail containing four biotinylated hybridization controls (BioB, BioC, BioD, and Cre) as recommended by the manufacturer. Samples were hybridized to an identical lot of Affymetrix MG-U74Av2 for 16 hours. After hybridization the GeneChips were washed, stained with SA-PE and read using an Affymetrix GeneChip fluidic station and scanner.

Analysis of microarray data was performed using the Affymetrix Microarray Suite 5.0, Affymetrix MicroDB 3.0 and Affymetrix Data Mining Tool 3.0 at the Array facility of the German Research Center for Biotechnology, GBF, Braunschweig, Germany. All array experiments were scaled to a target intensity of 150, otherwise using the default values of the Microarray suite. Filtering of the results was done as follows: Genes are considered as regulated when their fold change is greater than or equal to 2 or less than or equal to 2, the statistical parameter for a significant change is less than 0.001 (change p-Value for changes called increased (I)) or greater than 0.999 (change p-Value for changes called decreased (D)). Additionally, the signal difference of a certain gene should be greater than 100.

### 2.25 Liver perfusion, nuclei preparation and flow cytometry

Liver cells were collected by collagenase perfusion method. The cells were collected from the quiescent liver (non-operated) (n=5), 48hours (n=6) and 96hours (n=5) after PH from each group (mTERC<sup>+/+</sup> and G3 mTERC<sup>-/-</sup>). Mice were anesthetized and subjected to 70% partial hepatectomy and 10 $\mu$ L/gm body weight labeling reagent (10:1 ratio, 5-bromo-2-deoxyuridine and 5-fluoro-20-deoxyuridine, (Cell proliferation kit, Amersham) was administered 2 hours before liver perfusion. The abdomen of the mouse was wide opened and the liver was perfused through the portal vein by inserting SURFLO I.V catheter connected to ISMATEC pump with KRBI buffer (150mM NaCl, 5mM KCl, 5mM glucose, 25mM NaHCO<sub>3</sub>, 20mM HEPES, 1mM EDTA, pH 7.4) until the blood is completely drained-out followed by KRBII (150mM NaCl, 5mM KCl, 5mM glucose, 25mM NaHCO<sub>3</sub>, 20mM HEPES, 0.5mM CaCl<sub>2</sub>, 0.5mg/ml of collagenase) until the liver mass becomes soft and fragile. The above two buffers were kept at 37° C during the perfusion. Then the liver mass is suspended in 10ml of PBS and the single cell suspension was achieved by gentle pipeting. Then it is centrifuged at 50 x g for 3 minutes and the pellet which contains >90% hepatocytes was collected for nuclei preparation.

1 x 10<sup>6</sup> cells were suspended gently for 2 minutes without producing air bubbles in 2 ml of NPBT buffer (10mM TrisCl pH 7.4, 2mM MgCl<sub>2</sub>, 140mM NaCl, 0.5% Triton-X-100) and centrifuged through a 50% sucrose gradient (50% sucrose in NPB, 10mM TrisCl pH 7.4, 2mM MgCl<sub>2</sub>, 140mM NaCl) for 10 minutes at 13000 rpm. The nuclear pellet was re-suspended in suitable volume of PBS and again centrifuged at 50 x g for 2 minutes to remove non-lysed cells. The pure nuclei obtained from this procedure were used for flow cytometry.

### 2.26 Propidium iodide (PI) staining for FACS analysis

The isolated nuclei were re-suspended in 1ml of 1% BSA in PBS and centrifuged at 500x for 15 min at room temperature and the pellet was re-suspended in 200 $\mu$ l of PBS and then fixed in 5 ml of ice-cold 70% ethanol by adding ethanol drop by drop while vortexing and then incubated on ice for 30 min. Then the cells were centrifuged at 500x for 10 min at 4°C and the supernatant was aspirated and the pellet was re-suspended in 1 ml of 2N HCl + 0.5% Triton-X100 (17.2 ml of Conc. HCl and 0.5 ml of Triton-X100 in 82.3 ml of H<sub>2</sub>O) at room temperature for 30 min and then centrifuged at 500x for 10 min and the supernatant was

aspirated and the pellet was re-suspended in 1 ml of 0.1M NaB<sub>4</sub>O<sub>7</sub>, pH 8.5 and then centrifuged at 500x for 10 min and re-suspended in 1ml of 0.5% Tween-20/1% BSA/PBS and the cell concentration was adjusted to achieve 1 x 10<sup>6</sup> cells/test. Then it is centrifuged at 500x for 10 min and re-suspended in 0.5 ml of PBS + 5 µg (final conc.) of PI + 10 µl of 10 mg/ml RNase A.

### **2.27 Anti-BrdU (FITC) -PI double staining for FACS analysis**

The isolated nuclei were re-suspended in 1ml of 1% BSA in PBS and centrifuged at 500x for 15 min at room temperature and the pellet was re-suspended in 200µl of PBS and then fixed in 5 ml of ice-cold 70% ethanol by adding ethanol drop by drop while vortexing and then incubated on ice for 30 minutes. Then the cells were centrifuged at 500x for 10 min at 4°C and the supernatant was aspirated and the pellet was re-suspended in 1 ml of 2N HCl + 0.5% Triton-X100 (17.2 ml of Conc. HCl and 0.5 ml of Triton-X100 in 82.3 ml of H<sub>2</sub>O) at room temperature for 30 min and then centrifuged at 500x for 10 min and the supernatant was aspirated and the pellet was re-suspended in 1 ml of 0.1M NaB<sub>4</sub>O<sub>7</sub>, pH 8.5 and then centrifuged at 500x for 10 min and re-suspended in 1ml of 0.5% Tween-20/1% BSA/PBS and the cell concentration was adjusted to achieve 1 x 10<sup>6</sup> cells/test. Then the cells were incubated with 20µl of Anti-BrdU-FITC (Becton Dickinson) for 30 min per 10<sup>6</sup> cells at room temperature and then washed once in 1 ml of 0.5% Tween-20/1%BSA/PBS and centrifuged at 500x for 10 min and re-suspended in 0.5 ml of PBS + 5 µg (final conc.) of PI + 10 µl of 10 mg/ml RNase A. The nuclei collected from 0 hours and 21 days after PH were stained with only PI where as the nuclei from 48hrs and 96hrs after PH were double stained with PI and FITC-antiBrdU antibody (Becton Dickinson) as recommended by the manufacturer. Flow cytometric analysis was carried out with FACScan (Becton Dickinson) equipped with Cellquest software.

### **2.28 Quantitative real time PCR**

Quantitative real-time PCR was performed on ABI Prism 7700 Sequence detection system (PE Applied Biosystems) by using SYBR Green I (Sigma S9430) as a double-strand DNA-specific binding dye. Same RNA preparations from mice were used for micro-array analysis and quantitative RT-PCR. All the samples were analysed in triplicates and the expression was confirmed by three independent PCR runs. The cycle profile of PCR is as follows: An initial 10 min activation of Hot Star Taq<sup>TM</sup> DNA polymerase (Qiagen) at 95°C followed by denaturation at 94°C for 15 sec, annealing at 54°C for 15 sec, and extension at

72°C for 30 sec. 45 cycles of PCR amplification were performed to confirm the expression level and the house keeping gene RSP9 was used as an internal control for mouse and  $\beta$ -actin for primary human fibroblasts to normalize the expression levels. As SYBR Green I is not specific for the PCR product and binds to primer dimers formed non-specifically during all PCR reactions, optimum temperature for analysis of specific product was obtained after amplification by raising the temperature successively through 0.5°C steps and comparing the melting temperature of specific product with non-specific product obtained from a non-template control (NTC). The optimum temperature determined from melting point analysis was then used for quantitative PCR. The quantification data were analyzed with the ABI Prism 7700 analysis software. In all experiments the threshold value used to determine  $C_t$  during analysis was kept constant. For each primer pair the linearity of detection was confirmed to have a correlation coefficient of at least 0.98 over the detection area by measuring a fourfold dilution curve with cDNA prepared from liver samples and from primary cells. Fold difference was therefore calculated assuming 100% efficient PCR where each  $C_t$  was normalized to the house keeping gene RSP9 or  $\beta$ -actin expression. The results are shown as mean  $\pm$  SD for three different PCR reactions.

### **2.29 Cell culture**

Human fetal lung fibroblasts (IMR 90), human embryo lung fibroblasts (WI38) and human adult fibroblasts (HK1) were cultured in DMEM medium (Gibco) supplemented with 10% FBS (Sigma) and 1% penicillin / streptomycin in a CO<sub>2</sub> incubator (5% CO<sub>2</sub> and 20% O<sub>2</sub>) at 37°C. Cells were passaged serially in vitro and early passage and late passage cultures were used for this study. For experiments involving serum starvation and stimulation, cells were collected by trypsinization from serially passaged cultures of early and late passages and cultured in DMEM medium with 0.1% FBS for 120 hours and stimulated with 10% FBS in DMEM medium for 6, 12 and 24 hours. For drug (PD098059) inhibition studies cells were cultured in 0.1% FBS for 120 hours and incubated with 10 $\mu$ M final concentration of PD098059 1 hour before serum stimulation.

### **2.30 Retrovirus preparation and infection**

The onyx cells (packaging cell line) were cultured in DMEM medium with 10% FBS and were transfected with vector DNA (pBABEhygro-hTERT) by calcium phosphate transfection (20  $\mu$ g of plasmid DNA+125  $\mu$ l of 1M CaCl<sub>2</sub> with a final volume of 500  $\mu$ l was bubbled into 500 $\mu$ l of 2X HBS (280mM NaCl, 10mM KCl, 1.5mM Na<sub>2</sub>HPO<sub>4</sub>.2H<sub>2</sub>O, 50mM

HEPES, pH 7.5). The medium was changed after 12 hours and 5 ml of fresh medium was given. After 24 hrs the medium was filtered through 0.45µm filter and 5µl of polybrene was mixed and the primary fibroblasts were infected with this medium. Second round of infection was done exactly like before, after 48 hours. Then the successfully infected cells were selected with hygromycin (80µg/ml) for one week. Fresh medium with drug was given after every 24 hrs. After one week the cells resistant to hygromycin were cultured in DMEM medium without drug.

### **2.31 Cloning using the pGEMT-Easy vector**

Cloning of desired amplified full length cDNAs into pGEMT-Easy vector was done according to manufacturer protocol (Promega). The ligation reaction was set up by mixing 5µl 2X rapid ligation buffer, 1µl pGEMT-Easy vector, 1µl of PCR product, 1µl of T4 DNA Ligase and 2µl of dH<sub>2</sub>O. The contents were mixed and incubated for 2 hrs at room temperature. Then the ligation reaction tubes were briefly centrifuged to collect the contents at the bottom. Then 50µl high efficiency competent bacterial cells (JM 109, promega) were transformed with 2µl of the above reaction mix and incubated on ice for 20 min followed by a heat shock at 42°C for 1 min. Then the tubes were immediately transferred to ice for 5 min. Then 950µl of LB broth medium was added and incubated at 37°C for 2 hrs with shaking at 150 rpm in an orbital shaker. 100µl of transformation culture was plated onto duplicate LB/ampicillin/IPTG/X-gal plates. Then the plates were incubated overnight (14-16 hrs) at 37°C. This system facilitates blue/white screening, and white colonies generally contain inserts.

### **2.32 In-gel southern blotting for TRF (Telomere Restriction Fragment) length analysis**

Genomic DNA was extracted by phenol-chloroform method as described above (2.12). The DNA was rehydrated in TE buffer and an aliquot of undigested DNA was run in an agarose gel to check for DNA degradation. Only samples without any visible degradation were used for the assay. 15µg of total DNA was digested overnight at 37°C (with 3µl of HinfI + 12 µl of RsaI + 15µl NEB2 buffer with a final volume of 150µl with ddH<sub>2</sub>O). Complete digestion of the DNA samples was confirmed in a 1.5% agarose gel. Digested DNA was loaded into 0.8% agarose gel and run in TAE buffer overnight by applying 40V. Then the gel was carefully transferred on to a Whatman filter paper and vacuum dried at 60°C for 45 min. Then the dried gel was denatured in denaturation buffer (1.5M NaCl + 0.5M NaOH) followed by neutralization in neutralization buffer (1.5M NaCl + 1 M Tris-Cl, pH 7.5), 20 minutes

each. Then it was blocked with pre-hybridization mix (2.5ml 20X SSC, 100µl Phosphate wash, 1ml 50X Denhard's reagent, 6.4ml dH<sub>2</sub>O and 500µg Salmon sperm DNA) for 1 hour at 37°C followed by hybridization with radioactively labeled telomere probe (TTAGGG)<sub>3</sub> for 4 hours at 37°C in a narrow closed glass tube. (The radioactive probe was prepared by incubating (1µl TRF3 (50ng), 13.5µl H<sub>2</sub>O, 2 µl PNK buffer, 2.5 µl γATP, 1 µl T4 PNK for 1 hour at 37°C followed by a short wash with 50µl of dH<sub>2</sub>O and then centrifuged through a micro-spin G-25 coulumn and then denatured at 95°C for 10 min). After 4 hours the gel was washed three times each wash for 10 minutes with washing buffer (0.25X SSC pH 7.0 + 0.1% SDS). Then the gel was sealed into a plastic cover and exposed to Phosphoimager screen for over night in a Kodak film cassette. Then the film was read with Phosphoimager equipped with the software Bas Reader and PCBAS. All the calculations were performed with PCBAS and Microsoft Excel.

### **2.33 LB (Luria-Bertani) medium**

For 1 litre LB medium, 10gms select peptone, 5gms yeast extract and 10gms NaCl was dissolved in 950 ml of de-ionized water and the pH of the solution was adjusted to 7.0 with NaOH and then brought the volume to 1 litre with ddH<sub>2</sub>O. Then the solution was autoclaved on liquid cycle for 20 min at 15 psi. Then the solution was allowed to cool down to 55°C and the antibiotic was added if it is required (50µg/ml of either ampicilin or kanamycin). Then the medium was stored at 4°C in dark.

### **2.34 LB (Luria-Bertani) plates**

LB medium was prepared as described before and then 15gms/L agar was added before autoclaving. Then the solution was allowed to cool down to 55°C and the required antibiotic was added (50µg/ml of either ampicilin or kanamycin) and poured into 10 cm plates, let them hardened and then inverted and stored at 4°C in dark.

### **2.35 Bacterial transformation and culture**

100 ng of DNA was mixed with 100µl of competent bacterial cells and incubated on ice for 10 min. Then a brief 1 min heat-shock was given at 42°C in a water bath followed by incubation on ice for 10 min. Then 100 µl of LB medium without any antibiotic was added and the solution was shaken vigorously in an orbital shaker for 1 hr at 225 rpm. Then 300µl of LB medium with required antibiotic (ampicilin or kanamycin) was added, mixed and centrifuged and the bacterial pellet was resuspended in 100µl of LB medium and plated on to

LB plates and incubated at 37°C for overnight (12 to 14 hours). After that the plates were transferred to 4°C to avoid further growth of bacterial colonies. To culture bacteria, a single colony was picked up with a sterile pipette tip and inoculated into 2.5ml LB medium with desired antibiotic and shaken vigorously in an orbital shaker overnight (12 to 14 hrs).

### **2.36 Plasmid mini preparation**

1.5 ml of the above bacterial culture medium was taken into an eppendorf and centrifuged at 5000rpm for 5 min at room temperature. The supernatant was discarded and the bacterial pellet was re-suspended without producing air bubbles in 250µl of STET buffer (0.1M NaCl, 10mM Tris, 1mM EDTA, 5% Triton-100-X) and 10µl of lysozyme (10mg/ml) was added mixed and denatured at 95°C for 45 sec and then transferred to ice immediately and incubated for 5 min. Then it is centrifuged at 13,000 rpm for 20 min at 4°C and the supernatant was carefully transferred to a new eppendorf and the DNA was precipitated with ice cold iso-propanol and incubated at room temperature for 5 min and centrifuged at 13,000 rpm for 20 min at room temperature. The supernatant was discarded and the DNA pellet was washed with 500µl of 70% ethanol and centrifuged at 8000 rpm for 10 min at room temperature and the washing step was repeated twice. The supernatant was discarded and the pellet was air dried for 10 min and then dissolved in 50µl of TE (10mM Tris-HCl, 1mM EDTA) buffer.

### **2.37 Plasmid maxi preparation**

Plasmid maxi preparation was done by following Qiagen plasmid maxi kit manufacturer protocol. In brief 500µl of bacterial culture medium was inoculated into 200 ml of LB medium with desired antibiotic and continuously shaken for over night at 37°C in an orbital shaker at 225rpm. Then it is centrifuged at 6000 rpm for 15 min at 4°C and the supernatant was discarded and the pellet was re-suspended in 10 ml of buffer P1 and then 10 ml of buffer P2 was mixed and incubated at room temperature for 5 min. Then 10 ml of chilled buffer P3 was added mixed immediately but gently by inverting 4 to 6 times and incubated on ice for 20 min and centrifuged at 20,000 rpm for 30 min at 4°C and the supernatant containing plasmid DNA was collected and 2.5 ml of ER buffer was mixed and incubated on ice for 30 min. Then it is applied to a Qiagen-tip 500 which was already equilibrated with 10 ml of buffer QBT and allowed the column to empty by gravity flow. Then the Qiagen-tip was washed twice with 30 ml of buffer QC. Then the bound DNA was eluted with 15 ml of buffer QF. DNA was precipitated with 10.5 ml of room temperature iso-

propanol and centrifuged at 15,000 rpm for 30 min at 4°C. The supernatant was decanted and the pellet was washed with 70% ethanol and centrifuged at 8,000 rpm for 10 min. The pellet was air dried and dissolved in 300µl TE buffer.

### **2.38 Restriction digestion and insert verification**

1µg of DNA was digested with 1µl of restriction endonuclease (10U) in 2 µl of specific NEB buffer in a final volume of 10µl in dH<sub>2</sub>O at 37°C in a water bath for 2 hrs. Then the reaction mixer is incubated at 65°C to inactivate the enzyme. The insert of interest was checked by running the digest on 0.8% agarose gel and stained with ethidium bromide (20µl/100 ml of gel at 1mg/ml conc.) and compared with standard DNA markers of known size.

### **2.39 PCR Product extraction from the agarose gel**

QIAquick Gel Extraction Kit and manufacturer protocol was followed for extraction of PCR products from the agarose gels. The DNA fragments were excised from the agarose gel with a clean sharp scalpel. The gel slice was weighed in a colourless tube and three volumes of Buffer QG was mixed with 1 volume of gel (300µl of Buffer QG to 100mg of gel slice) and incubated at 50°C until the gel slice has completely dissolved. After the gel slice has dissolved completely, one gel volume of isopropanol was added to the sample, mixed and applied to the QIAquick column and centrifuged at 13,000rpm for 1 min at room temperature. Then the column was washed once with 750µl of Buffer PE and centrifuged at 13,000rpm for 1 min at room temperature. The flow through was discarded and the column was centrifuged once again to remove any residual ethanol. The QIAquick column was placed into a clean 1.5ml microfuge tube and the bound DNA was eluted with 30µl of dH<sub>2</sub>O and stored at -20°C until further use.

### **2.40 Freezing of cells**

The medium was discarded and the cells were washed once with PBS and trypsinized and re-suspended in 5 ml of fresh DMEM medium and centrifuged at 500 rpm for 10 min and the supernatant was discarded and the cell pellet was re-suspended in 1 ml of ice-cold freezing medium (90% FBS+10% DMSO), transferred to freezing vials (Nunc) and kept for 2 days at -80°C in a freezing chamber (Nunc) allowing slow freezing of the cells at a rate of approximately -1°C per hr. Finally the frozen cells were transferred to liquid nitrogen for long term storage.



#### **2.41 Thawing of cells**

The freezing vials in which the cells were stored are quickly thawed at 37°C, re-suspended in 5ml of fresh DMEM medium, centrifuged at 500rpm for 10 min and the cell pellet was resuspended in 10ml of medium and plated into culture dishes.

#### **2.42 Human liver cirrhosis samples and histology**

All samples were derived from explanted livers of patients undergoing liver transplantation. Collection of the samples was approved by the ethical committee of the Medical School Hannover. All liver samples were snap frozen in liquid nitrogen within 30 min after explantation and stored at -80°C until analysis. Histological analysis was performed on formalin-fixed paraffin embedded tissue samples at the Department of Pathology, Medical School Hannover. A collection of 64 samples from different cirrhosis groups AIH (n=12), Alcoholism (n=7), Viral hepatitis (n=12), PBC (n=7), PSC (n=13) and controls (n=15) were used for this study.

### 3. Results

#### 3.1 Telomere shortening limits the number of cells participating in organ regeneration

The resting liver is a mitotically inactive organ with over 95% of the cells in the G<sub>0</sub>-stage of the cell cycle. In response to partial hepatectomy (PH) liver cells re-enter the cell cycle in a highly synchronized fashion and regenerate lost mass by one to two rounds of replication within one week thus representing a system in which somatic cell division regenerates organ mass without a direct need for specific stem cell population (101, 102). To analyze the impact of telomere shortening on organ regeneration at the cellular level, continuous labeling of all the proliferating liver cells with BrdU was performed in G3 mTERC<sup>-/-</sup> and mTERC<sup>+/+</sup> controls until two rounds of replication (120hrs after PH) had been completed. After the first (72hrs after PH) as well as the second (120hrs after PH) round of DNA-replication the number of cells participating in liver regeneration was significantly reduced in G3 mTERC<sup>-/-</sup> mice compared to mTERC<sup>+/+</sup> mice (Figure 3.1.1A-B). These data indicated that telomere shortening inhibited a sub-population of liver cells from participating in organ regeneration.

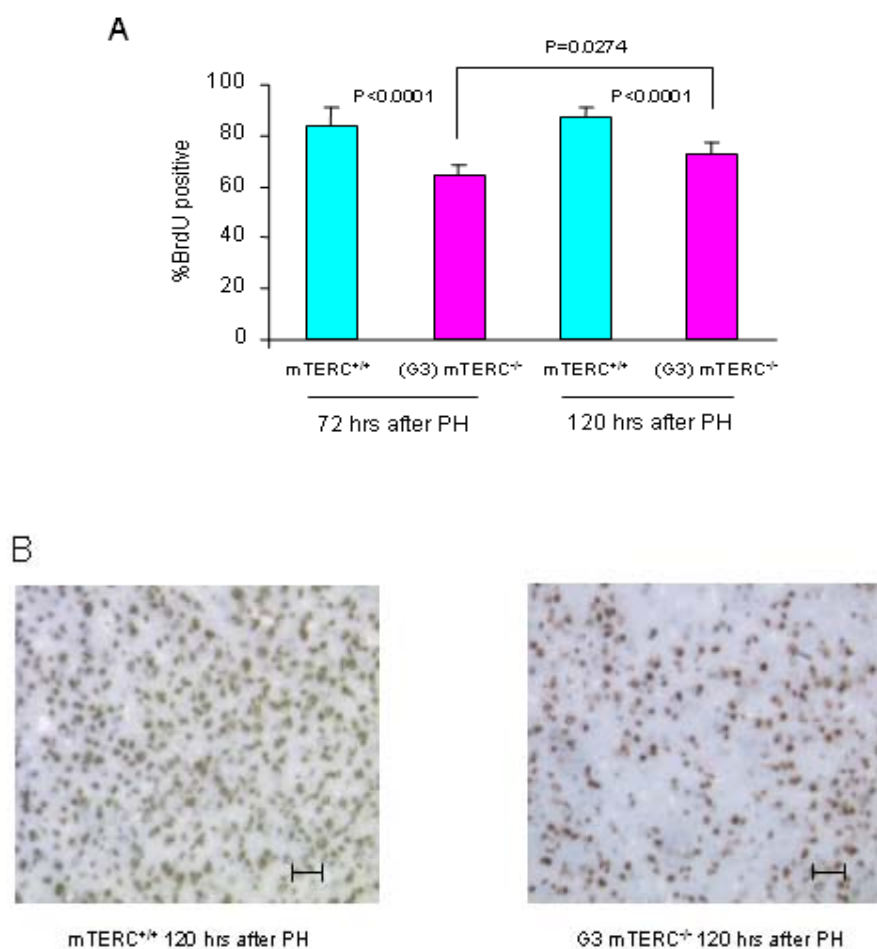


**Figure 3.1.1** The percentage of liver cells incorporating BrdU in response to PH under continuous BrdU labeling is higher in mTERC<sup>+/+</sup> compared to G3 mTERC<sup>-/-</sup> mice. **(A)** Rate of BrdU-labeled liver cells at 72 hrs after PH: 83.83±7.44% in mTERC<sup>+/+</sup> (n=5) vs 64.5±4.28% in G3 mTERC<sup>-/-</sup> (n=5), p<0.0001, and at 120 hrs after PH: 86.96±4.33 in mTERC<sup>+/+</sup> (n=5) vs 72.30±5.45% in G3 mTERC<sup>-/-</sup> (n=5), p<0.0001. **(B)** Representative photographs of BrdU staining pattern in mTERC<sup>+/+</sup> and G3 mTERC<sup>-/-</sup> mice 120hrs after PH under continuous BrdU infusion (magnification bar: 150µm).

Previous studies in late generation mTERC<sup>-/-</sup> mice have shown that telomere shortening leads to defective regeneration and impaired organ homeostasis (97-99). To test whether inhibited cell cycle entry of a sub-population of cells in G3 mTERC<sup>-/-</sup> mice is due to critical telomere shortening or due to lack of telomerase itself we followed the percentage of replicating liver cells at the first peak stage of S-phase (48 hours) after PH in mTERC<sup>+/+</sup>, G3 mTERC<sup>-/-</sup> and G1 mTERC<sup>-/-</sup> mice. G1 mTERC<sup>-/-</sup> mice lack telomerase activity but due to the long telomere length in mice do not have critically short telomeres and no signs of telomere dysfunction (93). As described above (Figure 3.1.1) the rate of BrdU-positive cells at the first peak stage of S-phase in response to PH was significantly decreased in G3 mTERC<sup>-/-</sup> mice compared to mTERC<sup>+/+</sup> mice. In contrast, G1 mTERC<sup>-/-</sup> mice have very similar rates of BrdU-positive cells compared to mTERC<sup>+/+</sup> mice (Figure 3.1.2 A, 44.45±5.26% in G1 mTERC<sup>-/-</sup> mice compared to 47.03±6.33% in mTERC<sup>+/+</sup> mice, p= 0.0934) indicating that not the absence of telomerase *per se* but the shortening of telomeres to a critical length inhibits a sub-population of cells from participating in organ regeneration. To test whether telomerase re-expression would rescue diminished organ regeneration induced by telomere shortening, G3 mTERC<sup>-/-</sup> mice were crossed with mTERC<sup>+/-</sup> mice as described previously (121). With this approach the G4 mTERC<sup>-/-</sup> have characteristic critical short telomeres and telomere dysfunction whereas the G4 mTERC<sup>+/-</sup> mice have a rescue of telomere function due to telomerase re-expression. When mice of this intercross were exposed to PH G4 mTERC<sup>-/-</sup> offspring showed a decreased number of liver cells participating in organ regeneration. In contrast, liver regeneration in G4 mTERC<sup>+/-</sup> offspring was rescued to levels comparable to mTERC<sup>+/+</sup> mice (Figure 3.1.2 B, rate of BrdU-positive liver cells 48 hours after PH: 45.52±4.65% in G4 mTERC<sup>+/-</sup> offsprings compared to 29.90±3.25% in G4 mTERC<sup>-/-</sup> offspring, p<0.0001). These results indicated that telomere stabilization by telomerase re-expression completely rescued impaired liver regeneration induced by inhibition of cell cycle re-entry in a subset of liver cells with critical short telomeres in mTERC<sup>-/-</sup> mice.

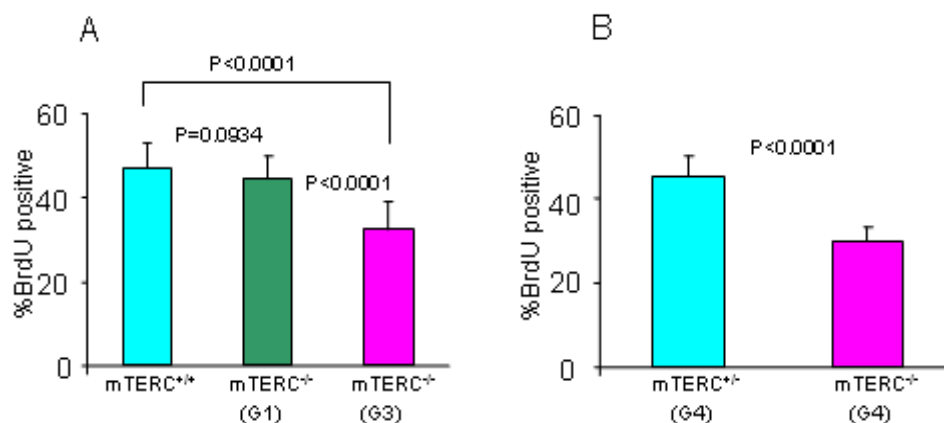


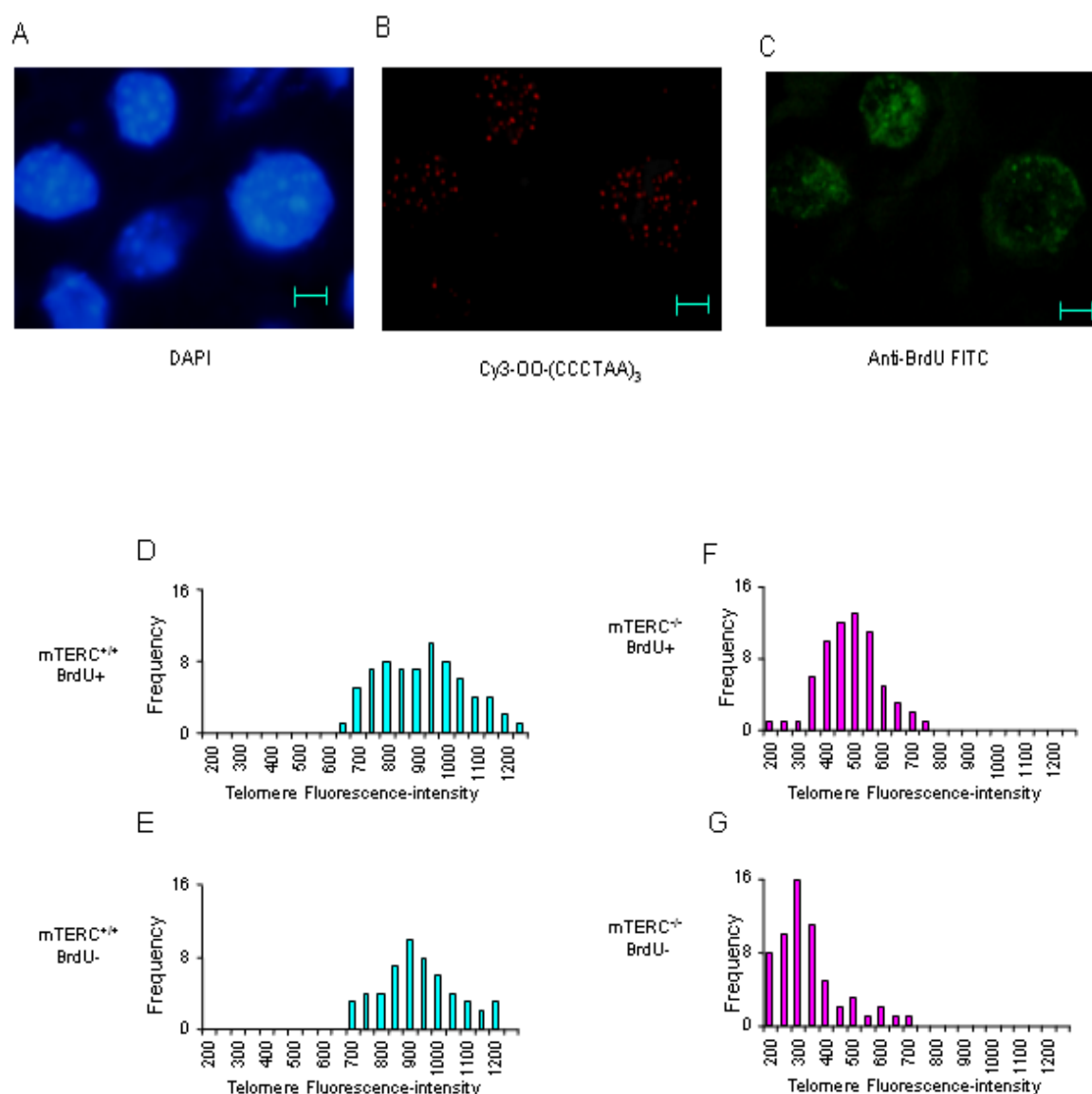
**Figure 3.1.2 (A)** Percentage of cells incorporating BrdU at the first peak stage of S-phase (48hrs after PH) under 2hrs of BrdU pulse labeling: 47.03±6.33% in mTERC<sup>+/+</sup> (n=5) vs 44.45±5.26% G1 mTERC<sup>+/-</sup> (n=5, p= 0.0934) and 32.31±6.65% G3 mTERC<sup>-/-</sup> (n=5, p<0.0001). A significant reduction in the BrdU-index is evident in G3 mTERC<sup>-/-</sup> mice, whereas G1 mTERC<sup>+/-</sup> mice show a similar rate of BrdU positive liver cells compared to mTERC<sup>+/+</sup> mice indicating that telomere length but not lack of telomerase impacts on the number of cells participating in organ regeneration. **(B)** Percentage of cells incorporating BrdU at the first peak stage of S-phase (48hrs after PH) under 2hrs of BrdU pulse labeling: 45.52±4.65% in G4 mTERC<sup>+/-</sup> (n=5) vs 29.90±3.25% G4 mTERC<sup>-/-</sup> (n=5, p<0.0001). G4 mTERC<sup>+/-</sup> mice show a rescue in the percentage of BrdU positive cells indicating that telomere stabilization by telomerase re-expression rescues suppression of cell cycle re-entry of a sub-population of cells.

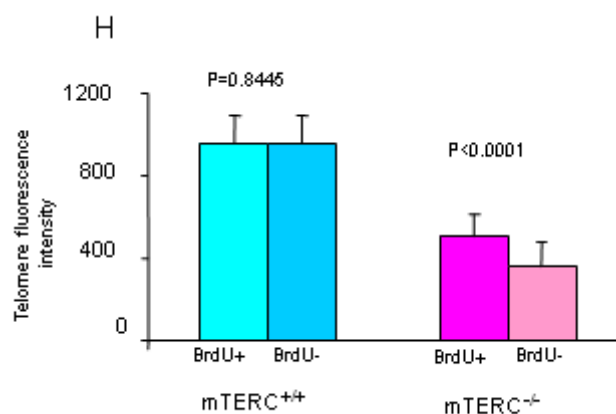
Together these data indicated that the phenotype of a decreased population of cells entering the cell cycle during organ regeneration is due to telomere shortening, independent of telomerase *per se*, but can be rescued by telomere stabilization in mice with critically short telomeres.

### 3.2 Critical telomere shortening at the cellular level blocks cell cycle re-entry of a sub-population of liver cells in G3 mTERC<sup>-/-</sup> mice

A possible explanation for the inhibition of cell cycle re-entry in a sub-population of cells in G3 mTERC<sup>-/-</sup> mice is that telomeres in cells of an organ system are heterogeneous and that only cells with critically short, dysfunctional telomeres are inhibited from entering the cell cycle. To test this hypothesis, telomere length was analyzed at the single cell level using quantitative fluorescence *in situ* hybridization (qFISH) (120) in combination with BrdU staining (Figure 3.2.1A-C). With this approach it is possible to directly compare telomere lengths between liver cells participating in organ regeneration (BrdU-positive) and liver cells inhibited (BrdU-negative) from cell cycle re-entry. In mTERC<sup>+/+</sup> mice BrdU positive and

negative liver cells (120 hrs after PH and continuous labeling with BrdU) showed similar mean telomere fluorescence intensities (Figure 3.2.1 D, E and H). As expected, the overall telomere fluorescence intensity was lower in G3 mTERC<sup>-/-</sup> mice compared to mTERC<sup>+/+</sup> mice. But interestingly within the liver of G3 mTERC<sup>-/-</sup> the telomere fluorescence intensity was significantly weaker in the sub-population of cells inhibited from cell cycle re-entry (BrdU negative) compared to the population of proliferating cells (BrdU positive) (Figure 3.2.1 F, G and H). The observation that the mean telomere fluorescence intensities between BrdU positive and BrdU negative cells 120 hrs after PH were similar in mTERC<sup>+/+</sup> mice indicates that BrdU staining and cell cycle stage did not interfere with hybridization and quantification of the telomeric probe at the telomeres. These data gave direct evidence that critically short telomeres at the cellular level limit the proliferative capacity of cells within an organ system.

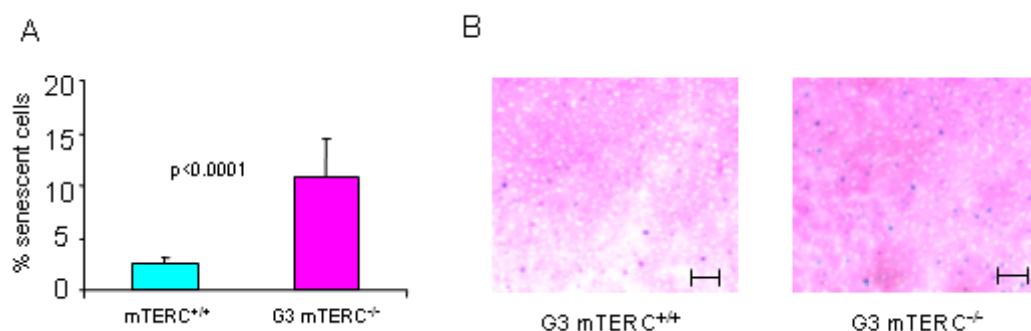




**Figure 3.2.1:** Telomere length analysis at cellular level by quantitative fluorescence in situ hybridization (qFISH) was combined with BrdU staining (A-C). (A) DAPI counter-staining (B) Q-FISH with a telomere specific probe Cy3-OO-(CCCTAA)<sub>3</sub>. (C) BrdU staining with anti-5-bromo-2'-deoxyuridine monoclonal antibody and FITC-conjugated secondary antibody. The liver samples from 120 hrs of continuous BrdU labeling after PH were used to measure and compare the telomere fluorescence intensities in BrdU positive and BrdU negative cells. In total, the fluorescence intensities of telomere spots were analyzed from 69 BrdU positive, 54 BrdU negative nuclei from mTERC<sup>+/+</sup> (n=5) and 66 BrdU positive and 60 BrdU negative nuclei from G3 mTERC<sup>-/-</sup> (n=5) mice. (D) Telomere fluorescence intensity of BrdU positive cells in mTERC<sup>+/+</sup> mice (E) BrdU negative cells in mTERC<sup>+/+</sup> mice (F) BrdU positive cells in G3 mTERC<sup>-/-</sup> mice (G) BrdU negative cells in G3 mTERC<sup>-/-</sup>. (H) The mean telomere fluorescence intensities of BrdU positive (952.53±144.19) and negative cells (957.44±130.57) in mTERC<sup>+/+</sup> and BrdU positive (509.65±101.30) and negative cells (364.94±116.45) in G3 mTERC<sup>-/-</sup> mice.

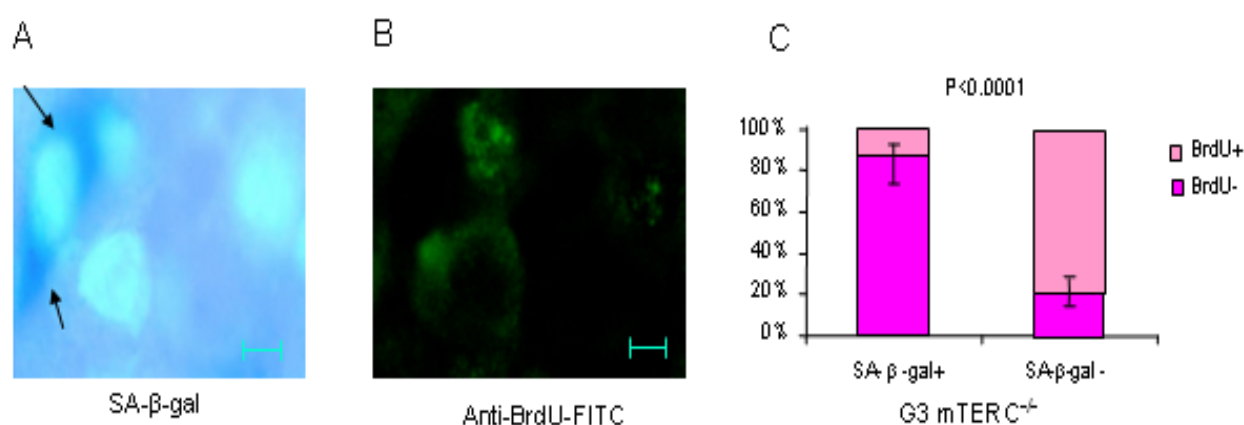
### 3.3 Non-proliferating cells with critically short telomeres in mTERC<sup>-/-</sup> are senescent

A possible mechanism for inhibition of cell cycle re-entry in a sub-population of cells is the induction of cellular senescence, which in primary human cells is induced after 50-70 cell doublings, first affecting sub-clones with critically short telomeres of a given cell line *in vitro* (19-21). To directly test whether the non-proliferating cells in G3 mTERC<sup>-/-</sup> entered senescence, SA-β-galactosidase staining (72) was conducted on liver samples at 120 hrs after PH to directly compare the percentage of SA-β-galactosidase positive cells with the percentage of non-proliferating cells (BrdU negative). This method revealed significantly increased rates of senescent cells in G3 mTERC<sup>-/-</sup> mice compared to mTERC<sup>+/+</sup> mice (Figure 3.3.1A-B).



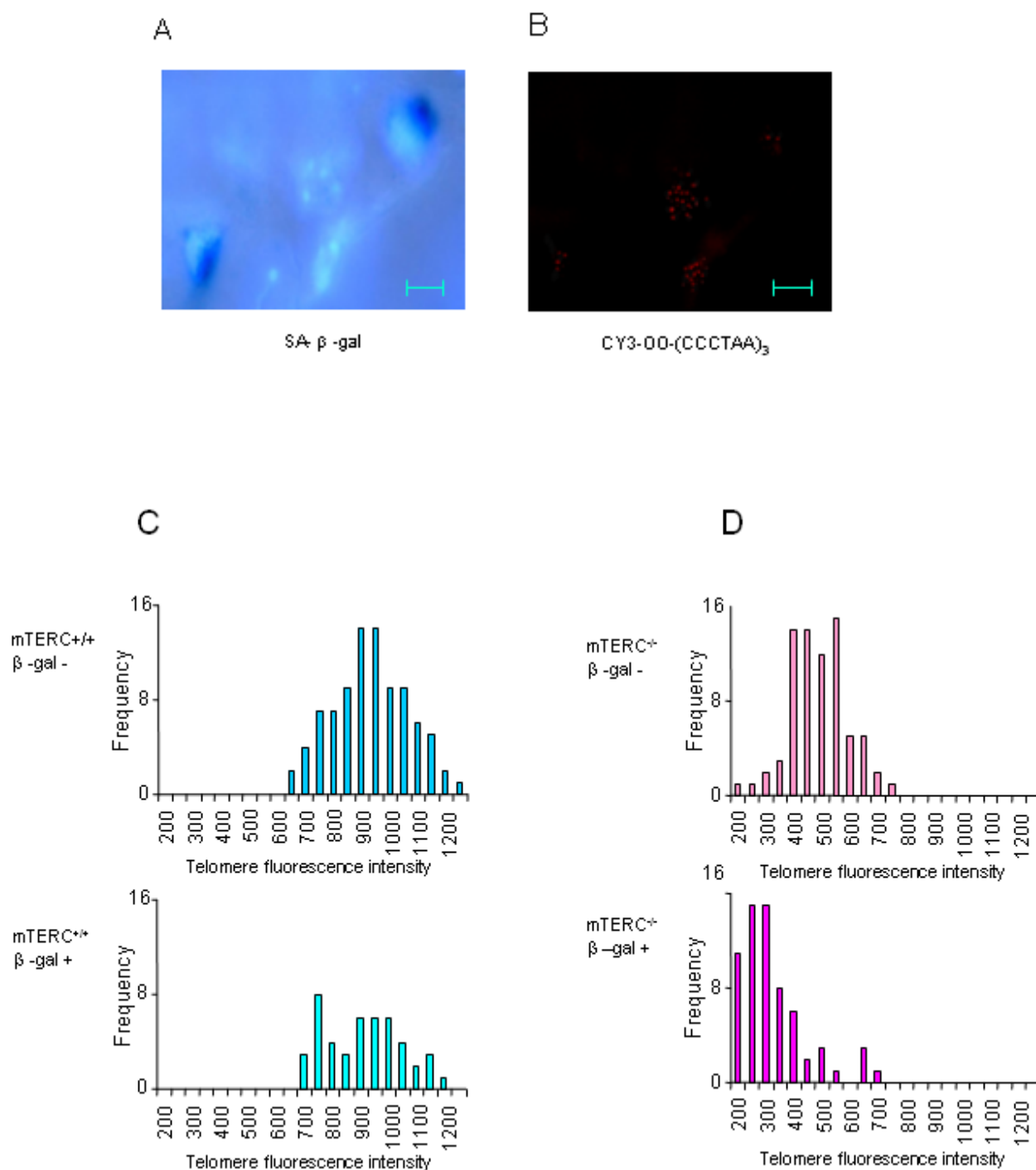
**Figure 3.3.1** (A) SA-β-gal staining at pH 6 shows higher number of positive cells in G3 mTERC<sup>-/-</sup> (n=5) mice (10.83±3.61%) compared to mTERC<sup>+/+</sup> (n=5) mice (2.54±0.7% p<0.0001). (B) Representative photographs of SA-β-gal stained liver sections (120 hrs after PH) of mTERC<sup>+/+</sup> and G3 mTERC<sup>-/-</sup> mice (magnification bar: 300μm).

Even though SA-β-galactosidase staining is widely used as a marker of senescence it has been shown that false positive results occur *in vitro* in cell cultures exposed to various stresses (122). To exclude unspecific non-senescence related SA-β-galactosidase staining a co-staining combining BrdU staining with SA-β-galactosidase staining was conducted. This co-staining revealed a strong coincidence of β-gal activity with non-proliferating cells (BrdU-negative) in G3 mTERC<sup>-/-</sup> mice. Specifically, only 13±4.84% of the SA-β-galactosidase positive cells were BrdU positive, whereas 79±6.2% of the SA-β-galactosidase negative fraction of cells showed BrdU incorporation (Figure 3.3.2 A-C).



**Figure 3.3.2** Co-localization of SA-β-gal activity in non-proliferating liver cells of G3 mTERC<sup>-/-</sup> mice. Representative photographs of (A) SA-β-gal staining (B) BrdU staining with anti-BrdU-FITC antibody showing the non proliferative cells are positive to SA-β-gal activity. (C) Histogram showing only 13±4.84% of SA-β-gal positive cells are BrdU positive, whereas 79±6.2% of the SA-β-gal negative cells are BrdU positive.

To directly show that the SA- $\beta$ -galactosidase positive cells in G3 mTERC<sup>-/-</sup> mice were inhibited from cell cycle re-entry by critically short telomeres a co-staining combining SA- $\beta$ -galactosidase staining with telomeric qFISH was carried out. As anticipated from the above results this analysis revealed significantly weaker telomere fluorescence intensities in SA- $\beta$ -galactosidase positive cells compared to SA- $\beta$ -galactosidase negative cells in G3 mTERC<sup>-/-</sup> mice (Figure 3.3.3 A-E). In contrast, mTERC<sup>+/+</sup> mice had no difference in the telomere fluorescence intensity comparing SA- $\beta$ -galactosidase positive and negative cells.





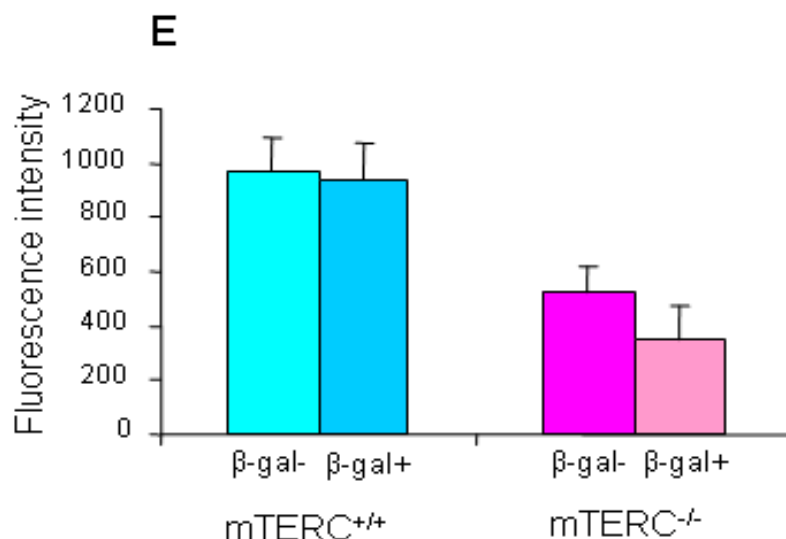


**Figure 3.3.3** SA-β-gal positive cells have critically short telomeres. Representative photograph of (A) SA-β-gal and (B) telomere probe co-staining showing that the fluorescent intensity of telomere spots are weaker in SA-β-gal positive cells. (C-E) The frequencies of mean telomere fluorescence intensities in nuclei of (top to bottom): (C) SA-β-gal negative cells in mTERC<sup>+/+</sup>, SA-β-gal positive cells in mTERC<sup>+/+</sup>, (D) SA-β-gal negative cells in G3 mTERC<sup>-/-</sup> and SA-β-gal positive cells in mTERC<sup>-/-</sup>. (E) The mean telomere fluorescence intensities of SA-β-gal negative and positive cells in mTERC<sup>+/+</sup> and SA-β-gal negative and positive cells in mTERC<sup>-/-</sup>. In total the fluorescence intensities of telomere spots are analyzed from 89 SA-β-gal negative (963.10±130.65) and 46 SA-β-gal positive cells (937.30±135) from mTERC<sup>+/+</sup> (n=5) and 75 SA-β-gal negative (521.86±100.16) and 65 SA-β-gal positive cells (352.13±119.63) from mTERC<sup>-/-</sup> (n=5) mice. Note that the telomere fluorescence intensity in mTERC<sup>+/+</sup> mice is similar between SA-β-gal positive and negative cells, indicating that SA-β-gal staining did not interfere with telomere probe hybridization and measurement.

Therefore, the low prevalence of SA-β-galactosidase positive cells in mTERC<sup>+/+</sup> mice was independent of telomere shortening possibly resembling the "premature senescence" phenotype induced by mitogenic stimulation such as ras-signaling (84). Although an interference of SA-β-galactosidase staining or senescence *per se* with telomere probe hybridization and measurement during qFISH remains formally possible, the data showing similar telomere fluorescence intensity in SA-β-gal positive and negative liver cells of mTERC<sup>+/+</sup> mice indicate that such an interference did not occur.

### 3.4 Differentially expressed genes in response to induction of senescence in vivo

The Rb- and p53-pathways have been prominently associated with cellular senescence (13-16, 66, 68, 79). To test for an activation of these senescence pathways in mTERC<sup>-/-</sup> mice, Affimetrix high density oligonucleotide microarray analysis was carried out in duplicate comparing gene expression levels in quiescent liver and at the G1/S transition of the cell cycle during liver regeneration (30-36 hrs after PH). This time point was chosen since most of the known senescence-pathways are active at this transition point and senescent cells can not overcome this G1/S checkpoint unless the cell cycle machinery is experimentally perturbed (79, 123). We monitored gene expression changes between these two time points and compared the differentially regulated genes in mTERC<sup>+/+</sup> mice and G3 mTERC<sup>-/-</sup> mice. This experiment identified several differentially expressed genes, 30 genes that were only regulated in mTERC<sup>+/+</sup> but not in G3 mTERC<sup>-/-</sup> mice and 76 genes that were only regulated in G3 mTERC<sup>-/-</sup> mice but not in mTERC<sup>+/+</sup> mice and 81 genes that were regulated in both mTERC<sup>+/+</sup> and G3 mTERC<sup>-/-</sup> mice. Comparison of the genes at quiescence stage between mTERC<sup>+/+</sup> and G3 mTERC<sup>-/-</sup> identified only 4 differentially regulated genes in G3mTERC<sup>-/-</sup> mice. The full dataset of this micro-array experiment and the experimental design is accessible in MIAME-format online ([www.gbf.de/array](http://www.gbf.de/array)) under downloads (under Satyanarayana et al.: Table1, Table2, and ExperimentalDesign).

**Table 3.4.1** Differentially expressed genes at G<sub>0</sub>-G<sub>1</sub>/S transition in mTERC<sup>+/+</sup> and mTERC<sup>-/-</sup> mice

No	Gene description	Gene symbol	$\Delta$ mTE RC <sup>+/+</sup>	$\Delta$ mTE RC <sup>-/-</sup>	Gene bank acc.#
<b>Stress and acute phase response</b>					
1	Heat shock protein, 86 kDa 1	Hsp86-1	2.83	2.77	J04633
2	Hypopolysaccharide binding protein	Lbp	2.28	2.43	X99347
3	Inter alpha-trypsin inhibitor, heavy chain 4	Itih4I	2.43	2.62	AF023919
4	Secretory leukocyte protease inhibitor	Slpi	2.13	3.86	AF002719
5	Serine protease inhibitor 2-2	Spi2-2	4.11	3.92	M64086
<b>Metabolism/Transport/Surface receptors/Cytoskeleton</b>					
6	Apolipoprotein A-IV	Apoa4	14.42	15.35	M64248
7	Aquaporin 8	Aqp8	-4.29	-2.16	AF018952
8	Carbonic anhydrase 13	Car13	-6.77	-12.64	AJ006474
9	Carboxylesterase 1	Ces1	-3.58	-2.95	Y12887
10	Cd63 antigen	Cd63	5.24	6.36	D16432
11	Cytochrome P-450	Cyp4a10	2.28	2.27	AB01842

12	Cytochrome P450, 1a2, aromatic compound Inducible	Cyp1a2	-2.39	-2.95	X04283
13	Cytochrome P450, 2a4	Cyp2a4	-8.75	-11.63	M19319
14	Cytochrome P450, 2f2	Cyp2f2	-2.91	-3.66	M77497
15	Cytochrome P450, 4a14	Cyp4a14	2.39	4.41	Y11638
16	Dynein, cytoplasmic, light chain 1	Dncl1	5.58	5.50	AF020185
17	Esterase 1	Es1	-3.48	-4.06	AW226939
18	Fatty acid binding protein 2, intestinal	Fabp2	3.07	3.53	M65034
19	Glutathione S-transferase, theta 1	Gstt1	-2.43	-2.14	X98055
20	Guanidinoacetate methyltransferase	Gamt	-2.60	-3.66	AF010499
21	Heat shock 70kD protein5(glucose-regulated protein)	Hspa5	2.45	2.16	AJ002387
22	Hepatic triglyceride lipase	Lipc	-2.36	-2.81	X58426
23	Hydroxysteroid 11-beta dehydrogenase 1	Hsd11b1	-2.31	-2.01	X83202
24	Hydroxysteroid dehydrogenase-5, delta<5>-3-beta	Hsd3b5	-4.17	-12.55	L41519
25	Lipocalin 2	Lcn2	377.41	145.01	X81627
26	Metallothionein-I	Mt1	2.54	2.38	V00835
27	Metallothionein II	Mt2	2.33	2.85	K02236
28	Nicotinamide N-methyltransferase	Nnmt	4.50	3.58	U86108
29	Niemann Pick type C1	Npc1	-2.91	-2.23	AF003348
30	Orosomucoid 1	Orm1	2.69	2.62	M27008
31	Orosomucoid 2	Orm2	10.70	16.56	M12566
32	Proteaseome (prosome, macropain) 28 subunit, 3	Psme3	2.11	2.58	AB007139
33	Selenium binding protein 1	Selenbp1	-2.33	-3.41	M32032
34	Serum amyloid A 1	Saa1	16.80	21.86	M13521
35	Serum amyloid A 2	Saa2	25.28	45.89	U60438
36	Serum amyloid A 3	Saa3	3.53	7.31	X03505
37	Serum amyloid P component	Sap	8.40	7.21	M23552
38	Solute carrier family 2 (facilitated glucose transporter), member 2	Slc2a2	-3.03	-2.45	X15684
39	Thioether S-methyltransferase	Temt	-18.13	-19.29	M88694
40	Tubulin, alpha 1	Tuba1	2.13	2.10	M28729
41	Tubulin, alpha 6	Tuba6	2.53	2.66	M13441
42	Tubulin, beta2	Tubb2	9.32	14.52	M28739
43	Tubulin, beta 3	Tubb3	3.14	4.69	AW050256
<b>Cell cycle, DNA damage and apoptosis</b>					
44	B-cell translocation gene 2, anti-proliferative	Btg2	5.10	2.13	M64292
45	Gro1 oncogene	Gro1	7.89	8.40	J04596
46	Growth arrest specific 1	Gas1	-2.43	-2.68	X65128
47	Histone H1 gene	His1a	3.05	2.43	J03482
48	Leukemia inhibitory factor receptor	Lifr	-5.39	-6.73	D17444
49	Nuclear factor, interleukin 3, regulated	Nfil3	3.25	2.64	U83148
<b>Growth, Differentiation &amp; Signal transduction</b>					
50	Activating transcription factor 5	Atf5	2.85	3.73	AB012276
51	Complement component 2	C2	-2.13	-2.38	M57891
52	Corticosteroid binding globulin	Cbg	-5.70	-6.68	X70533

					Results
53	Eukaryotic translation initiation factor 1A	Eif1a	3.27	2.28	AF026481
54	Insulin-like growth factor binding protein 1	Igfbp1	2.69	2.85	X81579
55	Peroxisome proliferator activated receptor alpha	Ppara	-2.07	-2.08	X57638
56	Polymeric immunoglobulin receptor	Pigr	-3.03	-3.20	AB001489
57	Regulator of G-protein signaling 16	Rgs16	-7.78	-9.71	U94828
58	RNA binding motif protein 3	Rbm3	2.17	2.89	AB016424
59	Serine protease inhibitor 2, related sequence 1	Spi2-rs1	3.58	3.92	X69832
60	Sphingosine kinase 2	Sphk2	-7.11	-7.06	AW047343
61	Stimulated by retinoic acid 14	Stra14	-2.36	-2.46	Y07836
62	Thyroid hormone responsive spot14	Thrsp	-5.90	-9.06	X95279
63	Ubiquitin specific protease 2	Usp2	-3.39	-3.78	AI846522
<b>Unknown Function</b>					
64	Camello-like 1	Cml1	-2.64	-2.91	AI840501
65	Sec61, gamma subunit	Sec61g	2.23	2.55	U11027
<b>ESTs</b>					
66	DnaJ(Hsp40)homolog, subfamily B,member11	Est	2.11	2.58	AW122551
67	Homologous to Arginine rich mutated in early tumors	Est	2.85	3.07	AW122364
68	Homologous to isovaleryl coenzyme A dehydrogenase	Est	-2.45	-2.66	AW047743
69	Homologous to stearoyl-CoA desaturase	Est	-3.07	-2.07	M21285
70	Leucine-rich alpha-2-glycoprotein	Est	3.46	3.07	AW230891
71	PLZF gene	Est	3.68	11.31	AI553024
72	Similar to Acetyl-CoA acyltransferase, 3-oxo acyl-CoA thiolase A, peroxisomal	Est	-2.81	-2.23	AW012588
73	Similar to prohepcidin	Est	-2.71	-2.69	AI255961
74	Similar to thyrotroph embryonic factor	Est	-5.66	-3.27	AI850638
75	Un-known gene	Est	-2.85	-2.58	AI853773
76	Un-known gene	Est	-7.26	-10.34	AI266885
77	Un-known gene	Est	2.25	3.14	AA921069
78	Un-known gene	Est	2.57	4.00	AI847162
79	Un-known gene	Est	2.17	3.05	AI848235
80	Un-known gene	Est	2.41	2.62	AW125178
81	Un-known gene	Est	2.35	2.28	AW049570

Δ Fold change, Acc.# Accession number

**Table 3.4.2** Differentially expressed genes at G<sub>0</sub>-G<sub>1</sub>/S transition only in mTERC<sup>+/+</sup> mice

No	Gene Description	Gene symbol	Δ mTER	Gene bank Acc.#
----	------------------	-------------	--------	-----------------

				Results
				C <sup>+/+</sup>
<b>Stress and acute phase response</b>				
1	Phospholipase A2	Pla2	2.68	AI845798
2	Stress induced phosphoprotein 1	Stip 1	2.14	U27830
<b>Metabolism/Transport/Surface receptors/Cytoskeleton</b>				
3	Beta III spectrin	Spnb3	-3.27	Af026489
4	Cytochrome P450 Cyp7b1	Cyp7b1	2.22	U36993
5	Cytochrome P450, 2b9, phenobarbital inducible	Cyp2b9	-11.96	M21855
6	Fatty acid synthase	Fasn	-2.07	X13135
7	Ia-associated invariant chain	Ii	-3.43	X00496
8	Immunophilin FKBP51	FKBP51	2.03	U16959
9	Peroxisomal/mitochondrial dienoyl-CoA isomerase ECH1p	ECH1p	2.14	Af030343
10	Proprotein convertase 4	pc4	-23.75	L21221
11	Sialyltransferase 4A (beta-galactosidase alpha-2,3-sialyltransferase	Siat4a	2.41	X73523
12	Squalene epoxidase	Sqle	2.10	D42048
13	Stearoyl-CoA desaturase	SCD	-2.35	M21285
<b>Cell cycle, DNA damage and apoptosis</b>				
14	Leukemia-associated gene	Lag	2.04	AI843359
15	MORF-related gene X	Mrgx	2.73	AB025049
16	Sirtuin 3 (silent mating type information regulation 2, homolog) 3	sirtuin 3	-2.20	AI849490
<b>Growth, Differentiation &amp; Signal transduction</b>				
17	CCAAT/enhancer binding protein (C/EBP), alpha	Cebpa	-2.07	M62362
18	CCAAT/enhancer-binding protein delta	Cebpd	3.25	X61800
19	Hemoglobin, beta adult major chain	Hbb-b1	-2.03	AV003378
20	Inhibin/activin bC subunit	Inhbc	2.17	X90819
21	Insulin-like growth factor binding protein-2	Igfbp2	-2.58	X81580
22	Traf and Tnf receptor associated protein	Ttrap	-3.14	AW228036
23	TRAM1	TRAM1	2.35	AA763937
<b>ESTs</b>				
24	Homologous to protocadherin gamma	EST	2.50	AA222943
25	Homologous to UMP-CMP kinase	EST	2.13	AI851401
26	Un-known gene	EST	3.89	AI853226
27	Un-known gene	EST	2.75	AW049360
28	Un-known gene	EST	4.63	AA874329
29	Weakly similar to Gastrulation specific protein G12	EST	-2.14	AI844396
30	Weakly similar to ribosomal protein L11 methyltransferase	EST	3.01	AI553401

Δ Fold change, Acc.# Accession number

**Table 3.4.3** Differentially expressed genes at G<sub>0</sub>-G<sub>1</sub>/S transition only in G3 mTERC<sup>-/-</sup> mice

No	Gene Description	Gene Symbol	Δ mTE	Gene Bank
----	------------------	-------------	-------	-----------

			RC <sup>-/-</sup>	Acc.#
<b>Stress and acute phase response</b>				
1	Inter-alpha-inhibitor3	Itih3	2.14	X70393
2	Orosomucoid 3	Orm3	2.73	S38219
<b>Metabolism/Transport/Surface receptors/Cytoskeleton</b>				
3	Actin gamma	Actg	2.27	M21495
4	Alpha tubulin isotope M-alpha-2	Tuba2	2.36	M28727
5	Aminolevulinic acid synthase 2, erythroid	Alas2	-2.75	M15268
6	Arginine vasopressin receptor 1A	Avpr1a	2.01	D49730
7	Calcium channel gamma 6	Cacng6	2.11	Ai849587
8	Carbonic anhydrase 14	Car14	-2.31	AB005450
9	Carbonic anhydrase 5a, mitochondrial	Car5a	-2.20	X51971
10	Cathepsin F	Ctsf	-2.16	AJ131851
11	Cytochrome p450, 2b10, phenobarbitol inducible type b	Cyp2b10	12.47	M21856
12	Cytochrome P450, 7a1	Cyp7a1	-8.17	L23754
13	Dopa decarboxylase	Ddc	3.89	AF071068
14	Ferridoxin 1	Fdx1	-2.06	L29123
15	Flotillin 1	Flot1	2.04	U90435
16	Frizzled homolog4	Fzd4	-2.23	Aw122897
17	Glutathione-S-transferase mu-3	Gstm3	-2.36	J03953
18	Glycerol kinase	Gyk	2.25	U48403
19	Hydroxysteroid dehydrogenase-2, delta<5>-3-beta	Hsd3b2	-2.68	M75886
20	Ornithine transcarbamylase	Otc	-2.36	X07092
21	Pyruvate dehydrogenase kinase like protein	Pdk4	8.69	Aj001418
22	Sarcosine dehydrogenase	Sardh	-2.53	AI839995
23	Serum/glucocorticoid regulated kinase	Sgk	2.27	AW046181
24	Solute carrier family 35 (UDP-galactose transporter), member 2	Slc35a2	2.55	D87990
25	Sterol-C5-desaturase	Sc5d	-2.41	AB016248
26	Tropomyosin isoform 1	Tpm1	2.30	M22479
<b>Circadian rhythms</b>				
27	Aryl hydrocarbon receptor nuclear translocator like	Arntl	7.16	Ab014494
<b>Cell cycle, DNA damage and apoptosis</b>				
28	Carnitine acetyl transferase	Crat	2.23	X85983
29	Cyclin dependent kinase inhibitor 1A, p21	Cdkn1a	8.63	Aw048937
30	Fas associated factor 1	Faf1	-4.62	U39643
31	Growth arrest and DNA damage inducible	Gadd45g	4.38	Af055638
32	Krupple like factor 4	Klf4	4.03	U20344
33	Neighbor of A-kinase anchoring protein-95	Nakap95	-2.01	Ab028921
34	NIMA (Nerve in mitosis gene-a) related expressed kinase-6	Nek6	2.38	Ai846534
35	Nucleobindin2	Nucb2	17.51	Aj222586
36	P <sup>87</sup> Wee1 kinase	Wee1	-6.36	D30743
37	Polo-like kinase	Plk	13.74	Av305987
38	Protein kinase inhibitor p <sup>58</sup>	Prkri	2.95	U28423
39	Ring finger protein 4	Rnf4	-2.10	Ai844517
40	Sarcosine oxidase	Pso	-2.48	U94700
41	Senescence marker protein 30	Smp-30	2.11	U28937
<b>Growth, Differentiation &amp; Signal transduction</b>				
42	Cytokine inducible SH-2 containing protein-3	Cish3	4.56	Av374868
43	Ectonucleotide pyrophosphatase/phosphodiesterase 2	Enpp2	-3.03	AW122933

				Results
44	Ets variant gene 6 (Tel oncogene)	Etv6	2.53	A1845538
45	Gamma-aminobutyric acid (GABA(A)) receptor-associated protein-like 1	Gabarapl1	-2.10	AF180518
46	Growth differentiation factor 5	Gdf5	-3.73	U08337
47	Growth factor receptor bound protein-2-associated protein-1	Gab1	-2.22	Ai046826
48	Kidney expressed gene 1	Keg1	-3.23	Ab028071
49	LPS-induced TN factor	Litaf	2.16	AI852632
50	Lymphocyte antigen-6 complex	Ly6d	3.46	X63782
51	Neural precursor cell expressed, developmentally down-regulated gene 4b	Nedd4b	2.25	AI840868
52	N-myc downstream regulated like	Ndr1	2.03	U52073
53	Nuclear factor I	Nfix	-2.08	Y07688
54	Pou domain class3, transcription factor1	Pou3f1	-7.52	X56959
55	Pre-B-cell colony-enhancing factor	Pbef	-2.01	AI852144
56	Prolactin receptor related sequence 1	Prlr-rs1	-2.36	M22957
57	Protein tyrosine kinase 6	Ptk6	-7.73	U16805
58	Ras homolog N (RhoN)	Arhn	2.57	Af016482
59	Retinoic acid early transcript gamma	Raet1c	-2.89	D64162
60	Ribosomal protein L22	Rpl22	2.46	AK008915
61	Ribosomal protein L30	Rpl30	2.07	K02928
62	S100 calcium binding protein A10 (calpactin)	S100a10	3.27	M16465
63	S100 calcium binding protein A8 (calgranulin A)	S100a8	5.03	M83218
64	Thymidine kinase	Tk	-2.64	X60980
65	Zeta chain (TCR) associated protein kinase	Zap70	-2.51	Ai386093
<b>Unknown Function</b>				
66	Bri3, Brain protein I 3	Bri3	-2.23	X61454
67	Glutathione S-transferase, mu 6	Gstm6	-2.25	AI326397
68	SEC61, alpha subunit	Sec61a	2.16	AI838624
69	Sulfotransferase-related protein	Sult-x1	-2.89	AF026074
<b>ESTs</b>				
70	Homologous to alpha-1-antiproteinase precursor	Est	-2.50	AI645694
71	Homologous to MCM10	Est	-3.39	AA867646
72	Protein disulfide isomerase-related protein	Est	2.16	AW045202
73	Similar to integral membrane transport protein UST5r	Est	-3.20	AI647632
74	Un-known gene	Est	2.69	AI849939
75	Un-known gene	Est	2.95	AW227650
76	Un-known gene	Est	2.36	AW046006

Δ Fold change, Acc.# Accession number

**Table 3.4.4** Differentially expressed genes at quiescence stage only in G3 mTERC<sup>-/-</sup> mice compared with mTERC<sup>+/+</sup> mice

No	Gene description	Gene symbol	Δ mTERC <sup>+/+</sup> Vs mTERC <sup>-/-</sup> 0 h	Gene bank acc.#
1	Cytochrome P450, 2b9, phenobarbitol inducible	Cyp2b9	-15.24	M21855

2	Cytochrome p450, 2b10, phenobarbital inducible type b	Cyp2b10	-2.30	M21856
3	Epidermal growth factor	Egfr	2.23	L06864
4	Retinoic acid early transcript gamma	Raet1c	2.16	D64162

$\Delta$  Fold change, Acc.# Accession number

From the differentially regulated genes in the micro-array experiments comparing resting liver and regenerating liver at 30-36 hours after PH between mTERC<sup>+/+</sup> mice and G3 mTERC<sup>-/-</sup> mice 8 target genes, which have a role in cell cycle regulation, were chosen and their differential expression was confirmed by rt-PCR (Table 3.4.5) with specific primers to each gene. The gene list include 4 downstream targets of p53 (p21, plk, Gadd45g, and KLF-4) which were all up-regulated in G3 mTERC<sup>-/-</sup> mice, two of these genes (p21 and Gadd45g) have been previously related to replicative senescence and DNA-damage response that leads to G1/S arrest (124, 125).

**Table 3.4.5** Differentially expressed cell cycle regulating genes at G<sub>0</sub>-G<sub>1</sub>/S transition in G3 mTERC<sup>-/-</sup> mice compared with mTERC<sup>+/+</sup> confirmed by real time quantitative PCR

N o	Gene description	Symbol	$\Delta$ RT- PCR	Function	Gene bank
1	Cyclin dependent kinase inhibitor 1A, p21	Cdkn1a	6.02	Senescence, DNA damage response, cell cycle regulation	Aw048937
2	Fas associated factor 1	Faf1	-4.08	Apoptosis	U39643
3	Growth arrest and DNA damage inducible	Gadd45	5.09	DNA damage response, Cell cycle arrest	Af055638
4	Krupple like factor 4	Klf4	5.77	DNA damage response	U20344
5	Nucleobindin2	Nucb2	12.9	Cell cycle regulation, growth arrest	Aj222586
6	P <sup>87</sup> Wee1 kinase	Wee1	-5.93	DNA damage response, cell cycle regulation	D30743
7	Polo-like kinase	Plk	8.63	DNA damage response, cell cycle regulation	Av305987
8	Protein kinase inhibitor p <sup>58</sup>	Prkri	3.60	Growth regulation	U28423

$\Delta$  – fold change of gene expression



**Table 3.4.6** Differential expression of eight target genes are confirmed by RT-PCR with specific primers and their comparative expression levels with microarray analysis

<b>No.</b>	<b>Gene</b>	<b><math>\Delta</math> RT- PCR</b>	<b><math>\Delta</math> Micro array</b>
1	Nucb2	12.90	17.51
2	Prkri	3.60	2.95
3	Plk	8.63	13.74
4	P21	6.02	8.63
5	Gadd45g	5.09	4.38
6	Faf1	-4.08	-4.62
7	Wee1	-5.93	-6.36
8	Klf4	5.77	4.03

$\Delta$ -Fold change

### **3.5 Cells with sufficient telomere reserves in G3 mTERC<sup>-/-</sup> mice compensate for impaired organ regeneration by an additional round of replication**

Synchronized liver regeneration in response to two-thirds partial hepatectomy (PH) takes approximately one and half rounds of replication to restore organ mass within one week after PH (101, 102). In the C57BL/6 mouse-strain used in our studies the first peak stage of S-phase was observed at 48 hours and was followed by a smaller second peak at 96 hours after PH (Figure 3.5.1). We evaluated S-phase onset and progression in response to PH in mTERC<sup>+/+</sup> mice and G3 mTERC<sup>-/-</sup> mice by BrdU pulse-labeling (Figure 3.5.1A-E). In response to PH the timing of the onset and the peak stages of S-phase were superimposable in mTERC<sup>+/+</sup> and G3 mTERC<sup>-/-</sup> mice. Nevertheless, the percentage of liver cells participating in the first round of replication was significantly lower in G3 mTERC<sup>-/-</sup> mice compared to mTERC<sup>+/+</sup> mice (Figure 3.5.1 C, D, E). In contrast, a significantly higher fraction of liver cells entered a second round of replication in G3 mTERC<sup>-/-</sup> mice compared to mTERC<sup>+/+</sup> mice (Figure 3.5.1 D, E).

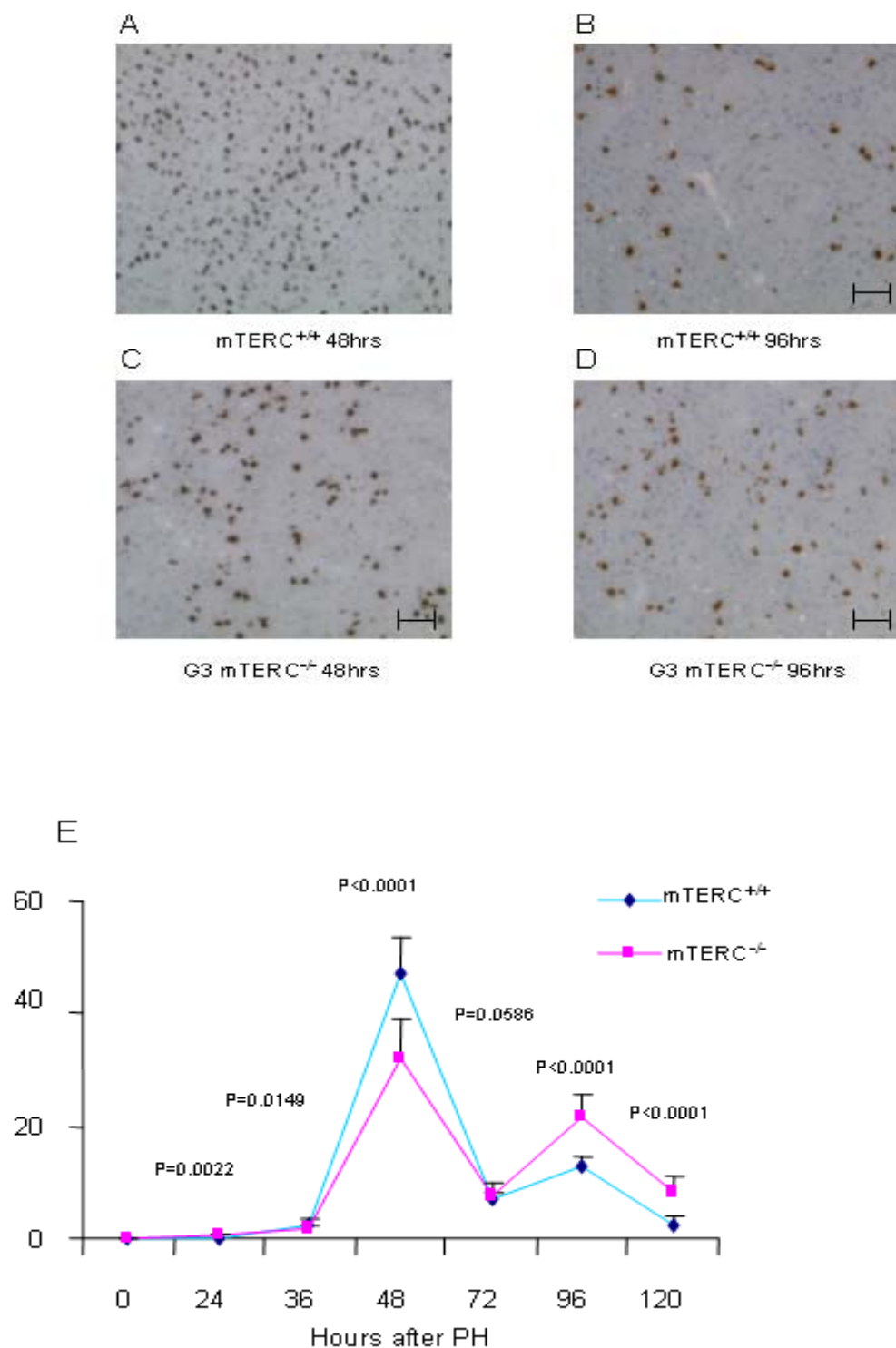


**Figure 3.5.1 (A-D)** Representative photographs of BrdU staining pattern at the two peak stages of S-phase in mTERC<sup>+/+</sup> and G3 mTERC<sup>-/-</sup> mice (Magnification bar: 150  $\mu$ m). **(E)** Percentage of BrdU positive cells at different time points after PH in mTERC<sup>+/+</sup> and (G3) mTERC<sup>-/-</sup> mice as determined by 2-hours of BrdU pulse labeling. mTERC<sup>+/+</sup> mice show a higher percentage of BrdU positive cells ( $47.03 \pm 6.33\%$ ,  $n=5$ ) at the first peak stage of S-phase (48hrs after PH) compared to G3 mTERC<sup>-/-</sup> mice ( $32.31 \pm 6.65\%$ ,  $n=5$ ,  $p<0.0001$ ). In contrast, at the second peak stage of S-phase (96h after PH) G3 mTERC<sup>-/-</sup> mice show higher percentage of BrdU-positive cells ( $21.58 \pm 4.24\%$ ,  $n=5$ ) compared to mTERC<sup>+/+</sup> mice ( $12.66 \pm 1.69\%$ ,  $n=5$ ,  $p<0.0001$ ).

To test whether impaired S-phase entry would impact on organ regeneration and whether the elevated second round of replication could compensate for impaired regeneration we followed the relative liver weight (liver weight/total body weight) of mTERC<sup>+/+</sup> and G3 mTERC<sup>-/-</sup> mice at different time points after PH. In parallel to the time course of S-phase, the liver weight of G3 mTERC<sup>-/-</sup> mice compared to mTERC<sup>+/+</sup> mice was significantly decreased after the first round of replication, 72 hours after PH (relative liver weight: 2.27% in G3 mTERC<sup>-/-</sup> mice compared to 2.74% in mTERC<sup>+/+</sup> mice,  $p=0.001$ ). In agreement with our hypothesis that liver cells with sufficient telomere reserves accomplished organ regeneration in G3 mTERC<sup>-/-</sup> mice by entering a second round of replication the liver weight was normalized in G3 mTERC<sup>-/-</sup> mice after the second round of replication, 120 hours after PH. Similarly, the difference in total number of BrdU labeled cells (after long-term labeling) between G3 mTERC<sup>-/-</sup> and mTERC<sup>+/+</sup> mice (Figure 3.1.1A) was significantly reduced after the second round of replication as compared to first round of replication (-4.69%,  $p=0.0274$ ).

### **3.6 Inhibition of S-phase entry, impaired G2/M progression, and additional round of cell division in regenerating liver of G3 mTERC<sup>-/-</sup> mice**

Together, our data indicated that impaired liver regeneration was due to inhibition of cell cycle re-entry in a sub-population of cells with critically short telomeres in G3 mTERC<sup>-/-</sup> mice but was compensated for by an additional round of replication by liver cells with sufficient telomere reserves capable of proliferation. An alternative explanation was that a sub-population of resting liver cells in G3 mTERC<sup>-/-</sup> mice was not in the G<sub>0</sub> stage but arrested in G2/M and was released from this block to exit mitosis and therefore re-entered the cell cycle at a delayed time-point after PH. To test this possibility cell cycle analysis was carried out by flow cytometry on resting and regenerating livers of mTERC<sup>+/+</sup> and G3 mTERC<sup>-/-</sup> mice (Figure 3.6.2).

Since in mouse liver a relatively high percentage of cells are bi-nucleated this analysis was carried out on cell nuclei, although cytopspins on liver cells did not show a difference in the percentage of mono-nuclear ( $22.51\pm7.77$  vs  $25.66\pm3.83$ ,  $p=0.2645$ ) as well as bi-nucleated ( $76.99\pm8.90$  vs  $74.32\pm3.82$ ,  $p=0.395$ ) cells in mTERC<sup>+/+</sup> and G3 mTERC<sup>-/-</sup> mice (Figure 3.6.1 A-C).

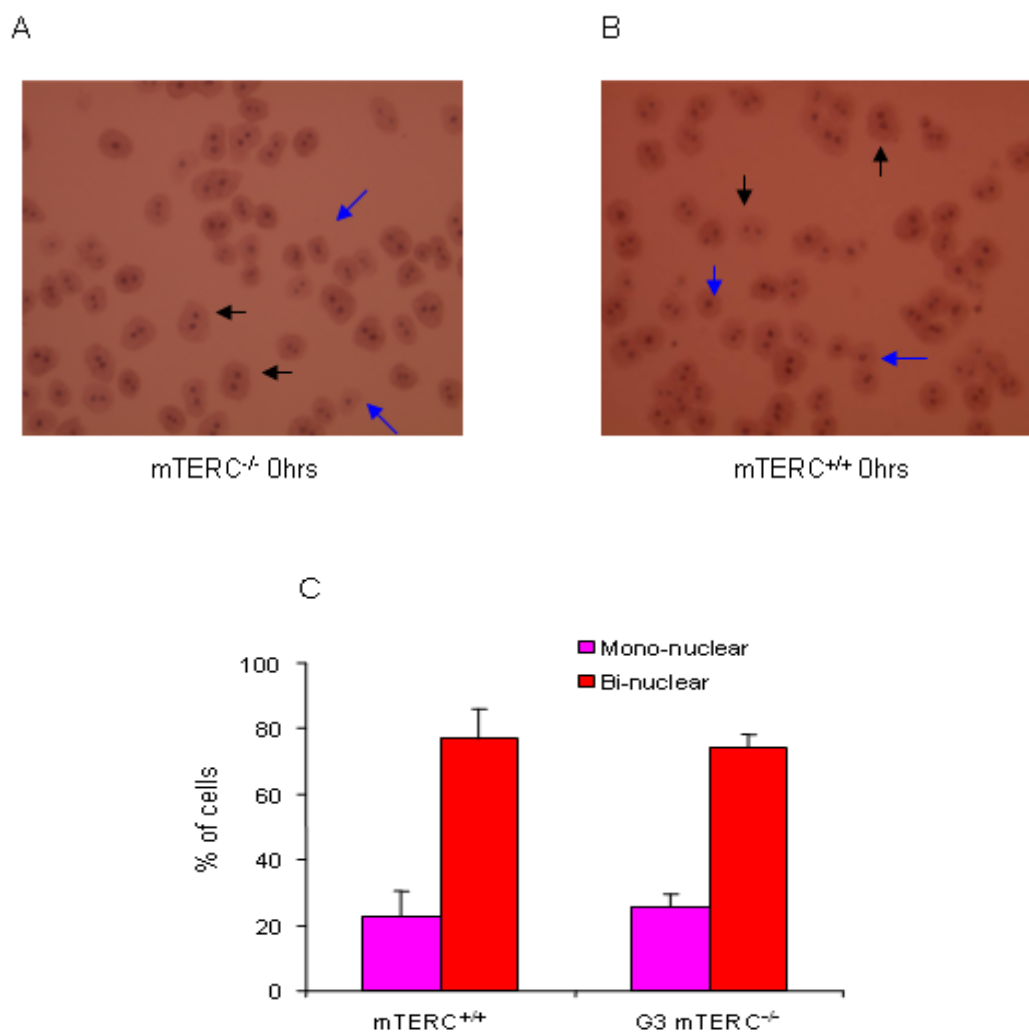


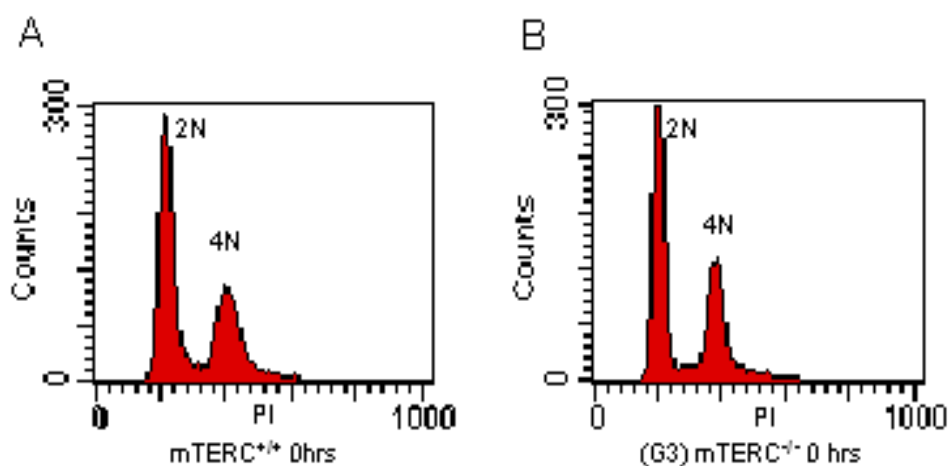
**Figure 3.6.1** The initial composition of the liver is similar in G3 mTERC<sup>-/-</sup> and mTERC<sup>+/+</sup> mice. **(A-B)** Representative H&E stained photographs of isolated liver cells from G3 mTERC<sup>-/-</sup> and mTERC<sup>+/+</sup> at quiescent stage (Blue arrows indicate mono-nuclear cells and black arrows indicate bi-nuclear cells). **(C)** Histogram showing the percentage of mono-nuclear ( $22.51 \pm 7.77$  vs  $25.66 \pm 3.83$ ,  $p=0.2645$ ) as well as bi-nucleated ( $76.99 \pm 8.90$  vs  $74.32 \pm 3.82$ ,  $p=0.395$ ) cells in mTERC<sup>+/+</sup> and G3 mTERC<sup>-/-</sup> mice.

In line with previous reports of flow cytometry on liver cell nuclei of several strains of mice (126, 127) our study revealed that beside a cell population with a 2n DNA content a proportion of resting liver cell nuclei had 4n DNA content. Cell cycle analysis of resting liver cell nuclei from G3 mTERC<sup>-/-</sup> and mTERC<sup>+/+</sup> mice revealed a similar distribution of nuclei with 2n and 4n DNA content in both groups (Table 3.6.1, Figure 3.6.2 A-B). In line with the BrdU-staining data the FACS analysis revealed that 48 hours after PH the overall number of cells in S-phase was significantly lower in G3mTERC<sup>-/-</sup> compared to mTERC<sup>+/+</sup> mice (Table 3.6.1, Figure 3.6.2 C-D, top panel). Interestingly, the suppression of S-phase entry in G3

mTERC<sup>-/-</sup> mice affected cells with 2n, 4n, and higher DNA content. Although it can not be excluded that some of the 4n and 8n cells were arrested at G2/M stage of the cell cycle, the inhibition of S-phase entry from 2n cells indicated that suppressed S-phase entry in G3 mTERC<sup>-/-</sup> was at least in part due to a pre-S-phase arrest.

As anticipated from the BrdU staining results (Figure 3.5.1) FACS analysis at 96 hours after PH revealed a higher percentage of liver cells in S-phase in G3 mTERC<sup>-/-</sup> compared mTERC<sup>+/+</sup> mice (Table 3.6.1, Figure 3.6.2 C-D, bottom panel). The fact, that this S-phase entry predominantly derived from cells with 4n and 8n DNA content suggested that the second peak of S-phase in G3 mTERC<sup>-/-</sup> mice did not result from 4n cells overcoming a G2/M-block to re-enter S-phase from a 2n-stage after completion of mitosis.

In addition to the above data on S-phase entry, the FACS analysis revealed an accumulation of cells with higher DNA content in G3mTERC<sup>-/-</sup> compared to mTERC<sup>+/+</sup> mice in the time course of liver regeneration following PH. These data are in line with previous reports of an impaired G2/M progression of regenerating liver cells in mTERC<sup>-/-</sup> mice (98). Cell cycle analysis 21 days after PH revealed again an almost similar ploidy distribution in mTERC<sup>+/+</sup> and G3 mTERC<sup>-/-</sup> mice (Figure 3.6.2 E-F) indicating that impaired G2/M progression in G3 mTERC<sup>-/-</sup> was either temporary or associated with decreased cell survival over time. It appears that the level of telomere dysfunction determines the proliferative fate of the cell and the activation of cell cycle checkpoints (Figure 3.6.3).



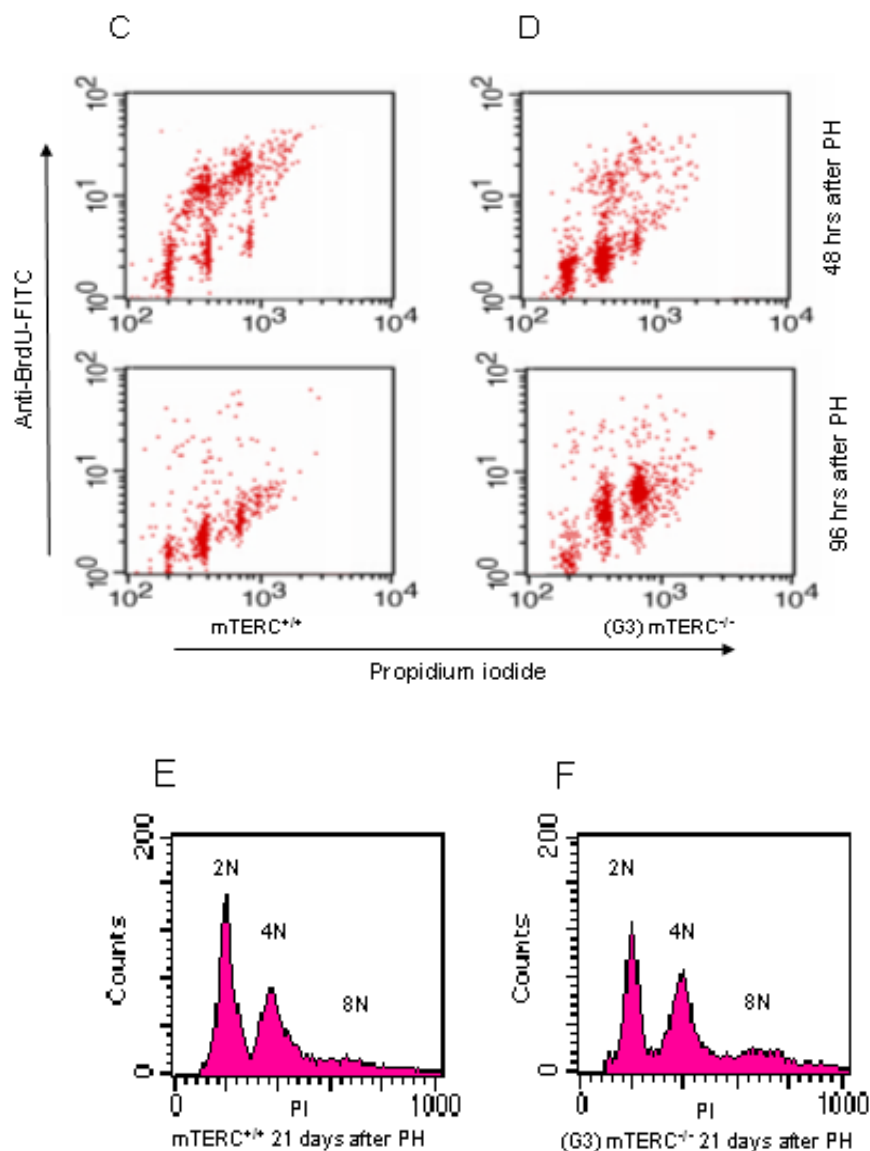


**Figure 3.6.2 (A-F)** Representative photographs of one of the five independent flow cytometric analysis of liver nuclei at each time point from mTERC<sup>+/+</sup> and G3 mTERC<sup>-/-</sup> mice. **(A) & (B)** Ploidy distribution of cell nuclei from quiescent liver showing an almost similar composition of 2n and 4n nuclei in mTERC<sup>+/+</sup> and G3 mTERC<sup>-/-</sup> mice. **(C) & (D)** Cell cycle profile of liver nuclei 48 hrs after PH (top panel) shows a significantly lower number of 2n ( $p=0.0031$ ) and 4n ( $p=0.0219$ ) nuclei are positive to BrdU in G3 mTERC<sup>-/-</sup> compared to mTERC<sup>+/+</sup> indicating that G1/S progression was inhibited in a subset of liver cells in G3 mTERC<sup>-/-</sup> mice. In contrast, an increased number of 2n ( $p=0.0516$ ), 4n ( $p=0.0005$ ) and 8n ( $p=0.0074$ ) nuclei incorporate BrdU at 96 hrs (lower panel) after PH in G3 mTERC<sup>-/-</sup> compared to mTERC<sup>+/+</sup> indicating that a higher number of liver cells in G3 mTERC<sup>-/-</sup> mice entered a second round of replication. Beside these differences in BrdU incorporation there is an accumulation of cells with higher DNA content in G3 mTERC<sup>-/-</sup> mice during the time course of liver regeneration indicating that G2/M progression was impaired. **(E) & (F)** Ploidy distribution of liver nuclei 21 days after PH showing again an almost similar DNA content in mTERC<sup>+/+</sup> and mTERC<sup>-/-</sup>: 2n ( $p=0.0683$ ), 4n ( $p=0.9831$ ) and 8n ( $p=0.0641$ ) indicating partial rescue of G2/M arrest in the course of time.

**Table 3.6.1** Ploidy distribution and cell cycle profile of quiescent and proliferating liver cells at the indicated time points after PH in mTERC<sup>+/+</sup> and G3 mTERC<sup>-/-</sup> as analysed by flow cytometry

Time	2N	4N	8N	2N S-phase	4N S-phase	8N S-phase
mTERC <sup>+/+</sup> 0 hrs	62.37±6.06	37.6±6.03	---	---	---	---
G3 mTERC <sup>-/-</sup> 0 hrs	58.94±4.88	41.09±4.93	---	---	---	---
mTERC <sup>+/+</sup> 48 hrs after PH	22.15±11.34	26.75±7.53	9.62±3.3	11.93±5.73	21.3±10.6	8.15±3.33
G3 mTERC <sup>-/-</sup> 48 hrs after PH	23.42±9.26	44.76±11.12	17±7.31	1.76±0.84	8.15±1.47	4.73±1.34
mTERC <sup>+/+</sup> 96 hrs after PH	43.18±17.25	40.87±13.46	10.98±7.77	1.58±0.83	1.49±1.13	1.36±1.13
G3 mTERC <sup>-/-</sup> 96 hrs after PH	20.14±6.42	43.26±8.68	25.46±9.86	2.84±1.02	4.41±0.62	4.05±1.29
mTERC <sup>+/+</sup> 21 d after PH	49.93±2.64	42.97±2.79	6.24±1.33	---	---	---
G3 mTERC <sup>-/-</sup> 21 d after PH	42.89±0.72	42.92±1.68	14.43±2.77	---	---	---

### 3.7 Apoptosis does not account for the differences in the regenerative response between mTERC<sup>+/+</sup> and G3 mTERC<sup>-/-</sup>

To analyze the role of other factors than impaired cell cycle re-entry that could explain the decreased rate of proliferation in G3 mTERC<sup>-/-</sup> mice, we evaluated apoptosis in this system. Apoptosis has been linked to impaired organ regeneration of highly self-renewing organs in mTERC<sup>-/-</sup> mice (94) and is induced by telomere shortening in clonally regenerating hepatocytes in the setting of acute liver failure (98). We assessed the possible impact of apoptosis in our experimental system using the TUNEL assay. Following PH, TUNEL staining showed very low but similar rates of apoptosis in the liver of mTERC<sup>+/+</sup> and G3 mTERC<sup>-/-</sup> mice (Figure 3.7.1) suggesting that this process did not account for the differences in regenerative response. Given that apoptosis is predominantly present in the setting of telomere shortening coupled with extensive regenerative pressure in mTERC<sup>-/-</sup> mice (94, 98) it seems possible that limited apoptotic response to PH was indicative of the more moderate regenerative stress in this setting.

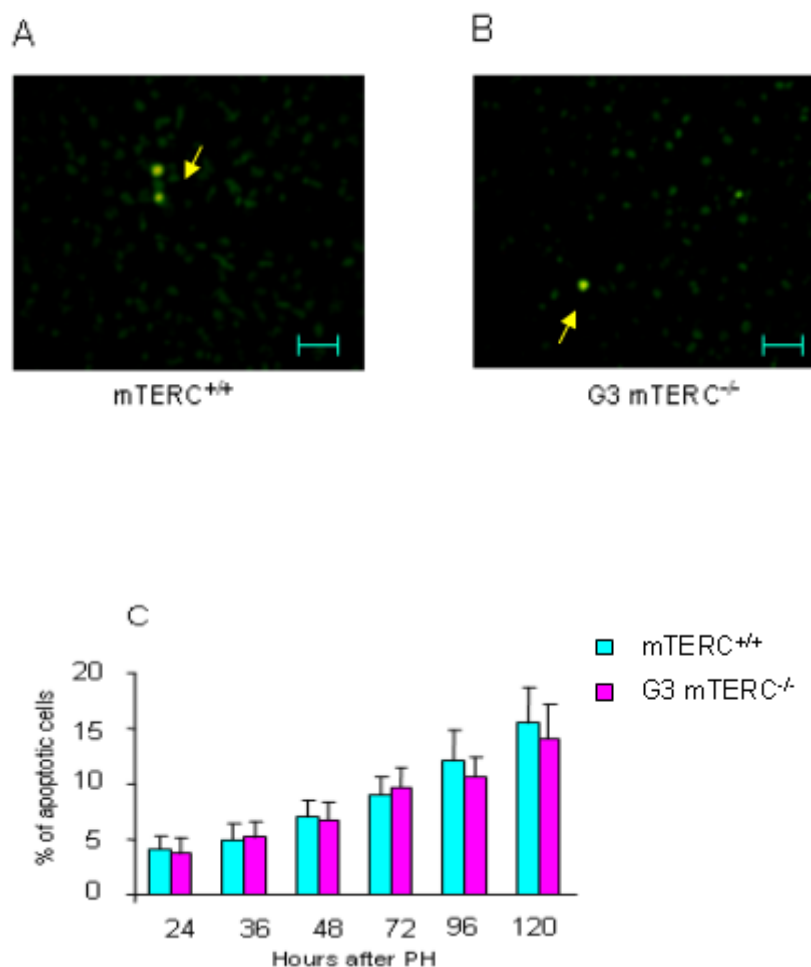


**Figure 3.7.1** Impaired organ regeneration induced by telomere shortening correlates to cellular senescence but not to apoptosis. **(A-B)** Representative photographs of TUNEL staining on liver sections of mTERC<sup>+/+</sup> and G3 mTERC<sup>-/-</sup> mice at 120 hours after PH (arrows indicate the apoptotic cells, magnification bar: 100µm). **(C)** Time-course changes of the TUNEL index in mTERC<sup>+/+</sup> and G3 mTERC<sup>-/-</sup> mice following 70% PH. The TUNEL index per 100 cells is similar in both groups.

### 3.8 Mitogenic responses are not disrupted by telomere shortening and are essential to reveal senescence phenotype in mTERC<sup>-/-</sup> mice

Initial mitogen responses such as the production of growth factors and cytokines are necessary for cell cycle re-entry and could be affected by telomere shortening. One of the prominent players in priming the liver cells to re-enter the cell cycle is IL-6 which after PH reaches peak levels 6-9 hours after operation (128, 129). Induction and peak levels of IL-6 in response to PH were similar in mTERC<sup>+/+</sup> and G3 mTERC<sup>-/-</sup> mice (Figure 3.8.1) indicating that other factors than the initial mitogen response inhibited cell cycle re-entry in liver cells with critical short telomeres. These data indicate that inhibition of cell cycle re-entry of a



fraction of liver cells during liver regeneration in G3 mTERC<sup>-/-</sup> mice is linked to cellular senescence induced by critical telomere shortening rather than impaired mitogenic responses or activation of apoptosis.

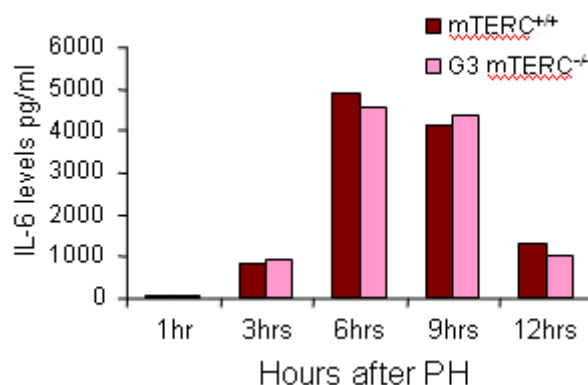


**Figure 3.8.1** IL-6 serum levels in mTERC<sup>+/+</sup> and G3 mTERC<sup>-/-</sup> mice show no difference in the induction and at peak stage in response to PH.

To test whether mitogen-stimulation would alter the replicative senescence phenotypes induced by telomere shortening, we monitored SA-β-Gal activity in quiescent liver and liver stimulated to divide in mTERC<sup>-/-</sup> and mTERC<sup>+/+</sup> mice. We used mTERC<sup>-/-</sup> mice of the first generation (G1), which lack telomerase activity but have long telomere reserves and no apparent phenotype (93), as well as G3 mTERC<sup>-/-</sup> mice, which have critically short telomeres (Figure 3.8.2A-D). The quiescent livers has very little mitotic activity with over 95% of the cells in the G<sub>0</sub>-stage of the cell cycle, but in response to PH over 90% of liver cells participate in organ regeneration and restore organ mass within 1 week (101, 102).

As described above there was an overall higher prevalence of β-Gal positive liver cells in G3 mTERC<sup>-/-</sup> mice harboring critically short telomeres compared to mTERC<sup>+/+</sup> mice (Figure 3.3.1). The increased incidence of SA-β-Gal positive cells in G3 mTERC<sup>-/-</sup> mice was mitogen dependent showing a strong increase after PH (Figure 3.8.2 A and D). In contrast mTERC<sup>+/+</sup> and G1 mTERC<sup>-/-</sup> mice showed only a slight increase in β-Gal positive cells (Figure 3.8.2 A-C) indicating that induction of SA-β-Gal activity *in vivo* depends on both telomere shortening and mitogen stimulation. The increase of β-Gal positive liver cells in G3 mTERC<sup>-/-</sup> mice after PH followed increased serum levels of IL-6 - the prominent mitogen regulating liver cell cycle re-entry in response to organ damage- and there was no difference in the mitogenic response between mTERC<sup>+/+</sup> and G3 mTERC<sup>-/-</sup> mice (Figure 3.8.1).

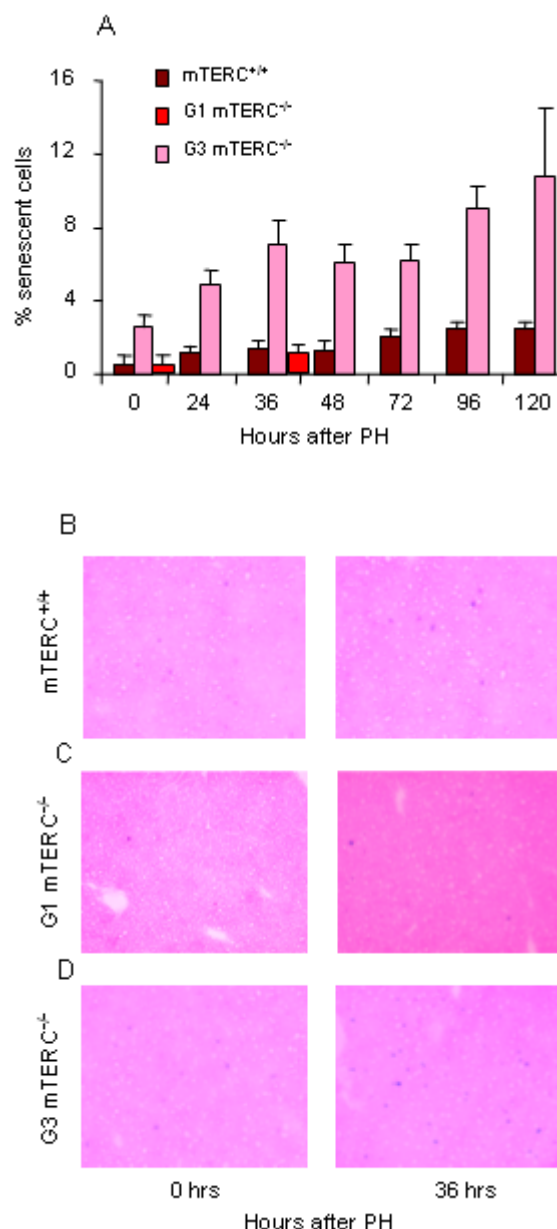


**Figure 3.8.2** The prevalence of SA-β-Gal staining in response to telomere shortening *in vivo* is mitogen dependent. **(A)** Histogram of the percentage of SA-β-gal positive cells in quiescent and regenerating liver of mTERC<sup>+/+</sup>, G1 mTERC<sup>-/-</sup> and G3 mTERC<sup>-/-</sup> mice showing a significant increase of β-gal positive cells in G3 mTERC<sup>-/-</sup> liver after PH but not in mTERC<sup>+/+</sup> liver. Note: SAβ-gal staining was analysed only on quiescent livers and 36 hrs after PH for G1 mTERC<sup>-/-</sup> which is comparable with mTERC<sup>+/+</sup> **(B-D)** Representative photographs of β-gal staining on liver samples from mTERC<sup>+/+</sup>, G1 mTERC<sup>-/-</sup> and G3 mTERC<sup>-/-</sup> at quiescence stage and 36 hrs after PH.

### 3.9 mTERC<sup>-/-</sup> have critically short telomeres and further telomere shortening in the subsequent cell division is not necessary to reveal increased senescence phenotype

Telomere length analysis by q-FISH showed the prevalence of critically shorter telomeres in G3 mTERC<sup>-/-</sup> compared to mTERC<sup>+/+</sup> (Figure 3.9.1 A-D). To test whether mitogen

stimulation itself is responsible for the increased incidence of senescence phenotypes or whether further telomere shortening in the subsequent cell division in response to mitogen stimulation lead to this phenomenon, we have analysed the S phase activity by two hours of BrdU pulse labeling in mTERC<sup>+/+</sup> and G3 mTERC<sup>-/-</sup>. Analysis of S-phase activity showed almost zero activity at 36 hrs but a sharp peak at 48 hrs after PH (Figure 3.9.1E-G) indicating that the senescence phenotypes in G3 mTERC<sup>-/-</sup> liver, which became detectable at 36 hour after PH (Figure 3.8.1), were independent of further telomere attrition induced by an additional round of cell division.

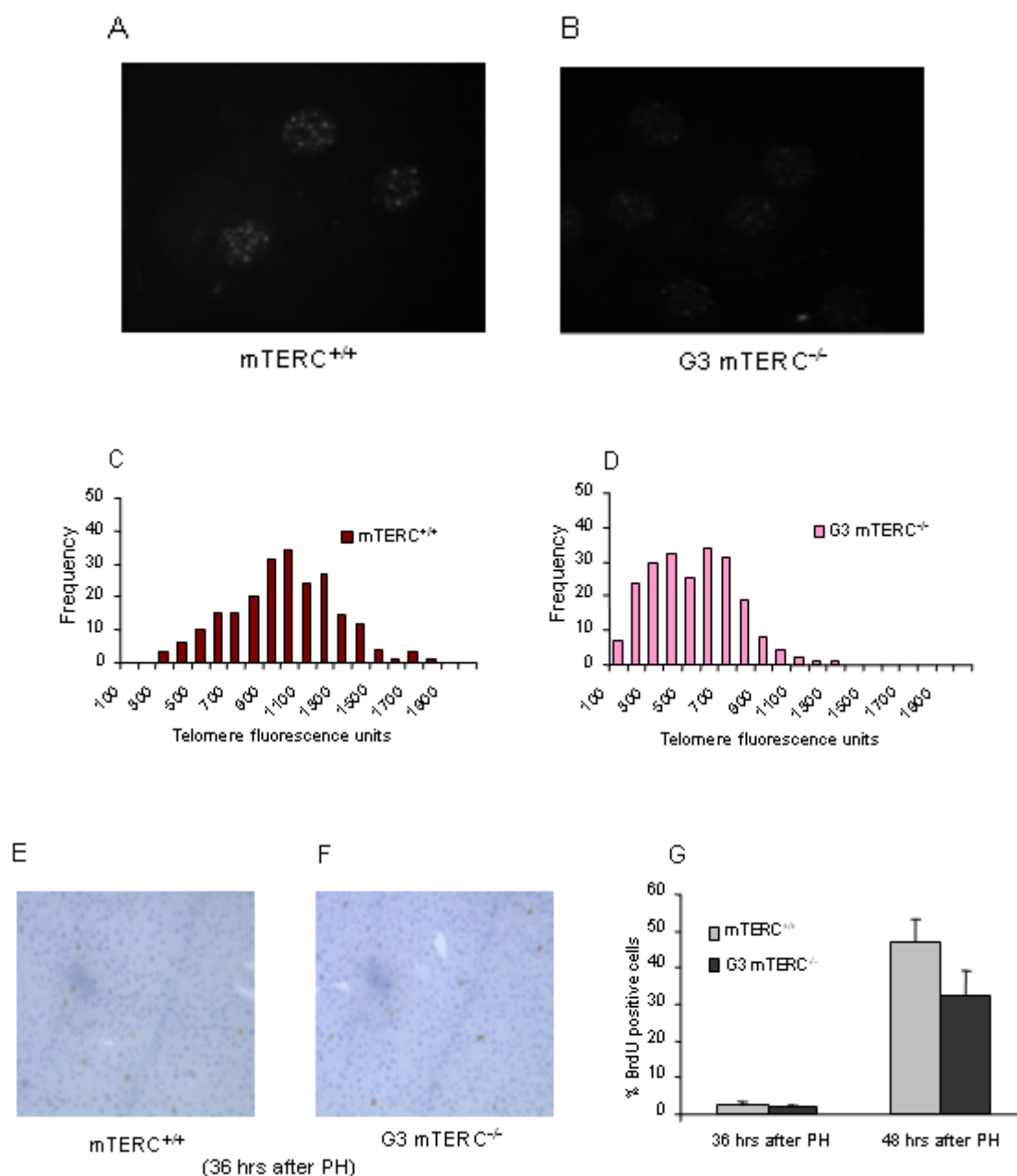
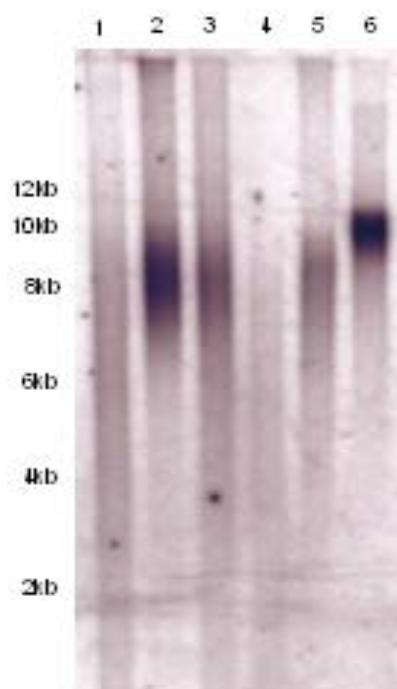


**Figure 3.9.1 (A-B)** Representative photographs of quantitative fluorescence in situ hybridization (Q-FISH) on interphase nuclei of liver cells from mTERC<sup>+/+</sup> and G3 mTERC<sup>-/-</sup>

mice hybridized with a telomere specific probe Cy3-OO-(CCCTAA)<sub>3</sub>. **(C-D)** Histogram on the distribution of mean telomere fluorescence intensities in nuclei of liver cells from G3 mTERC<sup>-/-</sup> mice (n=3) and mTERC<sup>+/+</sup> mice (n=3) showing a significantly reduced overall mean in G3 mTERC<sup>-/-</sup> mice compared to mTERC<sup>+/+</sup> mice ( $565 \pm 83.17$  Vs  $1027 \pm 135.23$ ,  $p < 0.0001$ ). **(E-F)** Representative photographs of BrdU staining pattern at the onset of S-phase (36 hrs after PH) in mTERC<sup>+/+</sup> and G3 mTERC<sup>-/-</sup> mice (Magnification bar: 150  $\mu$ m). **(G)** Percentage of BrdU positive cells at 36 hrs ( $2.3 \pm 1.08\%$  Vs  $1.75 \pm 0.77\%$ ) and 48 hrs ( $44.03 \pm 6.33\%$  Vs  $32.31 \pm 6.65\%$ ) after PH in mTERC<sup>+/+</sup> and G3 mTERC<sup>-/-</sup> mice as determined by 2hrs of BrdU pulse labeling.

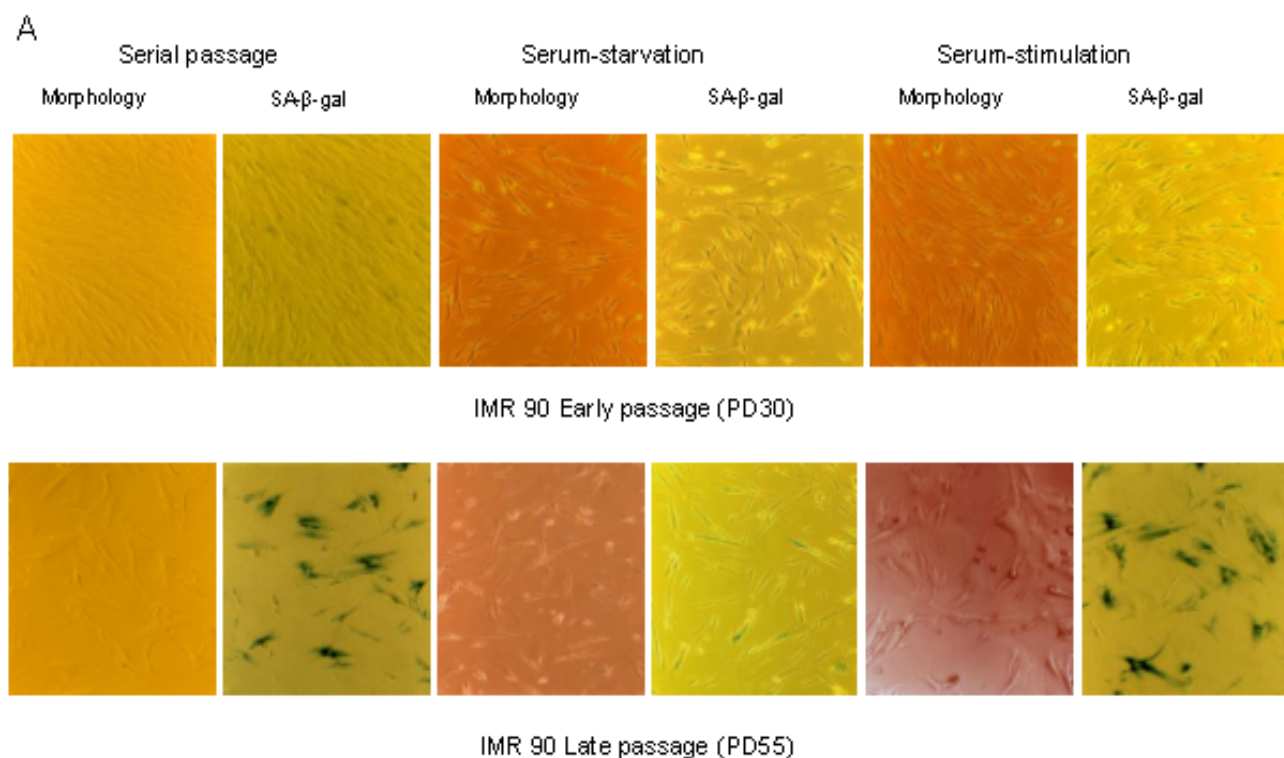
### 3.10 The *in vitro* phenotype of replicative senescence induced by telomere shortening is dependent on mitogen stimulation

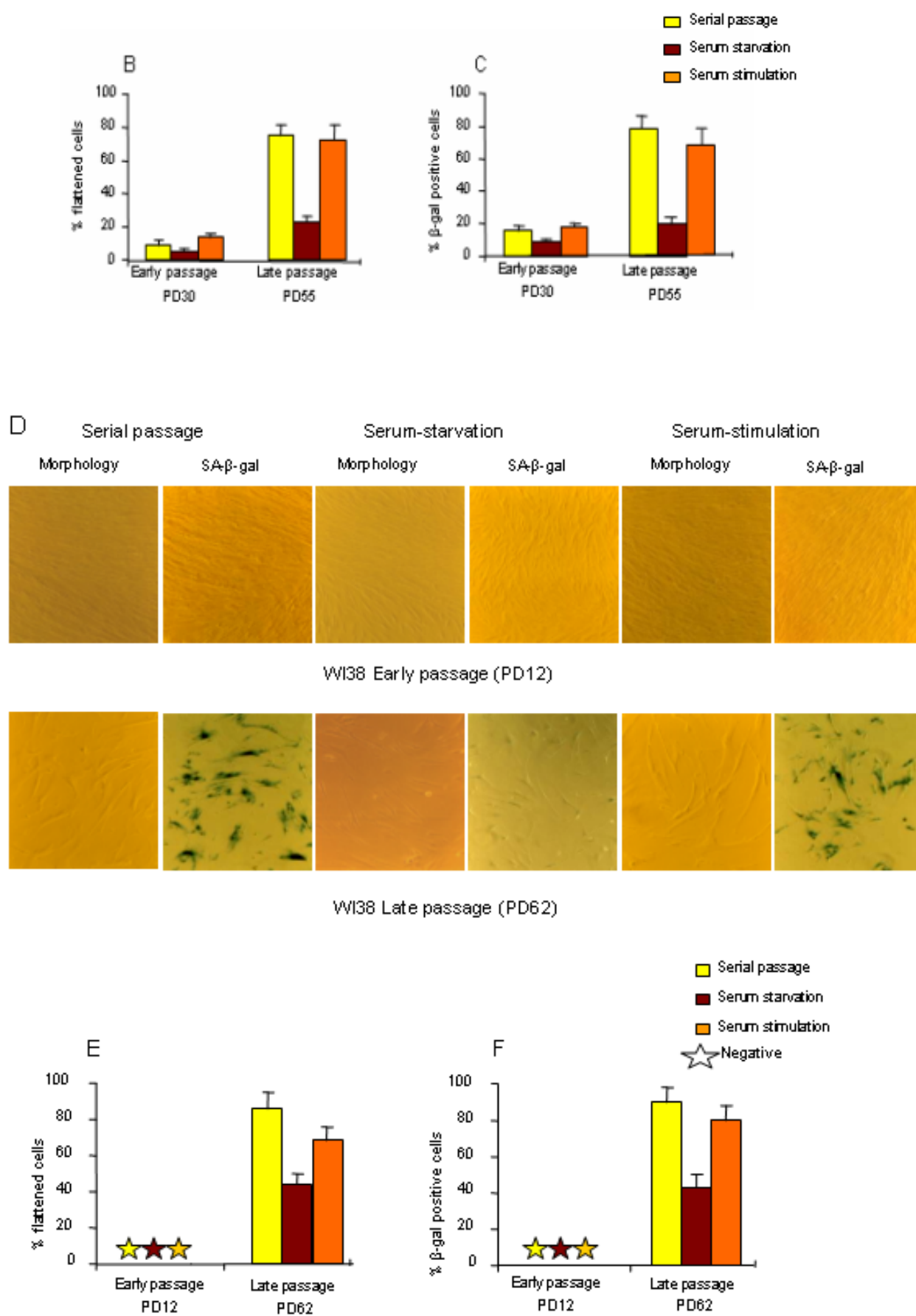
The modulations of senescence phenotype in response to mitogen stimulation *in vivo* lead us to explore this process further in detail. To analyze whether the senescence phenotype and signaling induced by telomere shortening is constitutively operative at the same level or amplified by mitogenic stimuli we explored this phenomenon in human fibroblast cultures using 3 different cell lines IMR90 (Human fetal lung fibroblasts), WI38 (human embryo lung fibroblasts) and HK-1 (human adult fibroblasts) (130-132). Serial passaging of primary human fibroblasts leads to telomere shortening after each round of cell division and after 60-80 PD's they enter replicative senescence due to critical telomere shortening. As described in previous studies telomeres were significantly shorter in late passage cells as compared to early passage (Figure 3.10.1) (130-132).



**Figure 3.10.1** The telomere restriction fragment (TRF) length was determined from early, late and hTERT IMR90 and HK1 cells. Representative In-gel southern blotting photograph, 1. Late passage (PD55) IMR90, 2. Early passage IMR90 (PD30) 3. hTERT-IMR90 (PD68) 4. Late passage HK1 (PD60) 5. Early passage HK1 (PD9) 6. hTERT-HK1 (PD90). The mean TRF length is significantly shorter in late passage IMR90 (5.7 kb) compared with early passage (8.5 kb) or hTERT-IMR90 (7.8 kb). The mean TRF length is significantly shorter in late passage HK1 (4.8 kb) compared with early passage (7.6 kb) or hTERT-HK1 cells (9.2 kb).

Decreasing cell proliferation at the onset of senescence correlated with an increasing prevalence of the markers of cellular senescence: 1. SA- $\beta$ -Gal activity at pH6 and 2. Senescence cell morphology (flattened, irregular cells with enlarged cytoplasm). Consistent with previous studies the percentage of cells being positive for both markers reached >60% in late passage cells whereas it was <20% at early passage (Figure 3.10.2). To test whether these markers of replicative senescence were modulated by altered mitogen stimulus their prevalence was quantitated 1. under serial passage, 2. after serum starvation (0.1% FBS for 120 hrs), and 3. after re-stimulation (10% FBS for 24 hrs) in early and late passage cells. Interestingly these experiments revealed that the increase in the percentage of cells showing a senescence-morphology or positive  $\beta$ -Gal-staining at late passage was strongly dependent on serum stimulation but almost completely disappeared in response to serum starvation (Figure 3.10.2A-I). The diminution of senescence markers in late passage cultures was detectable as early as 48 hrs after serum starvation and re-appeared 24 hrs after serum-stimulation.





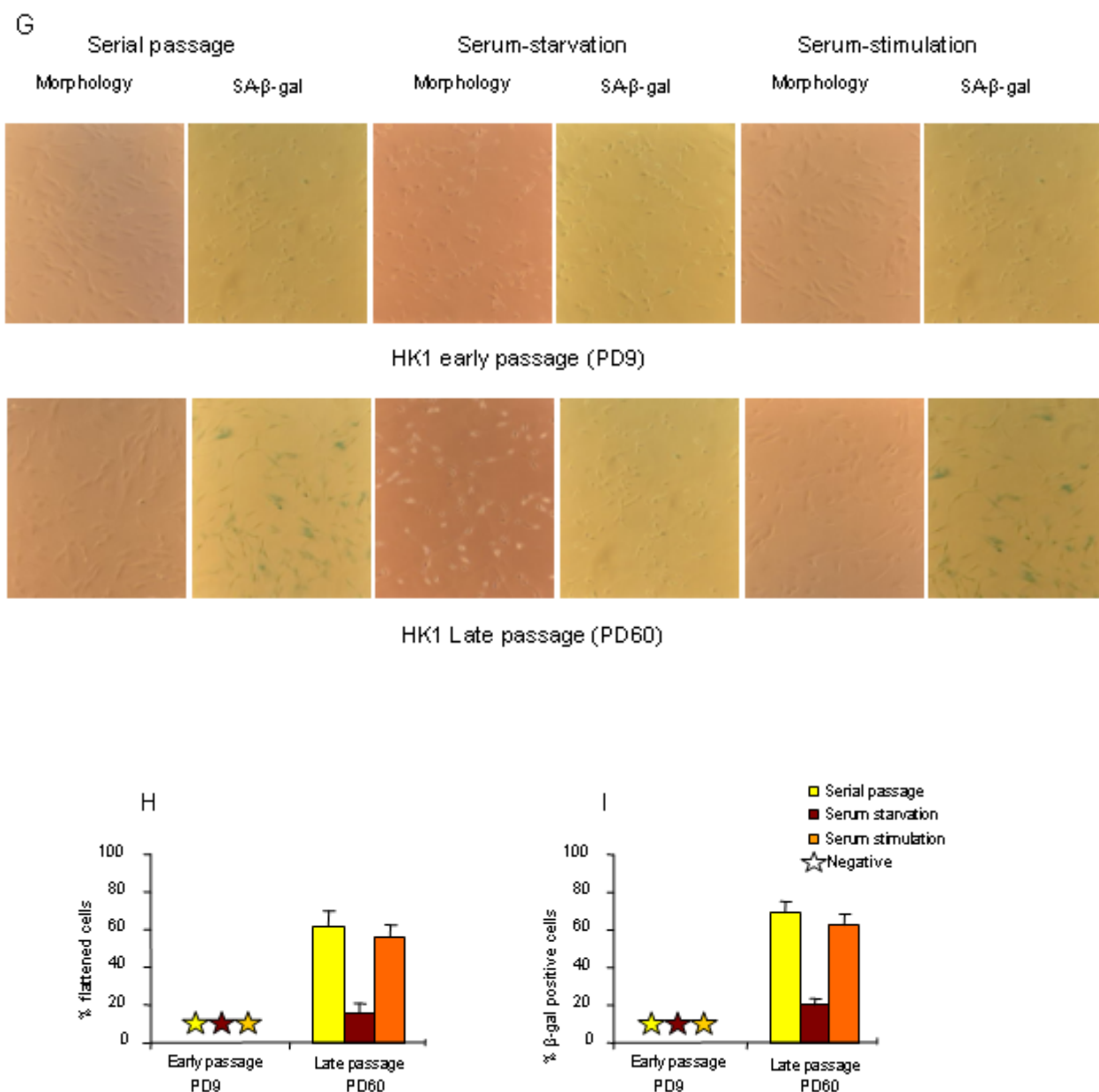


**Figure 3.10.2** The phenotype of replicative senescence of primary human fibroblasts is mitogen dependent. **(A)** Representative photographs of IMR90 cells at early passage, late passage at the indicated culture conditions. **(B, C)** Histogram showing the percentage of cells with senescent morphology **(B)** and the percentage of SA- $\beta$ -gal positive cells **(C)** in early (PD30) and late (PD55) passage IMR90 cells under serial passage in 10% FBS, after serum starvation in 0.1% FBS for 120 hrs, and after serum re-stimulation with 10% FBS for 24 hrs. The senescent morphology index and the number of SA- $\beta$ -gal positive cells for early passage IMR90 cells are low under all culture conditions. In contrast, late passage IMR90 show a high senescence morphology ( $75.36 \pm 6.14\%$ ) index and a high percentage of SA- $\beta$ -gal positive cells ( $78.34 \pm 7.62\%$ ) under serial passage, a significant diminution of senescence morphology ( $23.43 \pm 3.29\%$ ,  $p < 0.0001$ ) and  $\beta$ -gal activity ( $19.29 \pm 3.89\%$ ,  $p < 0.0001$ ) in response to serum starvation and a significant re-appearance of senescence morphology ( $72.9 \pm 8.17\%$ ,  $p < 0.0001$ ) and SA- $\beta$ -gal activity ( $67.58 \pm 8.86\%$ ,  $p < 0.0001$ ) in response to serum re-stimulation. **(D)** Representative photographs of early (PD12) and late (PD62) passage WI38 cells (PD75). **(E, F)** Histograms indicating the percentage of WI38 cells showing senescent morphology **(E)** and



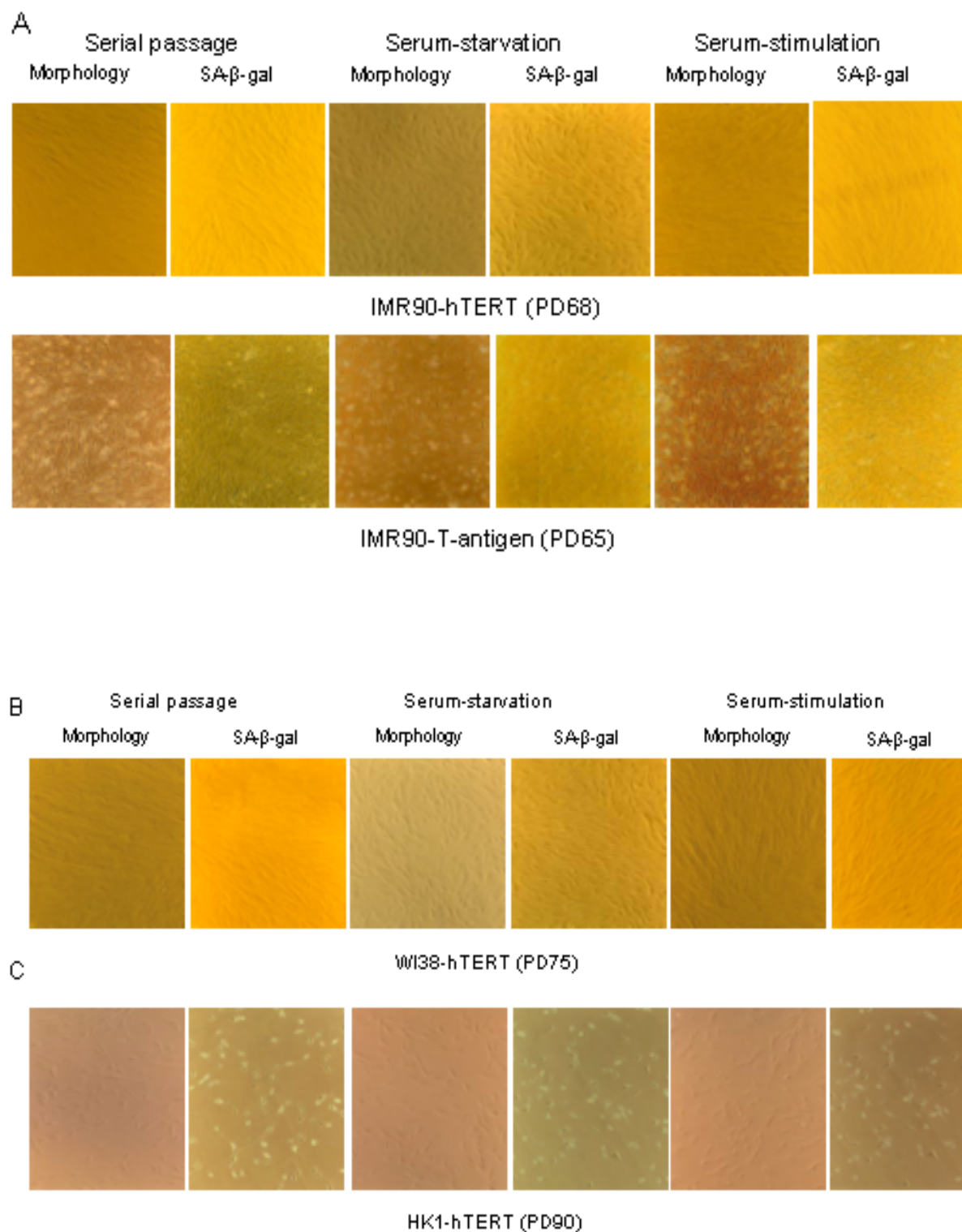
SA- $\beta$ -gal activity (**F**) in early (PD12) and late passage (PD62) under serial passage in 10% FBS, in response to serum starvation in 0.1% FBS for 120 hrs, and in response to serum-re-stimulation with 10% FBS for 24 hrs. Under serial passage late passage of WI38 cells show high rates of senescent morphology ( $85.62 \pm 9.69\%$ ) and SA- $\beta$ -gal activity ( $89.8 \pm 8.16\%$ ). Both markers are declined in response to serum starvation ( $44.27 \pm 5.52\%$  for senescence morphology,  $p < 0.0001$ , and  $43.2 \pm 6.56\%$  for SA- $\beta$ -gal activity,  $p < 0.0001$ ), but re-appeared in response to serum re-stimulation ( $68.06 \pm 8.19\%$  for senescence morphology,  $p < 0.0001$ , and  $79.69 \pm 9.05\%$  for SA- $\beta$ -gal activity,  $p < 0.0001$ ). (**G**) Representative photographs of early (PD9) and late passage (PD60) HK1 cells under different culture conditions. (**H-I**) Histograms indicating the percentage of HK1 cells showing senescent morphology (**H**) or SA- $\beta$ -gal activity (**I**) at early (PD9) and late passage (PD60) under serial passage in 10% FBS, in response to serum starvation in 0.1% FBS for 120 hrs, and in response to serum re-stimulation in 10% FBS. The early passage cells did not show any signs of senescence. Under serial passage late passage HK1 cells show high rates of senescent morphology ( $61.73 \pm 5.27\%$ ) and SA- $\beta$ -gal activity ( $68.93 \pm 6.11\%$ ). Both markers are declined in response to serum starvation ( $15.98 \pm 4.47\%$  for senescence morphology,  $p < 0.0001$ , and  $19.89 \pm 3.42\%$  for SA- $\beta$ -gal activity,  $p < 0.0001$ ), but re-appeared in response to serum re-stimulation ( $55.76 \pm 6.73\%$  for senescence morphology,  $p < 0.0001$ , and  $62.68 \pm 5.59\%$  for SA- $\beta$ -gal activity,  $p < 0.0001$ ).

To ensure that the phenotypes of senescence in late passage fibroblasts were induced by telomere shortening we performed an identical experiment on all 3 cell lines which had bypassed the replicative senescence by hTERT expression. The immortalization of WI38 by hTERT expression has been documented in previous studies (132), similarly hTERT expression is sufficient to immortalize HK-1 cells (S. Zimmermann and U. Martens, unpublished). There is some conflict on immortalization of IMR90 cells, however, in our laboratory conditions we have successfully established IMR90 cells that clearly by-passed the replicative senescence limit upon hTERT-over-expression (the cells were followed until PD115), which is in line with observations from other groups (133). It has been reported that even though TERT-expression elongates the lifespan of IMR90 cells they still reach a telomere-independent senescent arrest at very late passage (133). We can not exclude that such telomere independent factors impact on our *in vitro* data on IMR90 cells. However, the use of 3 different cell lines favors that our experiments are in fact relevant for replicative senescence induced by telomere shortening, which can be bypassed by hTERT expression.

Two of the three cell lines were tested and both of them showed telomere shortening upon serial passaging and both the cell lines showed telomere stabilization upon hTERT-expression (Figure 3.10.1) In all three cell lines there was no detectable senescence-morphology or  $\beta$ -Gal-staining at late passage independent of the culture conditions (Figure 3.10.3A-F). Similarly, simian virus T-antigen (SV40-T-Ag) expression, which blocks both the Rb and p53 pathways, which govern the senescence checkpoint (134), prevented induction of



senescence morphology and  $\beta$ -Gal activity in late passage IMR90 cells (Figure 3.10.3 A and D). Together, these data indicated that the classical senescence phenotype (induced by telomere shortening and bypassed by hTERT or SV40-T-Ag expression) in primary human cells can be modulated by altered mitogenic stimulation.



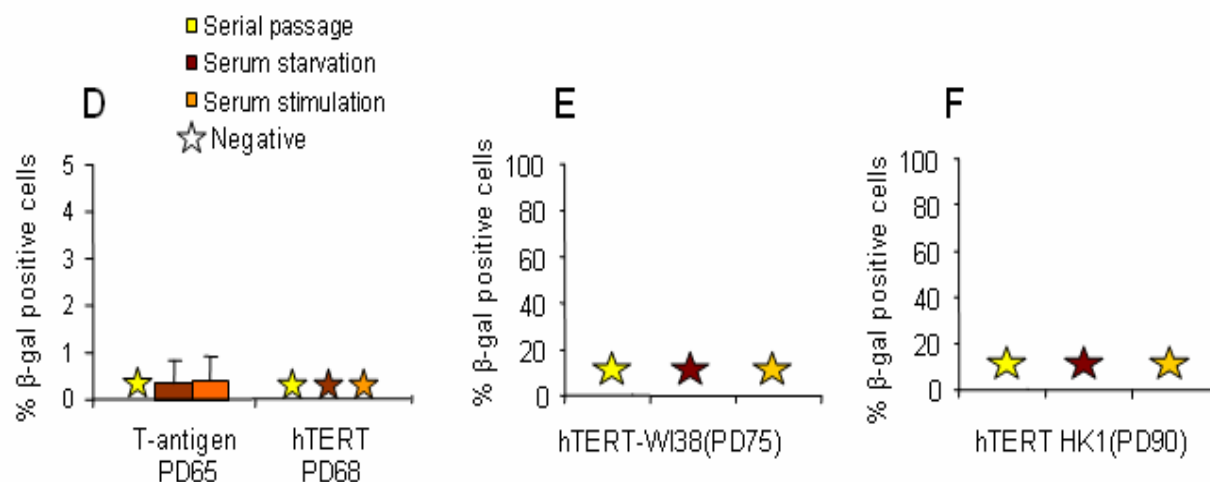


**Figure 3.10.3** (A) Representative photographs of hTERT expressing IMR90 cells at late passage (PD68), and SV40-T-Ag expressing IMR90 cells at late passage (PD65) showing no signs of either senescence morphology or SA-β-gal (B-C) Representative photographs of hTERT expressing WI38 cells at late passage (PD75), and hTERT expressing HK1 cells at late passage (PD90) showing no signs of either senescence morphology or SA-β-gal (D) Histogram showing the percentage of SA-β-gal positive cells in late passage IMR90 cells expressing SV-40 T-antigen (PD65) or hTERT (PD68) showing no senescence phenotype irrespective of the culture conditions. (E) Histogram showing absence of SA-β-gal positive cells in late passage (PD75) of hTERT-expressing WI38 cells in response to three different culture conditions. (F) Histogram showing absence of SA-β-gal positive cells in late passage (PD90) of hTERT-expressing HK1 cells at different culture conditions.

To rule out the possibility that further telomere shortening in the subsequent cell division might be the cause for this increased senescence phenotype in response to mitogenic stimulation we analyzed S-phase activity in IMR90 and HK1 cells. Early passage cells showed S-phase labeling under serial passage and resumption of replication 12-24 hrs after serum stimulation of serum starved cultures. In contrast, the late passage fibroblasts did not show any significant S-phase activity under serial passage or after serum stimulation of serum starved cultures (Figure 3.10.4, Table 3.10.1). These data excluded the possibility that the re-appearance of senescence phenotypes in response to serum stimulation of late passage human fibroblast cultures was due to further telomere shortening in subsequent cell division.

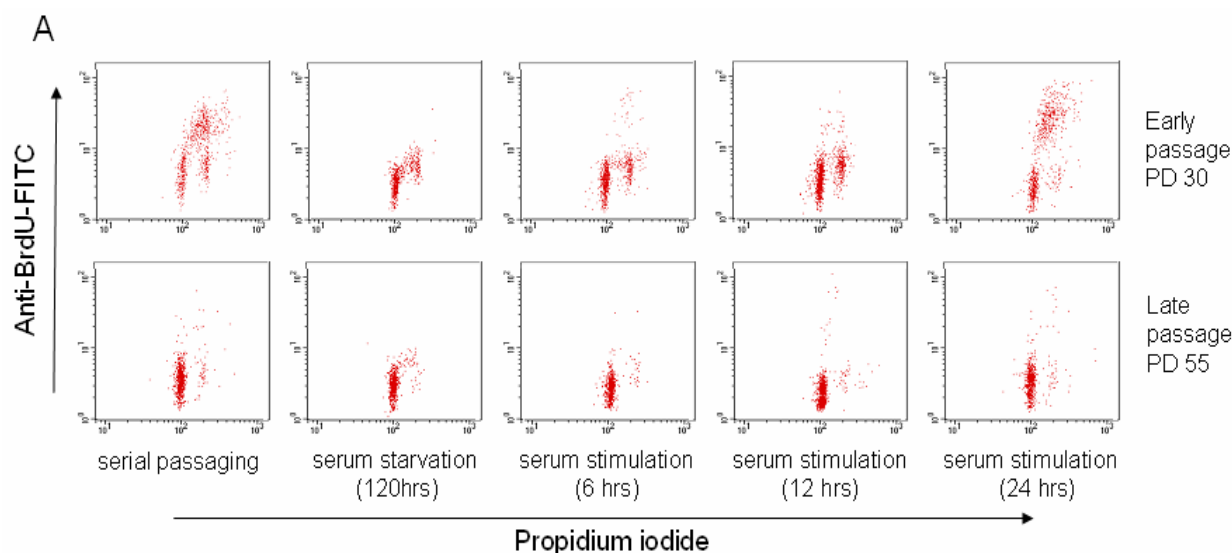


**Figure 3.10.4** Impaired cell cycle activity and accumulation of cells in G1 stage of the cell cycle in late passage. Representative photographs of one of the three independent flow cytometric analysis of early and late passage IMR90 cells at the indicated culture condition. About 90% of the late passage cells accumulated in G1 phase of the cell cycle even after 24 hrs of serum stimulation.

**Table 3.10.1** Cell cycle profile on early and late passage IMR90 and HK1 cells at the indicated time point and culture condition

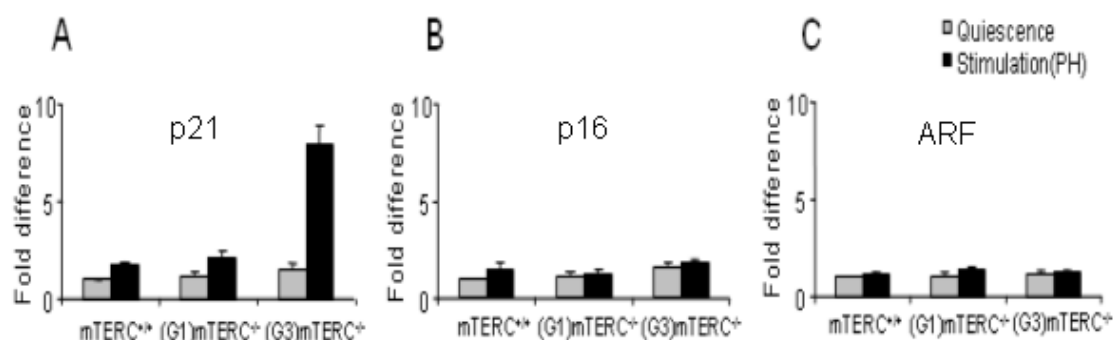
Culture condition	IMR 90 Early passage (PD30)			IMR 90 Late passage (PD55)		
	G1	S	G2/M	G1	S	G2/M
Serial passage	38.6±1.0	45.6±1.7	15.6±2.8	89.6±6.0	5.2±1.0	5.52±0.3
Starvation (120 hrs)	89.8±2.5	0.83±0.6	9.3±1.9	97.7±2.2	0.06±0.05	2.17±0.2
Stimulation (6 hrs)	81.4±2.0	4.2±0.3	14.2±1.8	96.1±5.1	1.0±0.5	3.1±0.1
Stimulation (12 hrs)	72.0±2.3	9.1±1.6	18.8±0.7	92.3±2.4	3.81±0.4	3.87±0.7
Stimulation (24 hrs)	31.7±3.2	60.5±2.1	7.6±1.8	87.6±4.9	7.0±0.7	5.35±0.4
Culture condition	HK1 Early passage (PD9)			HK1 Late passage (PD60)		
	G1	S	G2/M	G1	S	G2/M
Serial passage	35.4±2.2	53.0±0.2	11.5±2.1	81.7±1	11.2±1.7	6.92±1.3
Starvation (120 hrs)	90.7±0.4	0.93±0.2	8.3±0.5	97.0±2.0	0.0±0.0	2.90±2.0
Stimulation (6 hrs)	86.2±1.5	3.51±0.5	9.92±0.9	95.3±1.4	1.0±0.7	3.68±0.7
Stimulation	73.9±2.2	8.54±1.4	17.5±0.9	87.5±3.8	6.34±1.9	6.03±1.9

(12 hrs)						
Stimulation	30.4±4.0	61.6±6.4	7.6±2.1	78.5±4.6	13.0±2.7	8.36±1.9
(24 hrs)						

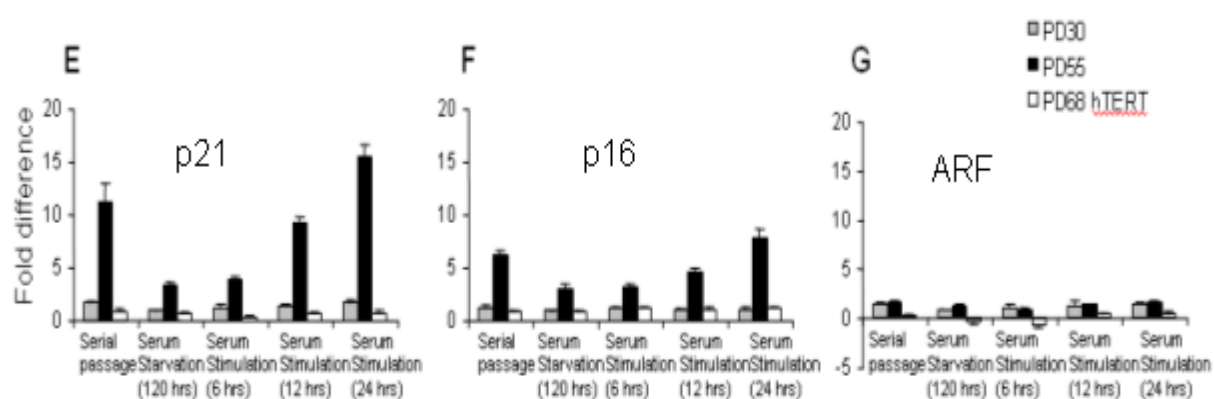
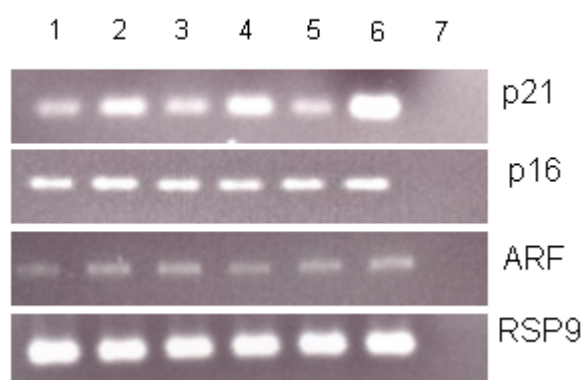
### 3.11 The enhanced expression of cell cycle inhibitors induced by telomere shortening is mitogen dependent.

To monitor molecular markers of replicative senescence we followed gene expression levels of cell cycle inhibitors regulating the senescence pathway, namely p21 and p16 (67, 135, 136) and expression levels of p19<sup>ARF</sup>, although its role in senescence is under debate (137, 138). As established in previous studies an increased expression of p21 was detected in late passage cells (135, 136) (Figure 3.11.1E-L). In our study an upregulation of p21 was identified in the regenerating liver of G3 mTERC<sup>-/-</sup> mice compared to mTERC<sup>+/+</sup> and G1 mTERC<sup>-/-</sup> mice (Figure 3.11.1A-D). Similarly an up-regulation of p16 was seen in late passage cells (136) (Figure 3.11.1E-L) but we did not observe an upregulation of p16 in the regenerating liver of G3 mTERC<sup>-/-</sup> mice (Figure 3.11.1A-D) in line with previously identified species differences in the regulation of p16 during senescence in mouse and human cells (13). We have not detected a significant up-regulation of p19<sup>ARF</sup> in either the *in vitro* or *in vivo* system (Figure 3.11.1).

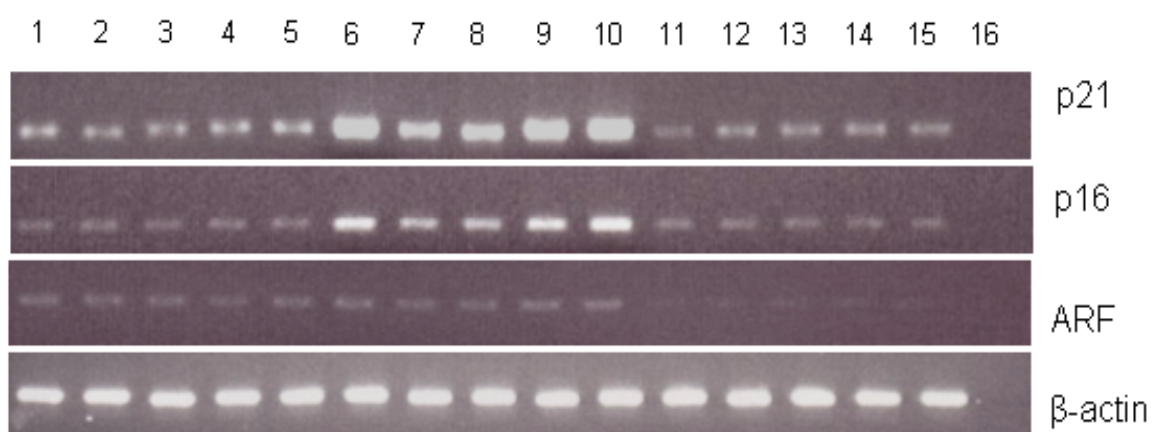
In accordance with our data on senescence morphology and SA-β-Gal-activity, the senescence-associated up-regulation of p21 in late passage cells and G3 mTERC<sup>-/-</sup> mice liver as well as the up-regulation of p16 in late passage cells were strongly induced when the cells were stimulated to enter the cell cycle by mitogen exposure (Figure 3.11.1A, D, E, F, H, I, J, L). Moreover, mitogen withdrawal reversed the up-regulation of these Cdk-inhibitors to a low, basal level when senescent late passage cells were transferred from serial passage in 10% FBS to serum starvation in 0.1% FBS (Figure 3.11.1 A, D, E, F, H, I, J, L).



D



H



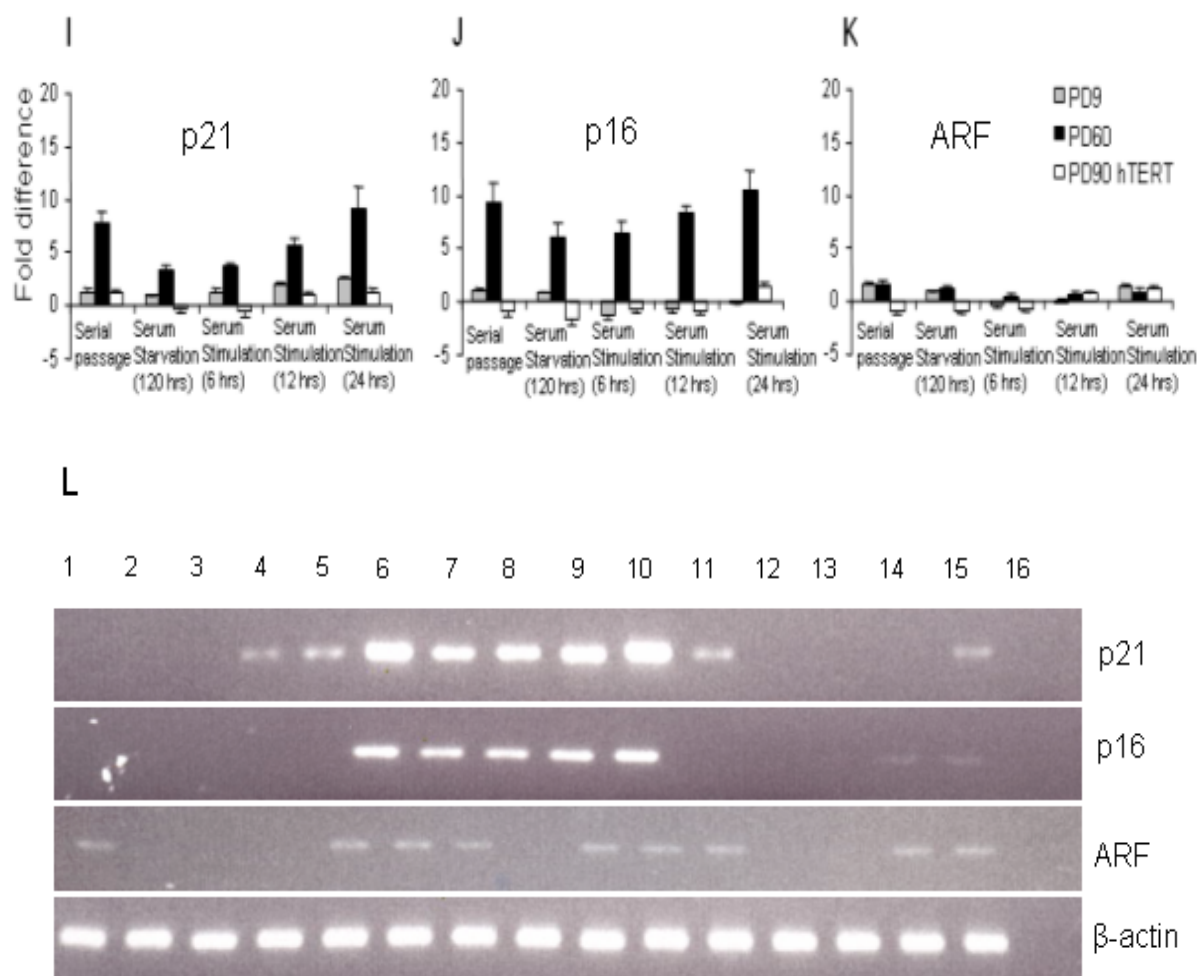


**Figure 3.11.1** Enhanced expression of cell cycle inhibitors associated with replicative senescence in response to telomere shortening is mitogen dependent. **(A-C)** Histograms on the level of mRNA expression of p21 **(A)**, p16 **(B)**, and p19<sup>ARF</sup> **(C)** in quiescent liver and regenerating liver (36hrs after PH) of mTERC<sup>+/+</sup>, G1 mTERC<sup>-/-</sup> and G3 mTERC<sup>-/-</sup> mice as revealed by RT-PCR. While p16 and p19ARF show no significant regulation, p21 was significantly over-expressed in G3 mTERC<sup>-/-</sup> mice only in response to partial hepatectomy (8±0.88 fold up-regulation compared to mTERC<sup>+/+</sup> quiescent liver) but not in the quiescent organ. **(D)** Representative gel electrophoresis photograph showing the RT-PCR products of p21, p16, and p19<sup>ARF</sup> (after 22 cycles) and the house keeping gene RSP9 (after 35cycles): Lane 1. Quiescent mTERC<sup>+/+</sup> liver, Lane 2. mTERC<sup>+/+</sup> liver 30-36 hrs after PH, Lane 3. Quiescent G1 mTERC<sup>-/-</sup> liver, Lane 4. G1 mTERC<sup>-/-</sup> liver 30-36 hrs after PH, Lane 5. Quiescent G3 mTERC<sup>-/-</sup> liver, Lane 6. G3 mTERC<sup>-/-</sup> liver 30-36 hrs after PH, Lane 7. Non-template control. **(E-G)** Histograms showing p21 **(E)**, p16 **(F)** and p19<sup>ARF</sup> **(G)** expression in early and late passage IMR90 cells and in late passage of hTERT expressing IMR90 cells. p21 and p16 were significantly up-regulated in late passage IMR90 cells but not in hTERT expressing cells. Note that serum starvation reversed the over-expression of p21 and p16, which re-appeared 12-24 hrs after serum re-stimulation. **(H)** Representative gel electrophoresis photograph showing the expression levels of p21, p16 and p19<sup>ARF</sup> (after 22 cycles) and the house keeping gene β-actin (after 30 cycles) in IMR90 cells in the following loading order: 1-5: early passage IMR90 (PD30): 1. serial passage, 2. serum starvation for 120 hrs, 3. serum stimulation (6 hrs), 4. serum stimulation (12 hrs), 5. serum stimulation (24 hrs). 6-10: late passage IMR 90 (PD55): 6. serial passage, 7. serum starvation (120 hrs), 8. serum stimulation (6 hrs), 9. serum stimulation (12 hrs), 10. serum stimulation (24 hrs). 11-15: late

passage of hTERT expressing IMR90 cells (PD68): 11. serial passage, 12. serum starvation (120 hrs), 13. serum stimulation (6 hrs), 14. serum stimulation (12 hrs), 15. serum stimulation (24 hrs). 16. Non-template control. **(I-K)** Histograms showing p21 **(I)**, p16 **(J)** and p19<sup>ARF</sup> **(K)** expression in early and late passage HK1 cells and in late passage of HK1 cells expressing hTERT. p21 and p16 were significantly up-regulated in late passage HK1 cells but not in hTERT expressing cells. Note that serum starvation partially reversed the over-expression of p16 and nearly completely rescued the over-expression of p21, which re-appeared 12-24 hrs after serum re-stimulation. **(L)** Representative gel electrophoresis photograph showing the expression levels of p21, p16 and p19<sup>ARF</sup> (after 22 cycles) and the house-keeping gene  $\beta$ -actin (after 30 cycles) in HK1 cells. The loading of PCR products for early (PD9), late (PD60) and hTERT immortalized (PD90) HK1 cells follow the same order as described for IMR90.

In the liver system it has been reported that p21 is induced during cell cycle re-entry of quiescent hepatocytes following PH (139) indicating that it plays a role in regulating cell cycle re-entry during liver regeneration. However, the up-regulation of p21 in G3 mTERC<sup>-/-</sup> mice in response to PH greatly exceeded this physiological up-regulation of p21 in wildtype or G1 mTERC<sup>-/-</sup> mice (Figure 3.11.1A & D).

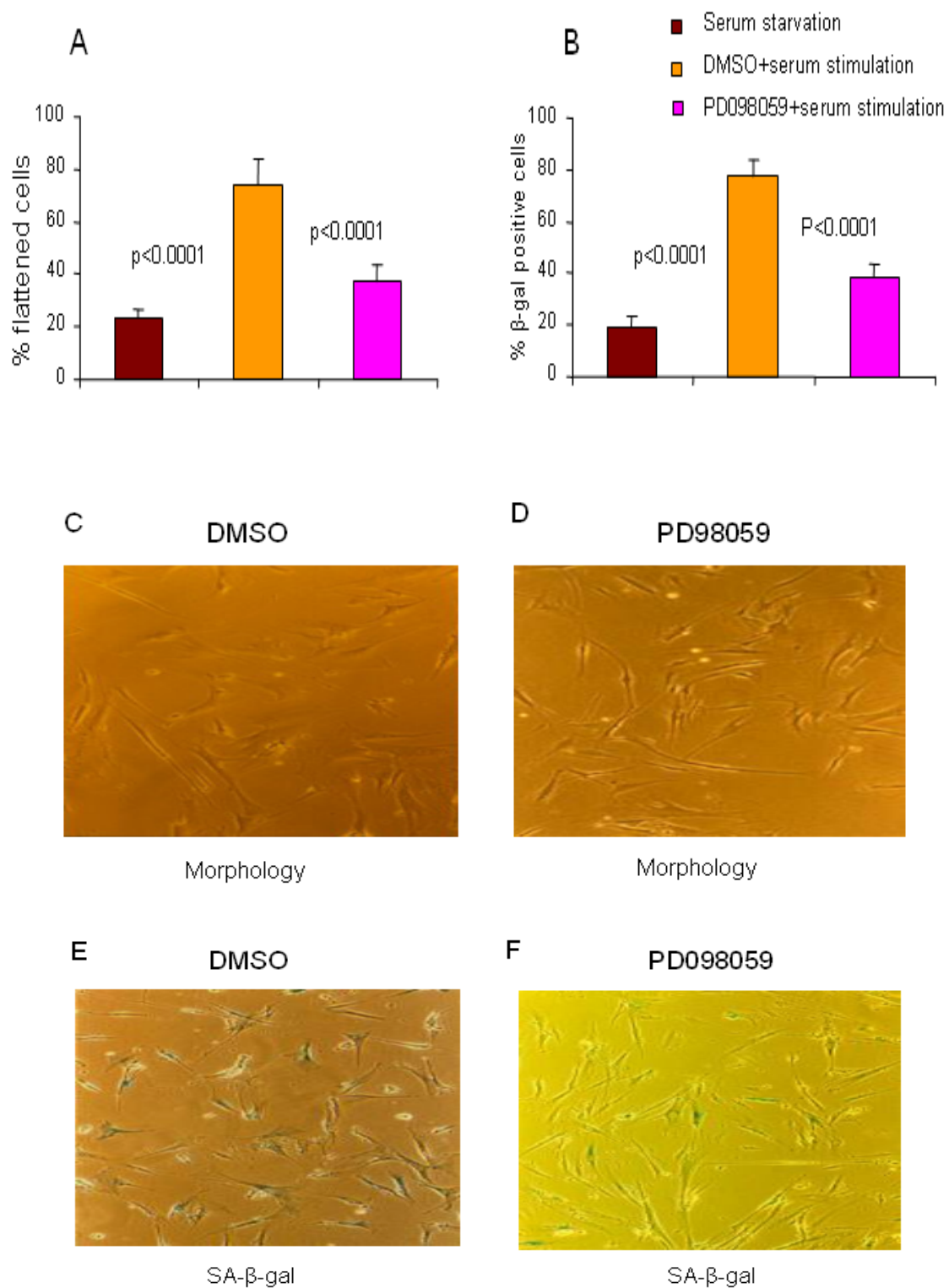
### **3.12 Inhibition of MEK/MAPK pathway partially abrogates the co-operation between mitogen stimulation and senescence signaling**

Treatment of cells with growth factors leads to activation of the mitogen activated protein kinases (MAPK) also called extracellular signal regulated kinases (ERK) by the MAPK/ERK-kinase (MEK). The Ras family members of onco-proteins activate this pathway in response to growth factor mediated dimerization of tyrosine-kinase receptors. Although necessary for normal cell proliferation, sustained over-stimulation of the Ras/MEK/MAPK-pathway induces premature senescence. Ras/MEK/MAPK-induced premature senescence is independent of telomere length and is characterized by the appearance of similar morphological and molecular markers as replicative senescence (84-86).

To test whether the same mitogenic pathway also plays a role in revealing the phenotype of replicative senescence a highly specific pharmacological inhibitor of MEK (PD098059) was used to block this pathway (140-141). When PD098059 was applied 1hr before and following serum stimulation of serum-starved late passage IMR90 cells the re-appearance of senescence phenotypes (cell morphology and SA- $\beta$ -Gal-activity, Figure 3.10.2) was partially prevented (Figure 3.12.1A-F). Similarly the up-regulation of p21 and p16 in late passage IMR90 in response to serum stimulation was significantly inhibited by addition of PD098059 (Figure 3.12.1G-I). Together, these data indicate that mitogen stimulation co-



operates with senescence signaling through the activation of MEK/MAKP-pathway to reveal replicative senescence phenotypes.





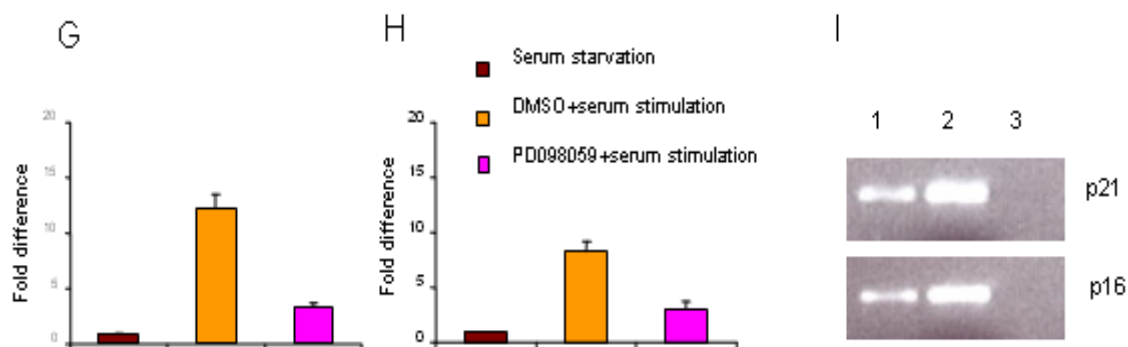


**Figure 3.12.1 (A, B)** Histogram of the percentage of cells with senescent morphology or positive  $\beta$ -gal-staining in late passage IMR90 cells 120 hrs after serum starvation and 24 hrs after serum stimulation after addition of DMSO or the MEK-inhibitor PD098059 1 hr before stimulation. **(C-F)** Representative photographs showing the senescent morphology and  $\beta$ -gal activity in late passage IMR90 cells in response to serum stimulation for 24 hours after addition of DMSO **(C, E)** or the MEK-inhibitor PD098059 **(D, F)**. **(G)** Fold difference of p21 in late passage IMR90 cells 120 hrs after serum starvation and 24 hours after serum stimulation after addition of DMSO or the MEK-inhibitor PD098059. **(H)** Fold difference of p16 in late passage IMR90 cells 120 hrs after serum starvation and 24 hrs after serum stimulation after addition of DMSO or the MEK-inhibitor PD098059. **(I)** Representative gel-electrophoresis photograph of 10  $\mu$ l of the RT-PCR products of p21 and p16 after 22 PCR-cycles: 1. Late passage IMR90 cells under serum stimulation plus PD098059, 2. Late passage IMR90 cells under serum stimulation plus DMSO, 3. Non-template control.

### 3.13.1 Hepatocyte-specific senescence in human liver cirrhosis

To test whether the induction of cellular senescence *in vivo* in the mouse model can also apply to human liver, senescence associated- $\beta$ -gal staining was conducted on human liver cirrhosis samples. In human liver cirrhosis, chronic hepatocyte destruction by viral hepatitis, AIH, PSC, PBC and concomitant hepatocyte regeneration accelerate telomere shortening in hepatocytes. If telomere shortening limits the regenerative capacity of hepatocytes signs of cellular senescence might be detectable in hepatocytes at the cirrhosis stage. To test this possibility,  $\beta$ -Gal staining was conducted on 49 of the cirrhosis samples and 15 of the control samples. In our study a strong correlation between senescence-associated- $\beta$ -Gal activity and cirrhosis was detectable: 41 of 49 cirrhosis samples (84%) had  $\beta$ -Gal activity, whereas only 1 of 15 control samples (7%) showed very weak  $\beta$ -Gal activity (Figure 3.13.1 A,  $P < 0.0001$ ).  $\beta$ -Gal activity was detectable at a high frequency in all sub-groups of cirrhosis: in 90% of the AIH, 75% of the viral hepatitis, 85% of the PSC, 86% of the PBC, and 86% of the cirrhosis samples induced by alcoholism (Figure 3.13.1B). Only hepatocytes stained positive for  $\beta$ -Gal whereas stellate cells in fibrotic septa did not stain positive for  $\beta$ -Gal in any samples tested

(Figure 3.13.1C). The  $\beta$ -Gal staining pattern of hepatocytes in cirrhosis is markedly pronounced at the edge of regenerative nodules as opposed to the center of the nodules (Figure 3.13.1C). Since the regenerative nodules in the cirrhotic liver represent clonal expansion of regenerating hepatocytes, the cells at the edge of these nodules have undergone more cell divisions than cells in the centre, providing a possible explanation for the increase in senescence-associated  $\beta$ -Gal activity in these regions. Quantification of the percentage of  $\beta$ -Gal-positive hepatocytes within cirrhosis samples showed that 32% of the cirrhosis samples have a weak  $\beta$ -gal activity (<5% of the hepatocytes), 32% have a moderate activity (5–15% of the hepatocytes), and 36% show strong activity (>15% of the hepatocytes). Together, our data show that there is a significant rate of hepatocellular senescence in cirrhosis limiting the regenerative capacity of the injured organ, thereby perturbing the balance of injury and regeneration, culminating in fibrotic scarring.

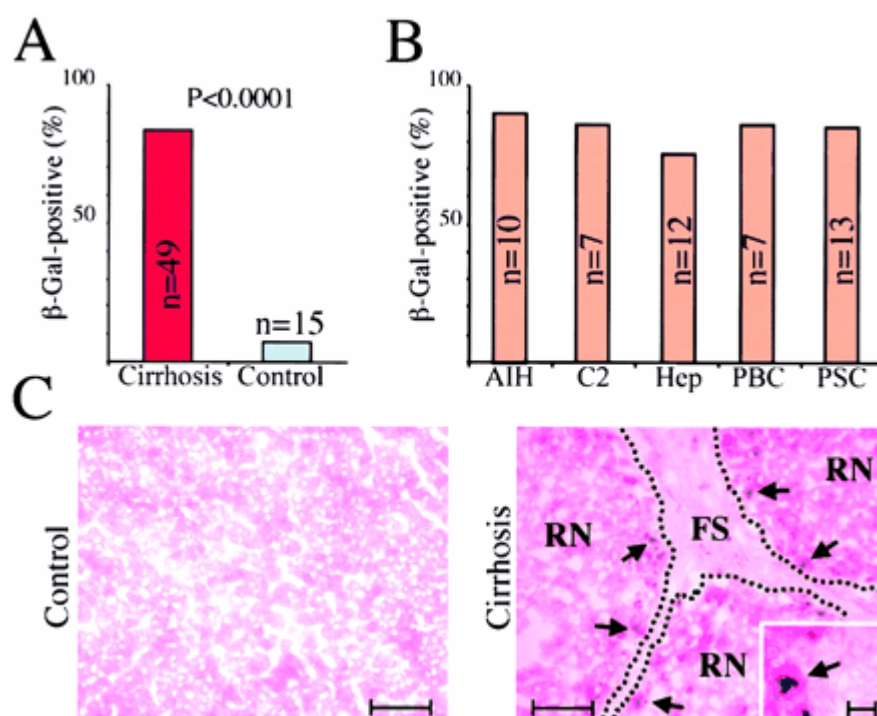


**Figure 3.13.1** Hepatocyte-specific senescence in cirrhosis. **(A)** 41 of 49 cirrhosis samples (84%) stain positive for senescence-associated  $\beta$ -Gal activity at pH 6, whereas only 1 of 15 control samples shows very weak  $\beta$ -Gal activity (7%,  $P < 0.0001$ ). **(B)** High rates of senescence-associated  $\beta$ -Gal activity are present in all subgroups of cirrhosis independent of its etiology: autoimmune hepatitis (AIH, 90%), alcoholism (C2, 86%), viral hepatitis (Hep, 75%), primary biliary cirrhosis (PBC, 86%), primary sclerosing cholangitis (PSC, 85%). **(C)** Representative photograph of a noncirrhotic control sample showing no staining for senescence-associated  $\beta$ -Gal activity (left site, Bar: 200  $\mu$ m), and a cirrhotic sample showing positive staining for senescence-associated  $\beta$ -Gal activity (right site, bar: 200  $\mu$ m). Positive  $\beta$ -

Gal staining of cirrhosis samples was restricted to hepatocytes and was not present in other cell types. Inlet: High magnification of an area showing hepatocyte-specific  $\beta$ -Gal staining (left site, arrow) at the edge to a fibrotic septum (right site); bar: 30  $\mu$ m.  $\beta$ -Gal-positive hepatocytes (arrows) are predominantly located at the edge of regenerative nodules (RN), whereas stellate cells in fibrotic septa (FS) do not show  $\beta$ -Gal activity.

### 3.14 Hepatocyte specific senescence correlates to fibrosis progression in cirrhosis

To test the hypothesis that limitation of hepatocyte regeneration by induction of senescence in hepatocytes triggers fibrotic scarring, we evaluated the correlation between the rate of senescent hepatocytes ( $\beta$ -Gal positive) and fibrosis. Cirrhosis samples were grouped into samples with mild fibrosis and samples with severe fibrosis according to the Ishak criteria (142). In line with our hypothesis, this analysis showed that samples with severe fibrosis have significantly higher rates of hepatocyte senescence than samples with milder fibrosis (Figure 3.14.1).

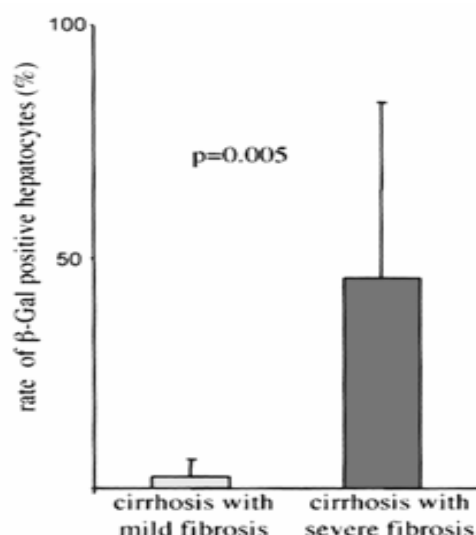


**Figure 3.14.1** Correlation between  $\beta$ -Gal activity and fibrosis progression. Cirrhosis samples were grouped into samples with mild fibrosis and samples with severe fibrosis according to the Ishak criteria (19). There was a significant increase in the percentage of hepatocytes staining positive for  $\beta$ -gal activity in cirrhosis samples with severe fibrosis compared with cirrhosis samples with mild fibrosis.

## 4. Discussion

Our current study demonstrates that telomere shortening at the cellular level affects organ regeneration *in vivo* by inhibiting a sub-population of cells with critically short telomeres from entering the cell cycle thereby limiting the pool of proliferating cells within an organ system. As a result there is an elevated regenerative pressure on the proliferating sub-population of cells to compensate for impaired organ regeneration by additional rounds of cell divisions which in turn accelerates the rate of telomere shortening and the imbalance of proliferating and non-proliferating cells. Our results are further strengthened by previous studies in mTERC<sup>-/-</sup> mice showing that it is not the average telomere length, but the prevalence of critically short telomeres leads to regenerative disorders (100). The new concept derived from our study is that the prevalence of critically short telomeres at the cellular level determines the proliferative capacity of cells within an organ system. Thus, the regenerative capacity of organs and tissues depends on the size of the population of cells with sufficient telomere reserves required for cell proliferation.

Which mechanism limits cell proliferation in the sub-population of cells with critically short telomeres? We show that mitogen signaling and apoptosis do not contribute to impaired liver regeneration in response to telomere shortening in our model system of PH. It seems likely that the lack of telomere-directed apoptosis reflects the modest regenerative stress induced by PH unlike previous studies which showed that critical telomere shortening induces prominent hepatocyte apoptosis during clonal expansion of hepatocytes following acute liver failure - a setting of potent regenerative stress (98). The prevalence of  $\beta$ -galactosidase positive cells and the coincidence of  $\beta$ -galactosidase activity with non-proliferating cells indicate that the cells with critically short telomeres have reached the senescence stage. In line with this hypothesis gene expression profiling and RT-PCR analysis of regenerating liver at the onset of S-phase revealed an up-regulation of downstream targets of p53 - a pathway critical for inducing cellular senescence in response to telomere shortening (62, 66).

At which stage of the cell cycle are the liver cells arrested? Previous studies in mTERC<sup>-/-</sup> mice have revealed that telomere shortening induces a biphasic cell cycle block in mouse embryonic fibroblasts (62) and impaired mitotic progression in regenerating liver (98).

In line with these studies, our current data on liver regeneration following PH show impaired cell cycle progression at 2 stages - at pre-S-phase and G2/M.: impaired S-phase entry in G3 mTERC<sup>-/-</sup> mice was independent of the DNA content of the cells demonstrating that G1/S progression was impaired, and the accumulation of cells with higher DNA ploidy in G3 mTERC<sup>-/-</sup> mice during the time course of liver regeneration indicated that G2/M progression was impaired. We hypothesize that if telomeres are dysfunctional in resting cells, cell cycle re-entry is inhibited at the G1/S transition. In addition, some cells will acquire dysfunctional telomeres during S-phase due to further telomere shortening during DNA replication and will consequently be withdrawn from the cell cycle at the G2/M stage.

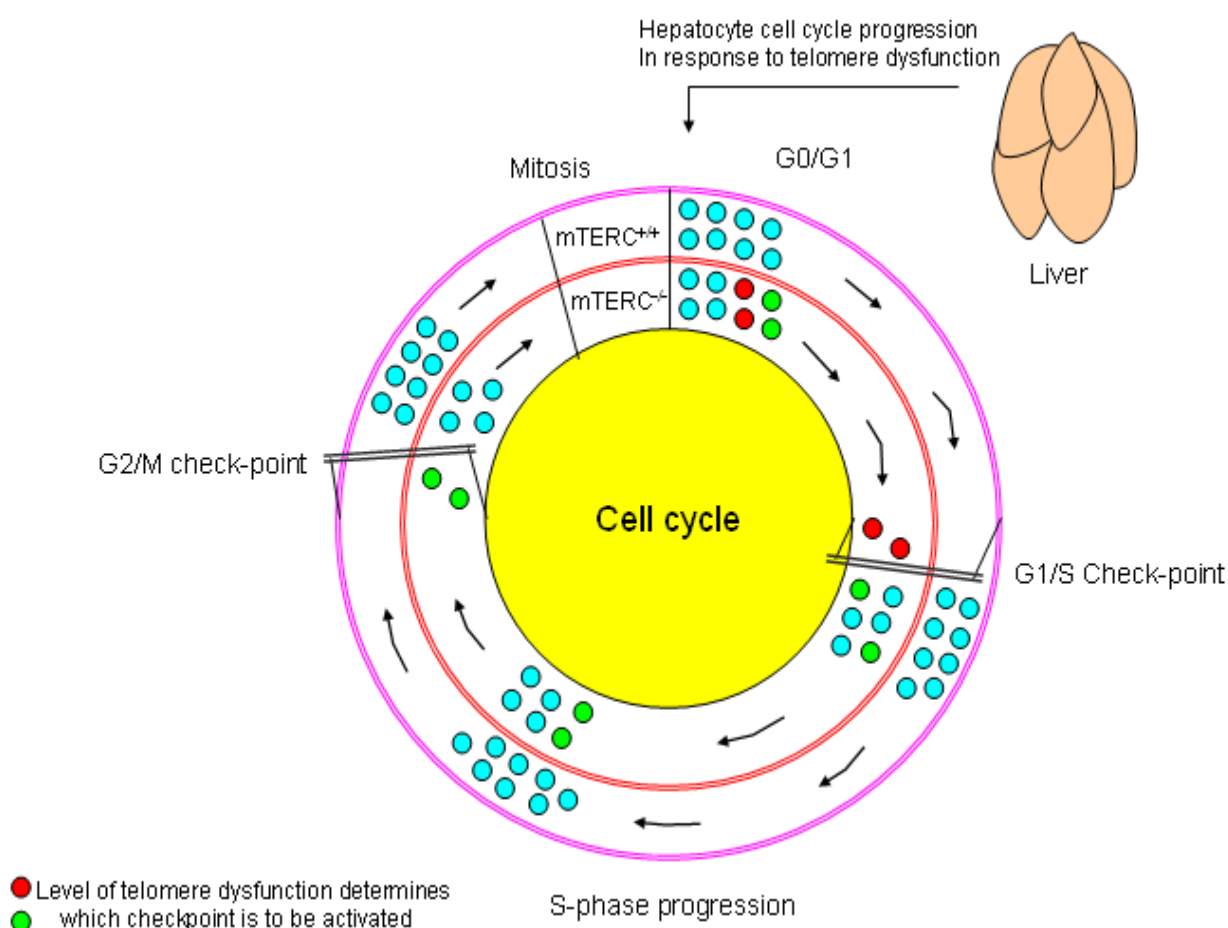


**Figure 4.1** Model on the consequences of telomere shortening at the cellular level on cell cycle progression. Telomere shortening is heterogeneous within the cells of an organ system. Cells with higher level of telomere dysfunction were inhibited from entering the cell cycle at G1/S transition whereas other cells with some telomere dysfunction enter the S phase and the consequent loss of a few more telomere repeats during S phase lead to telomere dysfunction and consequently these cells are inhibited at G2/M checkpoint of the cell cycle. So the level of

telomere dysfunction determines the proliferative fate of the cell and the activation of cell cycle checkpoints.

Our study supports a model that inhibition of cell cycle entry in a sub-population of cells with critically short telomeres results in delayed organ regeneration by requiring an additional round of replication by cells with sufficient telomere reserves. According to this model regenerative defects are determined by the size of the proliferating population of cells within an organ system necessary to maintain organ function and homeostasis. It seems likely that the differences in telomere length between individual cells within an organ reflect the replicative history of cells during organogenesis and postnatal life. In addition, other factors that possibly affect telomere length might be differences in metabolic rates and intracellular load of radical oxygen species. The percentage of liver cells inhibited from cell cycle re-entry in G3 mTERC<sup>-/-</sup> mice in our study was approximately 15%, most of them (~11%) in turn showed  $\beta$ -galactosidase activity.

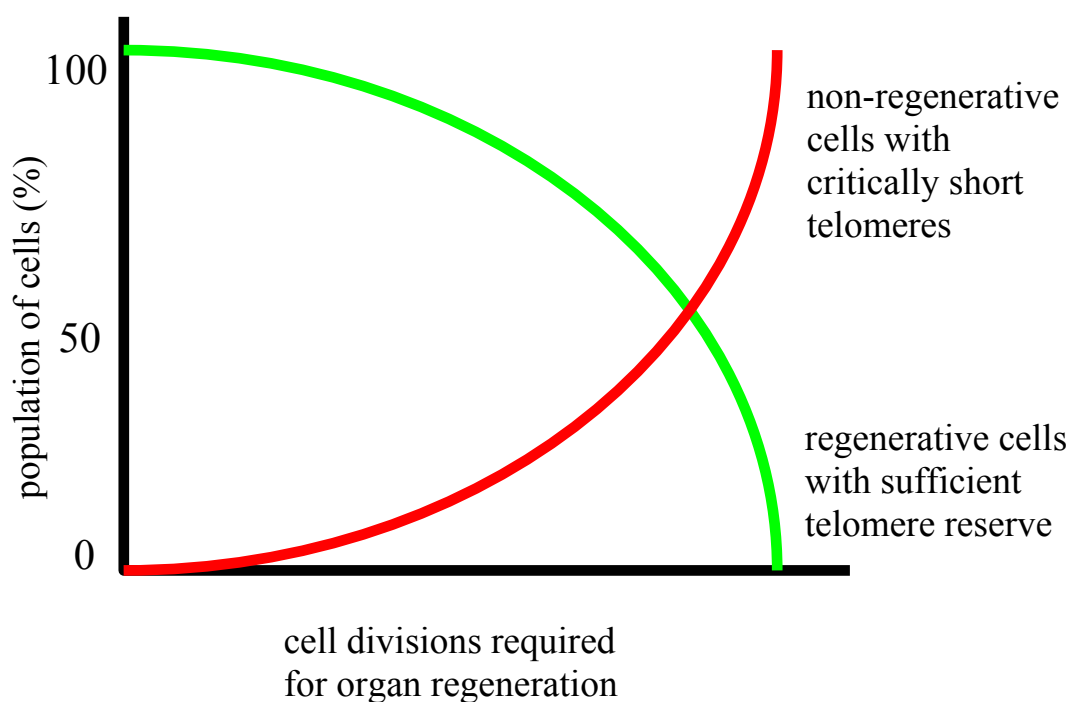


**Figure 4.2** Model of impaired regeneration of organs induced by telomere shortening at cellular level. Within a tissue or organ system heterogeneous telomere shortening inhibits a growing sub-population of cells from entering the cell cycle and the pool of proliferating cells will constantly decrease. This reduced pool of cells with sufficient telomere reserves has to undergo additional cell divisions to accomplish organ/tissue regeneration. This mechanism will lead to acceleration of telomere shortening and will further disturb the imbalance of proliferating and non-proliferating cells.

Similarly our present study shows that the phenotypes and signaling pathways of replicative senescence induced by telomere shortening in both *in vivo* and *in vitro* are revealed by mitogen stimulation. The senescent signaling become amplified to a higher level in cells that are stimulated to divide where as operate at a low, basal level in the absence of a growth response. We show that the morphological phenotypes as well as the molecular markers of cellular senescence are dramatically diminished in mitogen-deprived cells and organs despite the prevalence of critically short telomeres. The senescence markers (re-) appear in response to mitogen induced proliferative response both *in vitro* and *in vivo* indicating that responses to telomere dysfunction are still intact. Activation of the replicative senescence program in response to mitogenic stimuli signals in part through the MEK/MAPK-pathway inducing premature senescence in response to sustained over-stimulation of this pathway (84-86). Our data indicate that both senescence pathways (premature and replicative senescence) are linked to each other. We suggest the hypothesis that telomere shortening lowers the threshold at which MEK/MAPK-signaling induces growth arrest and senescence instead of cell proliferation. In line with this hypothesis previous studies have shown that premature senescence and replicative senescence are indistinguishable in terms of morphological and molecular markers (87). Recently it has been shown that the stress induced MAPK 38 - is over-expressed in both, replicative and premature senescence (89) indicating that there could be a cross-talk between mitogen stimulation and the stress induced MAPK 38 possibly functioning at a lower threshold in cells with shortened telomeres.

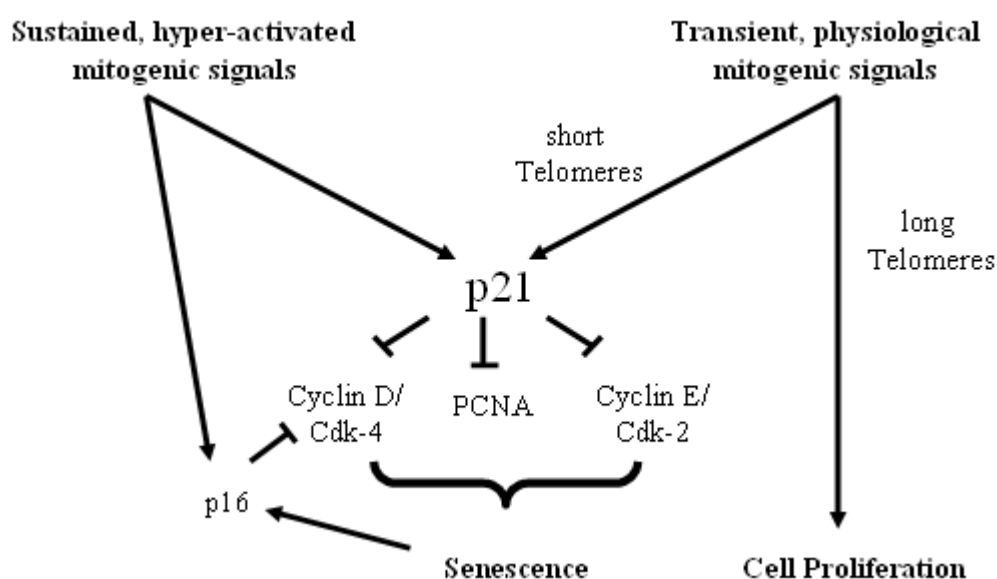


**Figure 4.3** Model showing the co-operation between mitogenic stimuli and telomere shortening to activate p21 signaling pathway to prevent the cells to enter cell cycle.

An explanation for the mitogen-dependence of replicative senescence is that a low level of cell cycle inhibitors is sufficient to counteract the actions of positive growth regulatory elements which are either absent or present at very low levels in growth deprived conditions (67). Quiescent young as well as senescent HDFs (Human diploid fibroblasts) express low levels of cyclin D1 and cyclin E and upon serum stimulation both their expression and their associated kinase activities increase during the mid and late G1 phases respectively in young HDFs which leads to pRb phosphorylation (67, 78, 79). In contrast to the young HDFs, in senescent HDFs even though there is abundant cyclin D-Cdk4/6 and cyclin E-Cdk2 complexes they lack cyclin E and cyclin D associated kinase activities which is due to increased inhibitory binding of p21 to these complexes rather than inhibitory phosphorylation of kinase activity (67, 79).

In our study the enhanced expression of p21 in response to serum stimulation reflects the fact that a higher level of p21 is essential to inhibit the growth stimulatory effects of cyclin D-Cdk4/6 and cyclin E-Cdk2 complexes. The moderate up-regulation of Cdk-inhibitors, which is the physiological response to mitogenic stimuli (139), gives a plausible explanation that there is a fine balance between expression levels of positive growth regulators and inhibitors for controlled proliferation of cells and the shift of this balance to either side depends on the physiological as well as molecular status of the cell.

Our study shows that in cells with shortened telomeres the up-regulation of p21 and p16 in response to mitogen stimulation greatly exceeded the normal physiological levels in order to prevent the cells from entering the cell cycle. In contrast to the almost complete diminution of p21 over-expression in human senescent cells by mitogen withdrawal, the diminution of p16 over-expression was partial and in-complete (Figure 3.11.1) indicating that the secondary upregulation and accumulation of p16 at the senescent stage is partially independent of mitogenic stimuli or that its decline is delayed. The disappearance of morphological characteristics of senescent cells is in correlation with diminution of expression levels of p21 and p16 in response to serum deprivation indicates that the expression levels of these cell cycle regulators determine not only the proliferative fate but also the morphological features of the cells. This explanation is in accord with previous reports that the induced expression of either p21 or p16 alone is sufficient to induce senescence which show all the



morphological markers of senescence including flattened morphology and SA- $\beta$ -gal activity (143-144) and inhibition of p21 and p16 leads to normal cell cycle progression and extension of life span with no signs of senescence (145, 146). In our current study the disappearance and reappearance of morphological features of senescence (flattened cells, SA- $\beta$ -gal activity) in response to serum starvation and stimulation are in correlation with the expression levels of p21 and p16. It appears that the expression levels of these genes can determine the morphological characteristics of cells through either activation or inhibition of a cascade of some unknown signal transduction pathways.

The classical model of replicative senescence is that critically short telomeres lose their capping-function at the chromosomal ends resulting in activation of a DNA-damage response culminating in cellular senescence (13-16, 66). Our findings that the morphological and molecular markers of senescence are revealed by mitogen stimulation independent of further telomere shortening in the subsequent cell division suggest that the "un-capped" chromosomal ends might not generate a DNA-damage signal as long as the cells are in the quiescent stage. Possible explanations are that the chromosomal ends might be protected by dense packing of the chromatin in G<sub>0</sub> cells as compared to cells entering the cell cycle, or those genes involved in DNA-damage recognition and signaling are actively suppressed in quiescent cells. The results of our study will impact on future analysis of the senescence-pathway and might help to identify the initial responses to telomere shortening leading to cell cycle arrest and senescence. Regarding the role of replicative senescence *in vivo* our findings indicate the need to monitor cell cycle activity in order to analyze the prevalence and consequences of senescence in different organs and tissues often containing large fraction of cells in the G<sub>0</sub>-stage of the cell cycle.

Does the telomere hypothesis of induction of cellular senescence and impaired organ regeneration in mouse models apply to humans? To date there is an accumulation of correlative data indicating that telomere shortening might impact on the regenerative capacity of human tissues during aging and chronic diseases. In addition, mutation of the essential RNA component of human telomerase has been implicated in premature aging, bone marrow failure, and liver cirrhosis among other phenotypes in patients with dyskeratosis congenita (147). Since it is not possible to study the consequences of telomere shortening in a regenerative model in humans, we explored the existence of cellular senescence in human

cirrhosis samples where continuous destruction and concomitant regeneration of liver cells occurs in response to a broad variety of liver diseases.

Our study revealed the existence of cellular senescence in human cirrhosis and the prevalence of senescent hepatocytes ranges from 2-15% in the vast majority of cases indicating that cellular senescence impairs regular organ regeneration in chronic liver disease in humans. Moreover, cellular senescence at the cirrhosis stage correlates with fibrosis progression. The determination of the rates of cellular senescence and the identification of new markers of senescence could be useful to test the relevance of senescence in limiting the regenerative capacity in different human tissues and organs during aging and chronic disease.

Our data support the telomere hypothesis of human cirrhosis, suggesting that chronic hepatocyte damage and concomitant hepatocyte regeneration accelerate telomere shortening in hepatocytes. When hepatocytes reach the senescent stage, liver regeneration decreases but the chronic liver damage continues. At this stage of disease, other cell types, like hepatic stellate cells, which usually do not participate in the regenerative process, become activated and form fibrotic scar tissue in areas of hepatocyte loss.

It will be important to identify the signals inducing hepatocellular senescence once telomeres have reached a critically short length. The tumor suppressor p53 has been identified as a downstream target of short dysfunctional telomeres in mouse and human cells (13) . Inhibition of p53 rescues the adverse effects of telomere dysfunction (62). The data on accumulation of p21 in cirrhotic samples indicate this pathway might also be activated at the cirrhosis stage (115). However, the mechanism of p53 activation and the role of other pathways in response to critical telomere shortening remain to be identified.

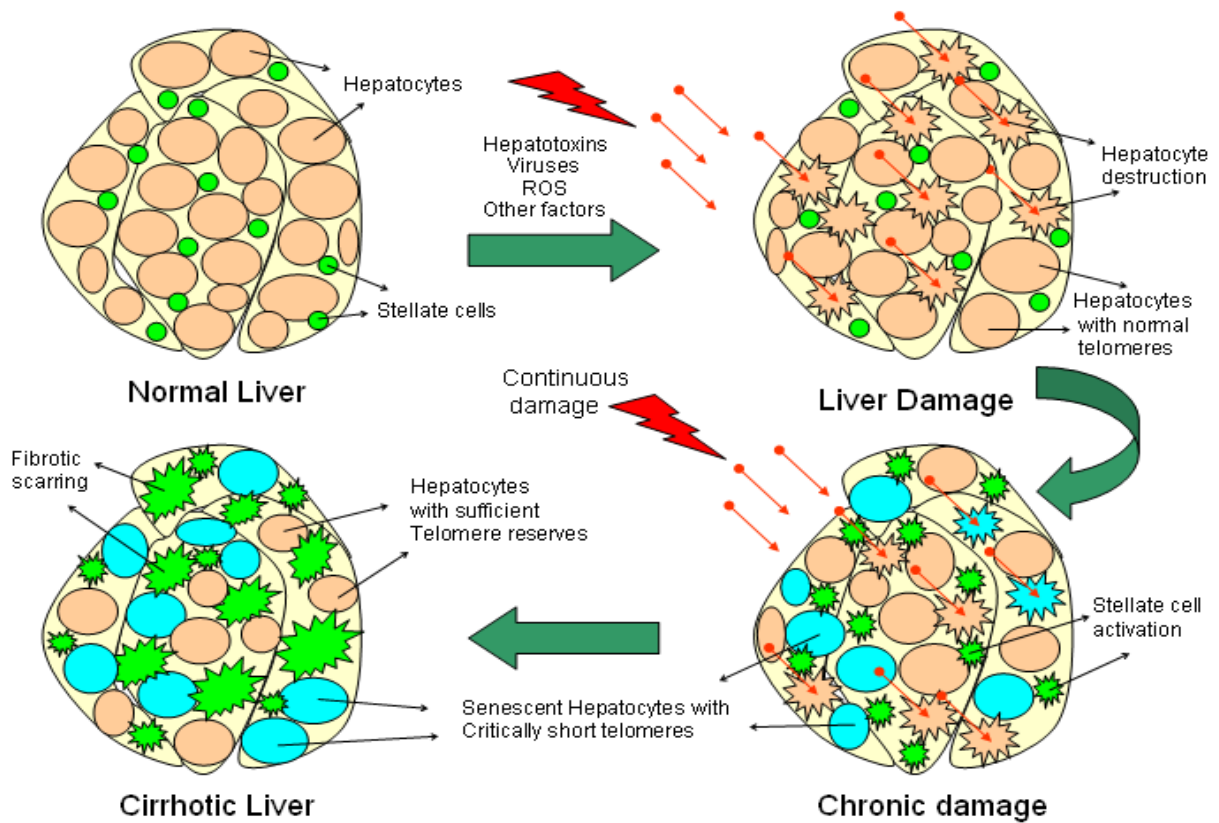


**Figure 4.4** Model of hepatocyte specific senescence and its correlation with cirrhosis formation and fibrosis progression. This model delineates that chronic liver diseases constitutively damage hepatocytes thus accelerating the rate of hepatocyte turnover, which in turn leads to hepatocyte telomere shortening and senescence. According to this model the formation of fibrotic scar is triggered by loss of hepatocyte regeneration and persistent organ damage which then leads to the activation of stellate cells with longer telomeres to replace organ mass by scar tissue compromising normal organ architecture and function.

## 5. References

1. Greider CW. Telomeres. *Curr Opin Cell Biol.* 1991, 3, 444-51.
2. Blackburn E.H. Structure and function of telomeres. *Nature*, 1991, 350, 569-73.
3. Hemann MT, Greider CW. Wild-derived inbred mouse strains have short telomeres. *Nucleic Acids Res.* 2000, 15, 28, 4474-8.
4. Aviv A, Levy D, Mangel M. Growth, telomere dynamics and successful and unsuccessful human aging. *Mech Ageing Dev.* 2003, 124, 829-37.
5. Liu Y, Kha H, Ungrin M, Robinson MO, Harrington L. Preferential maintenance of critically short telomeres in mammalian cells heterozygous for mTert. *Proc Natl Acad Sci U S A.* 2002, 99, 3597-602.
6. Moyzis RK, Buckingham JM, Cram LS, Dani M, Deaven LL, Jones MD, Meyne J, Ratliff RL, Wu JR. A highly conserved repetitive DNA sequence (TTAGGG)<sub>n</sub>, present at the telomeres of human chromosomes. *Proc Natl Acad Sci.* 1988, 85, 6622-6.
7. Shore D. Telomeric chromatin: replicating and wrapping up chromosome ends. *Curr Opin Genet Dev.* 2001, 11, 189-98.
8. Makarov, V. L., Y.Hirose, and J.P.Langmore. Long G tails at both ends of human chromosomes suggest a C strand degradation mechanism for telomere shortening. *Cell* 1997, 88, 657-666
9. Wright WE, Tesmer VM, Huffman KE, Levene SD, Shay JW. Normal human chromosomes have long G-rich telomeric overhangs at one end. *Genes Dev.* 1997, 11, 2801-9.
10. Griffith JD, Comeau L, Rosenfield S, Stansel RM, Bianchi A, Moss H, de Lange T. Mammalian telomeres end in a large duplex loop. *Cell* 1999, 97, 503-14.
11. Greider CW. Telomeres do D-loop-T-loop. *Cell* 1999, 97, 419-22.
12. Harrington L, Robinson MO. Telomere dysfunction: multiple paths to the same end. *Oncogene* 2002, 21, 592-7.
13. Smogorzewska A, de Lange T. Different telomere damage signaling pathways in human and mouse cells. *EMBO J* 2002, 21, 4338-48.
14. Blackburn EH. Switching and signaling at the telomere. *Cell* 2001, 106, 661-73.
15. Takai H, Smogorzewska A, de Lange T. DNA damage foci at dysfunctional telomeres. *Curr Biol.* 2003, 13, 1549-56.

16. Fagagna Fd F, Reaper PM, Clay-Farrace L, Fiegler H, Carr P, Von Zglinicki T, Saretzki G, Carter NP, Jackson SP. A DNA damage checkpoint response in telomere-initiated senescence. *Nature* 2003, 426, 194-8.
17. Chikashige Y, Ding DQ, Imai Y, Yamamoto M, Haraguchi T, Hiraoka Y. Meiotic nuclear reorganization: switching the position of centromeres and telomeres in the fission yeast *Schizosaccharomyces pombe*. *EMBO J* 1997, 16, 193-202.
18. Wright WE, Shay JW. Telomere positional effects and the regulation of cellular senescence. *Trends Genet.* 1992, 8, 197-7.
19. Hayflick, L. The limited in vitro lifetime of human diploid cell strains. *Exp. Cell Res.* 1965, 37, 614-636.
20. Allsopp R.C., Chang E., Kashefi-Azham M., Rogaev E.I., Piatyszek M.A., Shay J.W., Harley C.B. Telomere shortening is associated with cell division in vitro and in vivo. *Exp Cell Res.*, 1995, 220, 194-200.
21. Allsopp RC, Harley CB. Evidence for a critical telomere length in senescent human fibroblasts. *Exp Cell Res.*, 1995, 219, 130-6.
22. Tommerup H, Dousmanis A, de Lange T. Unusual chromatin in human telomeres. *Mol Cell Biol.* 1994, 14, 5777-85.
23. Van Steensel B, de Lange T: Control of telomere length by the human telomeric protein TRF1. *Nature* 1997, 385, 740-743.
24. Van Steensel B, Smogorzewska A, de Lange T. TRF2 protects human telomeres from end-to-end fusions. *Cell* 1998, 92, 401-413.
25. Li B, Oestreich S, de Lange T. Identification of human Rap1p: implications for telomere evolution. *Cell* 2000, 101, 471-83.
26. Zhou BS, Elledge SJ. The DNA damage response: putting checkpoints in perspective. *Nature* 2000, 408, 433-9.
27. Balagurumoorthy P, Brahmachari SK, Mohanty D, Bansal M, Sasisekharan V. Hairpin and parallel quartet structures for telomeric sequences. *Nucleic Acids Res.* 1992, 20, 4061-7.
28. Karlseder J. Telomere repeat binding factors: keeping the ends in check. *Cancer Lett.* 2003, 194, 189-97.
29. Broccoli D, Smogorzewska A, Chong L, de Lange T. Human telomeres contain two distinct Myb-related proteins, TRF1 and TRF2. *Nat Genet.* 1997, 17, 231-5.
30. Smith S, Giriat I, Schmitt A, de Lange T. Tankyrase, a poly(ADP-ribose) polymerase at human telomeres. *Science* 1998, 282, 1484-7.

31. Kim SH, Kaminker P, Campisi J. TIN2, a new regulator of telomere length in human cells. *Nat Genet.* 1999, 23, 405-12.
32. Loayza D, De Lange T. POT1 as a terminal transducer of TRF1 telomere length control. *Nature* 2003, 424, 1013-8.
33. Shay, JW: At the end of the millennium, a view of the end. *Nat Genet* 1999, 23, 382–383.
34. Zhu XD, Kuster B, Mann M, Petrini JH, de Lange T. Cell-cycle-regulated association of RAD50/MRE11/NBS1 with TRF2 and human telomeres. *Nat Genet.* 2000, 25, 347-52.
35. de Jager M, Dronkert ML, Modesti M, Beerens CE, Kanaar R, van Gent DC. DNA-binding and strand-annealing activities of human Mre11: implications for its roles in DNA double-strand break repair pathways. *Nucleic Acids Res.* 2001, 29, 1317-25.
36. Samper E, Goytisolo FA, Slijepcevic P, van Buul PP, Blasco MA. Mammalian Ku86 protein prevents telomeric fusions independently of the length of TTAGGG repeats and the G-strand overhang. *EMBO Rep.* 2000, 1, 244-52.
37. Rhodes D, Fairall L, Simonsson T, Court R, Chapman L. Telomere architecture. *EMBO Rep.* 2002, 3, 1139-45.
38. Lundblad V. The end replication problem: more than one solution. *Nat Med.* 1997, 3, 1198-9.
39. Blackburn E. Telomerases. *Annu Rev Biochem.* 1992, 61, 113-29.
40. Greider CW, Blackburn EH. Identification of a specific telomere terminal transferase activity in Tetrahymena extracts. *Cell* 1985, 43, 405-13.
41. Greider CW, Blackburn EH. A telomeric sequence in the RNA of Tetrahymena telomerase required for telomere repeat synthesis. *Nature* 1989, 337, 331-7.
42. Meyerson M, Counter CM, Eaton EN, Ellisen LW, Steiner P, Caddle SD, Ziaugra L, Beijersbergen RL, Davidoff MJ, Liu Q, Bacchetti S, Haber DA, Weinberg RA. hEST2, the putative human telomerase catalytic subunit gene, is up-regulated in tumor cells and during immortalization. *Cell* 1997, 90, 785-95.
43. Blackburn EH, The telomere and telomerase: nucleic acid-protein complexes acting in a telomere homeostasis system. A review. *Biochemistry (Mosc).* 1997, 62, 1196-201.
44. Holt SE, Aisner D, Baur J, et al. Functional requirement of p23 and hsp90 in telomerase complexes. *Gene Dev.* 1999, 13, 817-26.

45. Shay JW, Wright WE. Implications of mapping the human telomerase gene (hTERT) as the most distal gene on chromosome 5p. *Neoplasia* 2000, 2, 195-6.
46. Baur JA, Zou Y, Shay JW, Wright WE. Telomere position effect in human cells. *Science* 2001, 292, 2075-7.
47. Wright, W. E., Piatyszek, M. A., Rainey, W. E., Byrd, W., and Shay, J. W. Telomerase activity in human germline and embryonic tissue and cells. *Dev. Genet.* 1996, 18, 173-179.
48. Chiu, C. P., Dragowska, W., Kim, N. W., Vaziri, H., Yui, J., Thomas, T. E., Harley, C. B., and Lansdorp, P. M. Differential expression of telomerase activity in hematopoietic progenitors from adult human bone marrow. *Stem Cells* 1996, 14, 239-248.
49. Weng, N. P., Granger, L., and Hodes, R. J. Telomere lengthening and telomerase activation during human B cell differentiation. *Proc. Natl. Acad. Sci. USA* 1997, 94, 10827-10832.
50. Maini, M. K., Soares, M. V., Zilch, C. F., Akbar, A. N., and Beverley, P. C. Virus-induced CD8+ T cell clonal expansion is associated with telomerase up-regulation and telomere length preservation: a mechanism for rescue from replicative senescence. *J. Immunol.* 1999, 162, 4521-4526.
51. Martens, U. M., Brass, V., Sedlacek, L., Pantic, M., Exner, C., Guo, Y., Engelhardt, M., Lansdorp, P., M., Waller, C.F., and Lange, W. Telomere maintenance in human B lymphocytes. *Br. J. Haematol.* 2002, 119, 810-818.
52. Nakayama J, Tahara H, Tahara E, Saito M, Ito K, Nakamura H, Nakanishi T, Tahara E, Ide T, Ishikawa F. Telomerase activation by hTERT in human normal fibroblasts and hepatocellular carcinomas. *Nat Genet.* 1998, 18, 65-8.
53. Takahashi S, Kitamoto M, Takaishi H, Aikata H, Kawakami Y, Nakanishi T, Shimamoto F, Tahara E, Tahara H, Ide T, Kajiyama G. Expression of telomerase component genes in hepatocellular carcinomas. *Eur J Cancer* 2000, 36, 496-502.
54. Wright WE, Shay JW. The two-stage mechanism controlling cellular senescence and immortalization. *Exp Gerontol.*, 1992, 27, 383-9.
55. Gabet AS, Mortreux F, Charneau P, Riou P, Duc-Dodon M, Wu Y, Jeang KT, Wattel E. Inactivation of hTERT transcription by Tax. *Oncogene* 2003, 22, 3734-41.
56. Horikawa I, Cable PL, Mazur SJ, Appella E, Afshari CA, Barrett JC. Downstream E-box-mediated regulation of the human telomerase reverse transcriptase (hTERT)

- gene transcription: evidence for an endogenous mechanism of transcriptional repression. *Mol Biol Cell*. 2002, 13, 2585-97.
57. Satyanarayana A, Manns M.P, Rudolph K.L., Telomeres and Telomerase: A dual role in Hepatocarcinogenesis. *Hepatology* 2003 (In press)
  58. Henson JD, Neumann AA, Yeager TR, Reddel RR. Alternative lengthening of telomeres in mammalian cells. *Oncogene* 2002, 21, 598-610.
  59. Yeager TR, Neumann AA, Englezou A, Huschtscha LI, Noble JR, Reddel RR. Telomerase-negative immortalized human cells contain a novel type of promyelocytic leukemia (PML) body. *Cancer Res*. 1999, 59, 4175-9.
  60. Pignolo RJ, Martin BG, Horton JH, Kalbach AN, Cristofalo VJ. The pathway of cell senescence: WI-38 cells arrest in late G1 and are unable to traverse the cell cycle from a true G0 state. *Exp Gerontol*. 1998, 33, 67-80.
  61. Pang JH, Chen KY. Global change of gene expression at late G1/S boundary may occur in human IMR-90 diploid fibroblasts during senescence. *J Cell Physio*. 1994, 160, 531-8.
  62. Chin L., Artandi S.E., Shen Q., Tam A., Lee S.L., Gottlieb G.J., Greider C.W., DePinho R.A. p53 deficiency rescues the adverse effects of telomere loss and cooperates with telomere dysfunction to accelerate carcinogenesis. *Cell*, 1999, 97, 527-38.
  63. Bond JA, Haughton MF, Rowson JM, Smith PJ, Gire V, Wynford-Thomas D, Wyllie FS. Control of replicative life span in human cells: barriers to clonal expansion intermediate between M1 senescence and M2 crisis. *Mol Cell Biol*. 1999, 19, 3103-14.
  64. Bodnar AG, Ouellette M, Frolkis M, Holt SE, Chiu CP, Morin GB, Harley CB, Shay JW, Lichtsteiner S, Wright WE. Extension of life-span by introduction of telomerase into normal human cells. *Science* 1998, 279, 349-52.
  65. Linskens MH, Harley CB, West MD, Campisi J, Hayflick L. Replicative senescence and cell death. *Science* 1995, 267, 17.
  66. Vaziri H, Benchimol S. From telomere loss to p53 induction and activation of a DNA-damage pathway at senescence: the telomere loss/DNA damage model of cell aging. *Exp Gerontol.*, 1996, 31, 295-301.
  67. Stein, G. H., Drullinger, L. F., Soulard, A. Dulic, V. Differential roles for cyclin-dependent kinase inhibitors p21 and p16 in the mechanisms of senescence and differentiation in human fibroblasts. *Mol. Cell. Biol*. 1999, 19, 2109-2117.



68. Bringold F, Serrano M. Tumor suppressors and oncogenes in cellular senescence. *Exp Gerontol.* 2000, 35, 317-29.
69. Wong KK, Maser RS, Bachoo RM, Menon J, Carrasco DR, Gu Y, Alt FW, DePinho RA. Telomere dysfunction and Atm deficiency compromises organ homeostasis and accelerates ageing. *Nature* 2003, 421, 643-8.
70. Espejel, S., Franco, S., Rodriguez-Perales, S., Bouffler, S. D., Cigudosa, J. C. Blasco, M. A. Mammalian Ku86 mediates chromosomal fusions and apoptosis caused by critically short telomeres. *EMBO J.* 2002, 21, 2207-2219.
71. Bayreuther K, Rodemann HP, Hommel R, Dittmann K, Albiez M, Francz PI. Human skin fibroblasts in vitro differentiate along a terminal cell lineage. *Proc. Natl. Acad. Sci. USA.* 1998, 85, 5112-5116.
72. Dimri GP, Lee X, Basile G, Acosta M, Scott G, Roskelley C, Medrano EE, Linskens M, Rubelj I, Pereira-Smith O., Peacocke M., Campisi J. A biomarker that identifies senescent human cells in culture and in aging skin in vivo. *Proc. Natl. Acad. Sci. USA.* 1995, 92, 9363-9367.
73. Rittling SR, Brooks KM, Cristofalo VJ, Baserga R. Expression of cell cycle dependent genes in young and senescent WI38 fibroblasts. *Proc Natl Acad Sci USA.* 1986, 83, 3316-3320.
74. Seshadri T, Campisi J. c-fos repression and an altered genetic program in senescent human fibroblasts. *Science* 1990, 247, 205-209.
75. Hara E, Yamaguchi T, Nojima H, Ide T, Campisi J, Okayama H, Oda K. Id related genes encoding helix loop helix proteins are required for G1 progression and are repressed in senescent human fibroblasts. *J Biol Chem.* 1994, 269, 2139-2145.
76. Dimri GP, Hara E, Campisi J. Regulation of two E2F related genes in presenescent and senescent human fibroblasts. *J Biol Chem.* 1994, 269, 16180-16186.
77. Good LF, Dimri GP, Campisi J, Chen KY. Regulation of dihydrofolate reductase gene expression and E2F components in human diploid fibroblasts during growth and senescence. *J Cell Physiol.* 1996, 168, 580-588.
78. Stein GH, Beeson M, Gordon L. Failure to phosphorylate the retinoblastoma gene product in senescent human fibroblasts. *Science* 1990, 249, 666-669.
79. Weinberg, R.A. The retinoblastoma protein and cell cycle control. *Cell* 1995, 81, 323-330.
80. Wang E. Senescent human fibroblasts resist programmed cell death and failure to suppress bcl2 is involved. *Cancer Res.* 1995, 55, 2284-2292.

81. Macieira-Coelho A. Chromatin reorganization during senescence of proliferating cells. *Mutat Res.* 1991, 256, 81-104.
82. Itahana K, Dimri G, Campisi J. Regulation of cellular senescence by p53. *Eur J Biochem.* 2001, 268, 2784-91.
83. Matuoka K., Chen KY. Telomerase positive human diploid fibroblasts are resistant to replicative senescence but not premature senescence induced by chemical reagents. *Biogerontology* 2002, 3, 365-72.
84. Serrano, M., Lin, A.W., McCurrach, M.E., Beach, D. Lowe, S.W. Oncogenic ras provokes premature cell senescence associated with accumulation of p53 and p16INK4a. *Cell* 1997, 88, 593-602.
85. Zhu, J., Woods, D., McMahon, M. & Bishop, J.M. Senescence of human fibroblasts induced by oncogenic Raf. *Genes & Dev.* 1998, 12, 2997-3007.
86. Lin AW, Barradas M, Stone JC, van Aelst L, Serrano M, Lowe SW. Premature senescence involving p53 and p16 is activated in response to constitutive MEK/MAPK mitogenic signaling. *Genes & Dev.* 1998, 12, 3008-19.
87. Chen QM. Replicative senescence and oxidant-induced premature senescence. Beyond the control of cell cycle checkpoints. *Ann N Y Acad Sci.* 2000, 908, 111-25.
88. Toussaint O, Dumont P, Remacle J, Dierick JF, Pascal T, Fripiat C, Magalhaes JP, Zdanov S, Chainiaux F. Stress-induced premature senescence or stress-induced senescence-like phenotype: one in vivo reality, two possible definitions? *ScientificWorldJournal* 2002, 2, 230-47.
89. Iwasa H, Han J, Ishikawa F. Mitogen-activated protein kinase p38 defines the common senescence-signalling pathway. *Genes Cells* 2003, 8, 131-44.
90. von Zglinicki T. Oxidative stress shortens telomeres. *Trends Biochem Sci.* 2002, 27, 339-44.
91. Parrinello S, Samper E, Krtolica A, Goldstein J, Melov S, Campisi J. Oxygen sensitivity severely limits the replicative lifespan of murine fibroblasts. *Nat Cell Biol.* 2003, 5, 741-47.
92. Itahana K, Zou Y, Itahana Y, Martinez JL, Beausejour C, Jacobs JJ, Van Lohuizen M, Band V, Campisi J, Dimri GP. Control of the replicative life span of human fibroblasts by p16 and the polycomb protein Bmi-1. *Mol Cell Biol.* 2003, 23, 389-401.

93. Blasco MA, Lee HW, Hande MP, Samper E, Lansdorp PM, DePinho RA, Greider CW. Telomere shortening and tumor formation by mouse cells lacking telomerase RNA. *Cell* 1997, 91, 25-34.
94. Lee HW, Blasco MA, Gottlieb GJ, Horner JW 2nd, Greider CW, DePinho RA. Essential role of mouse telomerase in highly proliferative organs. *Nature* 1998, 392, 569-74.
95. Hemann MT, Rudolph KL, Strong MA, DePinho RA, Chin L, Greider CW. Telomere dysfunction triggers developmentally regulated germ cell apoptosis. *Mol Biol Cell*. 2001, 12, 2023-30.
96. Herrera, E., Samper, E., and Blasco, M. A. Telomere shortening in mTR<sup>-/-</sup> embryos is associated with failure to close the neural tube. *EMBO J*. 1999, 18, 1172-1181.
97. Herrera, E., Samper, E., Martin-Caballero, J., Flores, J. M., Lee, H.-W., and Blasco, M. A. Disease states associated with telomerase deficiency appear earlier in mice with short telomeres. *EMBO J*. 1999, 18, 2950-2960.
98. Rudolph, K. L., Chang, S., Millard, M., Schreiber-Agus, N., and DePinho, R. A. Inhibition of experimental liver cirrhosis in mice by telomerase gene delivery. *Science* 2000, 287, 1253-1258.
99. Rudolph, K. L., Chang, S., Lee, H.-W., Blasco, M., Gottlieb, G. J., Greider, C., and DePinho, R. A. Longevity, stress response, and cancer in aging telomerase-deficient mice. *Cell* 1999, 96, 701-712.
100. Hemann MT, Strong MA, Hao LY, Greider CW. The shortest telomere, not average telomere length, is critical for cell viability and chromosome stability. *Cell*, 2001, 107, 67-77.
101. Fausto N. Liver regeneration. *Journal of hepatology*, 2000, 32 (suppl.1):19-31.
102. Kountouras J, P Boura, NJ Lygidakis. Liver Regeneration after Hepatectomy. *Hepato-gastroenterology*, 2001, 48, 556-562.
103. Su AI, Guidotti LG, Pezacki JP, Chisari FV, Schultz PG. Gene expression during the priming phase of liver regeneration after partial hepatectomy in mice. *Proc Natl Acad Sci U S A*. 2002, 99, 11181-6.
104. Haber BA, Mohn KL, Diamond RH, Taub R. Induction patterns of 70 genes during nine days after hepatectomy define the temporal course of liver regeneration. *J Clin Invest*. 1993, 91, 1319-26.
105. Taub R. Liver regeneration 4: transcriptional control of liver regeneration. *FASEB J*. 1996, 10, 413-27.

106. Fausto N, Mead JE, Braun L, Thompson NL, Panzica M, Goyette M, Bell GI, Shank PR. Proto-oncogene expression and growth factors during liver regeneration. *Symp Fundam Cancer Res.* 1986, 39, 69-86.
107. Kang, M. K., Swee, J., Kim, R. H., Baluda, M. A., and Park, N. H.. The telomeric length and heterogeneity decrease with age in normal human oral keratinocytes. *Mech. Ageing Dev.* 2002, 123, 585-592.
108. Satoh, H., Hiyama, K., Takeda, M., Awaya, Y., Watanabe, K., Ihara, Y., Maeda, H., Ishioka, S., and Yamakido, M. Telomere shortening in peripheral blood cells was related with aging but not with white blood cell count. *Jpn. J. Hum. Genet.* 1996, 41, 413-417.
109. Furugori E., Hirayama R., Nakamura, K. I., Kammori, M., Esaki, Y. Takubo, K. Telomere shortening in gastric carcinoma with aging despite telomerase activation. *J. Cancer. Res. Clin. Oncol.* 2000, 216, 481-485.
110. Yang, L., Suwa, T., Wright, W. E., Shay, J. W., and Hornsby, P. J. Telomere shortening and decline in replicative potential as a function of donor age in human adrenocortical cells. *Mech. Ageing Dev.* 2001, 122, 1685-1694.
111. Aikata, H., Takaishi, H., Kawakami, Y., Takahashi, S., Kitamoto, M., Nakanishi, T., Nakamura, Y., Shimamoto, F., Kajiyama, G., and Ide, T. Telomere reduction in human liver tissues with age and chronic liver inflammation. *Exp. Cell. Res.* 2000, 256, 578-582.
112. Takubo, K., Nakamura, K., Izumiyama, N., Furugori, E., Sawabe, M., Arai, T., Esaki, Y., Mafune, K., Kammori, M., Fujiwara, M., Kato, M., Oshimura, M., and Sasajima, K. Telomere shortening with aging in human liver. *J. Gerontol. A. Biol. Sci. Med. Sci.* 2000, 55, B533-536.
113. Ohashi K, Tsutsumi M, Kobitsu K, Fukuda T, Tsujiuchi T, Okajima E, Ko S, Nakajima Y, Nakano H, Konishi Y. Shortened telomere length in hepatocellular carcinomas and corresponding background liver tissues of patients infected with hepatitis virus. *Jpn J Cancer Res.* 1996, 87, 419-22.
114. Kitada T., Seki S., Kawakita N., Kuroki T., Monna T. Telomere shortening in chronic liver diseases. *Biochem Biophys Res Commun.*, 1995, 211, 33-9.
115. Wagayama H, Shiraki K, Sugimoto K, Ito T, Fujikawa K, Yamanaka T, Takase K, Nakano T. High expression of p21WAF1/CIP1 is correlated with human hepatocellular carcinoma in patients with hepatitis C virus-associated chronic liver diseases. *Hum Pathol.* 2002, 33, 429-34.

116. Delhay M, Louis H, Degraef C, Le Moine O, Deviere J, Gulbis B, Jacobovitz D, Adler M, Galand P. Relationship between hepatocyte proliferative activity and liver functional reserve in human cirrhosis. *Hepatology* 1996, 23, 1003-11.
117. Takahashi S, Kitamoto M, Takaishi H, Aikata H, Kawakami Y, Nakanishi T, Shimamoto F, Tahara E, Tahara H, Ide T, Kajiyama G. Expression of telomerase component genes in hepatocellular carcinomas. *Eur J Cancer*. 2000, 36, 496-502.
118. Kirk KE, Harmon BP, Reichardt IK, Sedat JW, Blackburn EH. Block in anaphase chromosome separation caused by a telomerase template mutation. *Science* 1997, 275, 1478-81.
119. Higgins GM, Anderson RM. Experimental pathology of the liver. I. Restoration of the liver of the white rat following partial surgical removal. *Arch Pathol.*, 1931, 12, 186-202.
120. Poon, S. S., Lansdorp, P. M. *Current Protocols in Cell Biology* 2001, 18.41-18.4.21.
121. Samper E, Juana M. Flores and Blasco M.A. Restoration of telomerase activity rescues chromosomal instability and premature aging in *Terc*<sup>-/-</sup> mice with short telomeres. *EMBO reports*, 2001, 2, 800-807.
122. Severino J, Allen RG, Balin S, Balin A, Cristofalo VJ. Is beta-galactosidase staining a marker of senescence in vitro and invivo? *Exp Cell Res.*, 2000, 225, 162-71.
123. Chen KY. Transcription factors and the down-regulation of G1/S boundary genes in human diploid fibroblasts during senescence. *Front Biosci.*, 1997, 2, 417-26.
124. Dulic V, Beney GE, Frebourg G, Drullinger LF, Stein GH. Uncoupling between phenotypic senescence and cell cycle arrest in aging p21-deficient fibroblasts. *Mol Cell Biol*, 2000, 20, 6741-54.
125. Vairapandi M, Balliet AG, Hoffman B, Liebermann DA. GADD45b and GADD45g are cdc2/cyclinB1 kinase inhibitors with a role in S and G2/M cell cycle checkpoints induced by genotoxic stress. *J Cell Physiol*, 2002, 192, 327-38.
126. Severin E, Willers R, Bettecken T. Flow cytometric analysis of mouse hepatocyte ploidy. II. The development of polyploidy pattern in four mice strains with different life spans. *Cell Tissue Res*, 1984, 238, 649-52.
127. Danielsen H, Lindmo T, Reith A. A method for determining ploidy distributions in liver tissue by stereological analysis of nuclear size calibrated by flow cytometric DNA analysis. *Cytometry*, 1986, 7, 475-80.

128. Li W, Liang X, Leu JI, Kovalovich K, Ciliberto G, Taub R. Global changes in interleukin-6-dependent gene expression patterns in mouse livers after partial hepatectomy. *Hepatology* 2001, 33, 1377-86.
129. Cressman DE, Greenbaum LE, DeAngelis RA, Ciliberto G, Furth EE, Poli V, Taub R. Liver failure and defective hepatocyte regeneration in interleukin-6 deficient mice. *Science* 1996, 274, 1379-1383.
130. Veelken H, Jesuiter H, Mackensen A, Kulmburg P, Schultze J, Rosenthal F, Mertelsmann R, Lindemann A. Primary fibroblasts from human adults as target cells for ex vivo transfection and gene therapy. *Hum Gene Ther.* 1994, 5, 1203-10.
131. Ouellette MM, Aisner DL, Savre-Train I, Wright W.E., Shay JW. Telomerase activity does not always imply telomere maintenance. *Biochem Biophys Res Commun.* 1999, 254, 795-803.
132. Kim H, You S, Farris J, Kong BW, Christman SA, Foster LK, Foster DN. Expression profiles of p53-, p16(INK4a)-, and telomere-regulating genes in replicative senescent primary human, mouse, and chicken fibroblast cells. *Exp Cell Res.* 2002, 272, 199-208.
133. Nicholas R., Forsyth. NR, Evans. AP, Shay.JW, Wright. WE. 2003. *Aging Cell* (In press).
134. Wright, W.E. & Shay, J.W. Re-expression of senescent markers in deinduced reversibly immortalized cells. *Exp. Gerontol.* 1992, 27, 383-9.
135. Brown, J.P., Wei, W. Sedivy, J.M. Bypass of senescence after disruption of p21CIP1/WAF1 gene in normal diploid human fibroblasts. *Science* 1997, 277, 831-834.
136. Hara E, Smith R, Parry D, Tahara H, Stone S, Peters G. Regulation of p16CDKN2 expression and its implications for cell immortalization and senescence. *Mol. Cell. Biol.* 1996, 16, 859-867.
137. Wei, W., Hemmer, R.M., Sedivy, J.M. Role of p14(ARF) in replicative and induced senescence of human fibroblasts. *Mol. Cell. Biol.* 2001, 21, 6748-6757.
138. Dimri, G.P., Itahan, K., Acosta, M., Campisi, J. Regulation of a senescence checkpoint response by the E2F1 transcription factor and p14(ARF) tumor suppressor. *Mol. Cell. Biol.* 2000, 20, 273-285.
139. Albrecht JH, Meyer AH, Hu MY. Regulation of cyclin-dependent kinase inhibitor p21(WAF1/Cip1/Sdi1) gene expression in hepatic regeneration. *Hepatology* 1997, 25, 557-63.

140. Dadley, D.T., Pang, L., Decker, S.J., Bridges, A.J. & Saltiel, A.R. A synthetic inhibitor of the mitogen-activated protein kinase cascade. *Proc. Nat. Acad. Sci. USA*. 1995, 92, 7686-7689.
141. Davies, S.P., Reddy, H., Caivano, M., Cohen, P. Specificity and mechanism of action of some commonly used protein kinase inhibitors. *Biochem. J.* 2000, 351, 95-105.
142. Ishak, K., Baptista, A., Bianchi, L., Callea, F., De Groote, J., Gudat, F., Denk, H., Desmet, V., Korb, G., MacSween, R. N., et al Histological grading and staging of chronic hepatitis. *J. Hepatol.* 1995, 22,696-699.
143. McConnell BB, Starborg M, Brookes S, Peters G. Inhibitors of cyclin-dependent kinases induce features of replicative senescence in early passage human diploid fibroblasts. *Curr Biol.* 1998, 8, 351-4.
144. Fang L, Igarashi M, Leung J, Sugrue MM, Lee SW, Aaronson SA. p21Waf1/Cip1/Sdi1 induces permanent growth arrest with markers of replicative senescence in human tumor cells lacking functional p53. *Oncogene* 1999, 18, 2789-97.
145. Macip S, Igarashi M, Fang L, Chen A, Pan ZQ, Lee SW, Aaronson SA. Inhibition of p21-mediated ROS accumulation can rescue p21-induced senescence. *EMBO J.* 2002, 21, 2180-8.
146. Duan J, Zhang Z, Tong T. Senescence delay of human diploid fibroblast induced by anti-sense p16INK4a expression. *J Biol Chem.* 2001, 276, 48325-31.
147. Vulliamy T, Marrone A, Goldman F, Dearlove A, Bessler M, Mason PJ, Dokal I. The RNA component of telomerase is mutated in autosomal dominant dyskeratosis congenita. *Nature*, 2001, 413, 432-435.

## Curriculum Vitae

Name	:	Ande Satyanarayana
Date of Birth	:	05-06-1975
Plate of Birth	:	Vijayawada, Andhra Pradesh, India
Nationality	:	Indian
Sex & Marrital Status	:	Male & Un-married
Father's Name	:	Ande Veeraiah
Mother's Name	:	Ande Koteswaramma
Present Address	:	A. Satyanarayana c/o Dr.K.L.Rudolph Department of Gastroenterology, Hepatology & Endocrinology Hannover Medical School Hannover, 30625, Germany

### Education

10 <sup>th</sup> standard	1990	S.K.P.V.V.H.H.School, Vijayawada, India
Intermediate (12 <sup>th</sup> )	1993	P.B.Siddhartha College, Vijayawada, India
Bachelor of Science (B.Sc)	1996	Nagarjuna University Guntur, India
Master of Science (M.Sc)	1998	Nagarjuna University Guntur, India
Doctoral Research	2003	Department of Gastroenterology, Hepatology & Endocrinology Hannover Medical School Germany

### Achievements

GATE 1998 (Graduate aptitude test for Engineering ) - 89.17 percentile

NET (National Eligibility Test ) - Lecture Ship



**Publications:**

1. **A. Satyanarayana**, S.U. Wiemann, J. Buer, J. Lauber , K.E.J. Dittmar, T. Wüstefeld, M. Blasco, M. P. Manns, K. L. Rudolph. **(2003)** Telomere shortening impairs organ regeneration by inhibiting cell cycle re-entry of a sub-population of cells. **EMBO J.** Aug 1;22(15):4003-4013.
2. Wiemann SU\*, **Satyanarayana A\***, Tsahuridu M\*, Tillmann HL, Zender L, Klempnauer J, Flemming P, Franco S, Blasco MA, Manns MP, Rudolph KL. **(2002)** Hepatocyte telomere shortening and senescence are general markers of human liver cirrhosis. **FASEB J.** Jul;16(9):935-42 (\* *first three authors contributed equally to this work*)
3. **A.Satyanarayana**, M.P. Manns, K.L.Rudolph **(2003)** Telomeres and Telomerase: A duel role in regeneration, Cirrhosis and Carcinogenesis. (***In Press, Hepatology***).
4. **A. Satyanarayana**, R.A. Greenberg, S. Schaezlein, J. Buer, K. Masutomi, W. C. Hahn, S. Zimmermann, U. Martens, M.P. Manns, K.L. Rudolph. **(2004)**. Mitogen stimulation co-operates with telomere shortening to activate DNA damage responses and senescence signaling (***In press, Mol.Cell.Biol.***).